Goethite liquid crystals and magnetic field effects

Universiteit Utrecht

Cover:
Front - Small-angle X-ray scattering pattern of the biaxial nematic phase of goethite.
Back - Polarization microscopy picture of goethite in a magnetic field of 250 mT, around the isotropic-nematic interface, after 6 hours.

ISBN 978-90-393-5346-2
Subject headings: Goethite/liquid crystals/biaxial phases/X-ray scattering/polarization microscopy/magnetic fields/colloids.

Goethite liquid crystals and magnetic field effects

Vloeibare kristallen van goethiet en magneetveld effecten

(met een samenvatting in het Nederlands)

Proefschrift

ter verkrijging van de graad van doctor aan de
Universiteit Utrecht op gezag van de rector magnificus,
prof. dr. J.C. Stoof, ingevolge het besluit van het
college voor promoties in het openbaar te verdedigen
op woensdag 23 juni 2010 des middags te 2.30 uur

door

Esther van den Pol

geboren op 1 augustus 1982 te Middelburg

Promotor: Prof. dr. H.N.W. Lekkerkerker

Co-promotoren: Dr. G.J. Vroege

Dr. A.V. Petukhov

Dr. D.M.E. Thies-Weesie

This work is part of the research program of the 'Stichting voor Fundamenteel Onderzoek der Materie' (FOM), which is financially supported by the 'Nederlandse Organisatie voor Wetenschappelijk Onderzoek' (NWO). Support by the 'Deutsche Forschungsgemeinschaft' (DFG) through the 'Sonderforschungsbereich Transregio 6' (SFB TR6) is acknowledged.

Contents

1

General introduction

1.1. Colloids

A colloid is a particle with at least one dimension of the order of 1 nm – 1 μm. Colloids are dispersed in a medium to form a stable system. The lower limit of this size range is determined by the fact that the particles should be significantly larger than the solvent molecules, so that the medium can be treated as a homogeneous background. An important property of these particles is that they exhibit Brownian motion, which gives the higher limit of the size range. Thermal fluctuations of the solvent molecules make the particles move in a random way and prevent the particles to sediment quickly. Brownian motion was observed for the first time by Robert Brown in 1827 [1], who studied plant pollen in water. A theoretical explanation of this phenomenon was given by Albert Einstein in 1905 [2] and an experimental verification followed by Jean Baptiste Perrin [3, 4].

Colloids and the medium in which they are dispersed can be in the gas, liquid or solid phase. Examples of colloidal systems are milk, paint, cream, clay, ink, blood, fog, smoke, etc. Experimental and theoretical studies of colloidal dispersions can give new insights in the behavior of all these systems.

Because of the similarities in the behavior of molecules or atoms and colloids, showing for example all kinds of phase transitions, colloidal systems are also widely studied as a model system [5, 6]. An advantage of colloids is that they are relatively large, so that it is possible to visualize them with a microscope. Their size makes them also slower and easier to follow. Furthermore, both the interactions between the colloids and their size and shape can easily be tuned to be able to model different types of systems. These interactions can usually be described by the so-called DLVO (Derjaguin-Landau-Verweij-Overbeek) potential, which sums the Van der Waals attraction and the electrostatic repulsion. For example, the electrostatic interaction can be tuned by changing the pH of the dispersion, thereby modifying the surface charge, or by adding salt to the dispersion, thereby screening the charges.

The relatively large size of colloids, and their density difference with the solvent, causes sedimentation to play an important role in these systems. A sedimentation profile develops and different phases can be observed in one sample. The higher order phases, lower in the sample, will experience a higher osmotic pressure.

1.2. Liquid crystals

Spherical colloids can show different phases: the gas, liquid, crystal or glass phase [7]. Anisometric particles, however, can even show phases in between the liquid and the crystal state. Because of their shape they can show orientational order together with a possible positional order. When particles have orientational order and maximum 2D positional order they are called liquid crystals. They combine properties of liquids and

solids. A system with only orientational order is called nematic. A smectic phase combines orientational order with a 1D positionally ordered layer structure with liquidlike positional order within the layers. In a columnar phase columns are formed which arrange themselves in a regular way. Within the columns the structure is still liquidlike, so there is 2D positional order.

Liquid crystal phases have special optical properties, like birefringence, which can be tuned by applying external fields. This makes them suitable for display applications; liquid crystal displays (LCDs) are widely used nowadays.

In 1888, botanical physiologist Reinitzer and physicist Lehmann noticed for the first time that there was a state in between the liquid and the crystal state [8, 9]. They studied various derivatives of cholesterol, which are now known as cholesteric liquid crystals. These are examples of thermotropic liquid crystal, which form different phases as a function of temperature. Another type of liquid crystals is called lyotropic, where the concentration determines their state.

When colloidal particles form liquid crystals they are lyotropic. One type of colloidal liquid crystals are mineral liquid crystals [10–12], which were recognized for the first time by Zocher in 1925 [13]. He studied suspensions of vanadium pentoxide (V_2O_5) which formed a nematic phase. Some other examples are California bentonite clay (the first nematic phase of platelike particles found by Langmuir [14]), akagenite [15], boehmite [16], gibbsite [17, 18] and layered double hydroxides [19].

A theoretical model for hard particles was developed in the 1940s by Onsager [20]. He described the transition from the disordered isotropic phase to the orientationally ordered nematic phase in terms of the excluded volumes between the particles. Going to the nematic phase the orientational entropy decreases, but at the same time the free volume available for the particles increases. At a certain concentration the gain in packing entropy will exceed the loss in orientational entropy and the system undergoes an isotropic-nematic phase transition.

1.3. Goethite

Mineral liquid crystals have some advantages over molecular liquid crystals [11, 12]. These particles are electron rich and are therefore highly susceptible to external influences, like electric and magnetic fields. Furthermore, they are thermally stable and also the liquid crystal phases remain stable over a wide range of temperatures. Finally, some of these systems can be found in nature and are therefore very cheap.

One of the mineral liquid crystals that is extremely susceptible to an external magnetic field is goethite (α-FeOOH). It is named after Johann Wolfgang von Goethe, the German philosopher and poet who was also a mineralogist. Goethite is an iron bearing oxide mineral which can be found everywhere. It has been used as a pigment since prehistoric times. Besides, goethite plays an important role in the migration of heavy

metal cations and of certain anions in the natural environment and it is used as a model adsorbent in soil science and in environmental science and technology [21]. Furthermore, thermal reduction of goethite particles gives elongated metallic iron particles which can be used as a magnetic carrier in magnetic recording systems [22].

The dispersed form of goethite has also been studied for a long time. In 1902, Majorana examined the magnetic-field-induced birefringence of the "fer de Bravais", a mixture of various iron oxide and hydroxide particles in suspension, one of which was goethite. He observed field-induced linear birefringence when applying a transverse magnetic field to this dispersion [23]. This is now called the Majorana effect. The analogous effect for molecular liquids is called the Couton-Mouton effect, named after the scientists who discovered it a few years later [24]. These effects are different from the earlier found Faraday effect, which is the occurrence of circular birefringence when a magnetic field is applied along the optic axis [25].

Majorana, Cotton and Mouton also found some other intriguing behavior in the same dispersion [26,27]. They observed a non-monotonical dependence of the birefringence on the field intensity. A positive birefringence was measured in small fields, then it reached a maximum after which it decreased again to reach even negative values. This effect was attributed to the fact that the dispersion consisted of a mixture of iron oxide and hydroxide particles, giving different contributions to the birefringence. About 100 years later, Lemaire *et al.* studied the properties of pure goethite in dispersion. They found that similar birefringence effects were also observed for this dispersion [28]. It turned out that the boardlike goethite particles bear a weak permanent magnetic moment along the long axis of the particles. This was not expected since goethite is antiferromagnetic, containing opposite spin lattices, which completely compensate in the bulk crystal. In crystallites of colloidal size there are probably uncompensated surface spins. Because the magnetic easy axis of the particles is along the shortest dimension, a reorientation of the particles is observed in a magnetic field. In a small field they are aligned along the field, but in a large field they will reorient to have a perpendicular alignment.

A model for the magnetic energy of a goethite particle was developed, assuming that the particles are rodlike [29]. This is a simplification since the particles are actually boardlike with three different dimensions. If a particle is placed in a magnetic field B, at an angle θ with respect to B, the magnetic energy E_{m} per particle is given by

$$E_{\mathrm{m}} = -\mu B \cos\theta - \frac{\Delta\chi V}{2\mu_0} B^2 \cos^2\theta \tag{1.1}$$

with μ the permanent magnetic moment, $\Delta\chi = \chi_{\parallel} - \chi_{\perp}$ the magnetic susceptibility anistropy, which is negative in this case, and V the volume of the particles. The first term describes the interaction between the particle dipole and the field and the second term the induced magnetization. In small fields, the first term dominates which has a minimum at $\theta = 0$ and the particles will indeed align parallel to the field. However,

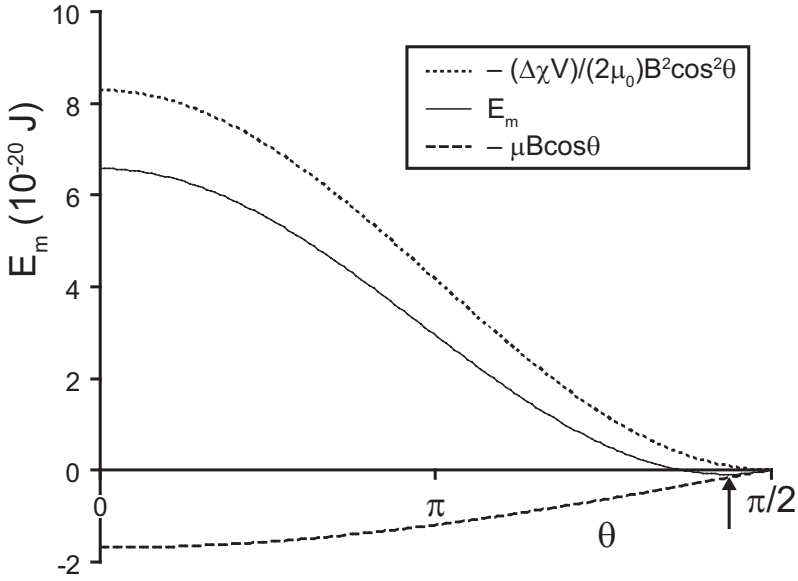

Figure 1.1. Plot of the magnetic energy of a goethite particle at an angle θ with respect to a magnetic field B of 1 T.

in large fields the second term dominates which has its minimum at $\theta = \pi/2$ and the particles will align perpendicular to the field. The exact angle of $\pi/2$ will never be the minimum in energy because the $\cos\theta$ term will always have a larger contribution than the $\cos^2\theta$ close to $\pi/2$. In Figure 1.1 a plot is given of the two separate terms of E_m and the sum of the two in a field of 1 T. For the parameters, values measured for goethite are used (see Chapter 9). The arrow indicates the energy minimum.

In more concentrated dispersions, this single-particle behavior couples to the interparticle interaction and more complicated behavior arises especially within liquid crystal phases. The reorientation behavior of colloidal goethite in dispersion has been observed in the isotropic and nematic phase [28–30]. A columnar phase has also been found in samples with a higher volume fraction of particles and a magnetic-field-induced nematic-columnar phase transition can occur [31, 32]. The structure of the columnar phase is centered rectangular (*c2mm*), which is a distorted form of the hexagonal columnar phase. In our group, even a smectic *A* phase was found in these dispersions [33, 34]. Surprisingly, this phase was present in a system with a length polydispersity of 55%. Apparently, goethite dispersions form a versatile liquid crystal system.

1.4. Outline of this thesis

In this thesis the liquid crystal phase behavior of colloidal goethite is described. Except for the last chapter, we studied aqueous dispersions of charged goethite particles. The main technique used for these studies is small-angle X-ray scattering (SAXS). In Part 1, the general liquid crystal phase behavior is described with only gravity as an external field. Chapter 2 focuses on the influence of polydispersity; fractionation and sedimentation play an important role in these systems. In Chapter 3 it is shown that specific particle dimensions can lead to biaxial phases. Clear experimental evidence is given for the existence of these phases, which is still a highly debated issue in thermotropics. A closer look at the smectic A phase is taken in Chapter 4, where a detailed analysis of the undulation fluctuations of the smectic layers is performed.

In Part 2, an external magnetic field is used to influence the phase behavior. Chapter 5 briefly describes the behavior of the different liquid crystal phases occurring in goethite dispersions. A more detailed study of the smectic A phase in a field is performed in Chapter 6, where a comparison is made between systems with different polydispersities. In Chapter 7 it is shown that nematic-nematic phase separation can occur when a field is applied around the critical field strength where the goethite particles reorient. The phase separation process is studied over time, using polarization microscopy. Around the isotropic-nematic interface also interesting behavior is observed when applying different field strengths to the system, as is shown in Chapter 8.

In the last part of this thesis (Part 3), different modified systems are studied. Chapter 9 describes the phase behavior of goethite modified with the elements Cr, Al and Co. A study of the changes in magnetic properties is performed and also nematic-nematic phase separation in a mixed system of normal and Al-goethite is studied. In Chapter 10 a new type of columnar structure, found in Cr-goethite, is discussed. This simple rectangular columnar phase can also be switched to the centered columnar structure using a magnetic field. Finally, Chapter 11 compares dispersions of charge stabilized goethite particles with dispersions of sterically stabilized particles. Their phase behavior is studied with and without an external magnetic field.

Part 1

Liquid crystal phase behavior of goethite

2

Influence of polydispersity on the liquid crystal phase behavior

Abstract

The effect of fractionation on the phase behavior of colloidal goethite dispersions with different polydispersities (17%, 35% and 55% in length) has been studied by small-angle X-ray scattering and transmission electron microscopy. All systems show a nematic and smectic A phase. The occurrence of the latter phase at such a high polydispersity is remarkable. It is shown that in the highly polydisperse systems strong fractionation occurs, which is able to reduce the local length polydispersity by up to a factor of two. In addition, a columnar phase was found, but only in the 35% and 55% polydisperse systems. It seems that the columnar phase accommodates the particles that do not fit into the smectic layers and, thus, reduces the length polydispersity within the smectic phase even further. The fact that a columnar phase was not found in the system of lowest polydispersity indicates that the smectic phase is the most stable phase at higher concentrations.

2.1. Introduction

Lyotropic mineral liquid crystals were found for the first time by Zocher in 1925 [13]. Although considerably more attention has been paid to organic liquid crystals, which are well known for their applications like LCD screens, there is now renewed interest in mineral liquid crystals [10,12]. Compared to organic liquid crystals they have enhanced electrical, optical and magnetic properties, together with a better thermal stability [11]. An interesting example are colloidal dispersions of the mineral goethite (α-FeOOH). Magneto-optical linear birefringence in iron oxide dispersions containing goethite was already recognized by Majorana in 1902 [26] and further studied by Cotton and Mouton in 1907 [24]. Lemaire *et al.* [28–32] revealed the nature of this behavior.

In contrast to highly monodisperse viruses [35–38], colloidal dispersions of synthetic particles always have an inherent polydispersity. This polydispersity can sometimes suppress the formation of ordered phases [39,40]. It was shown by computer simulations on hard spherocylinders, in the limit of infinite aspect ratio, that a smectic phase can only form if the length polydispersity is below 18% [41]. Above this terminal polydispersity a columnar phase rather than a smectic phase is expected at high volume fractions. A columnar phase can accommodate broader length distributions because particles do not have to fit into layers.

There are, however, recent theories that show that there is an influence of fractionation in polydisperse systems. It was first shown for bidisperse systems that fractionation occurs for isotropic-nematic phase separation in rod dispersions [20,42,43]. The longer rods tend to orient first and already form a nematic phase while the shorter rods remain behind in the isotropic phase, which leads to a widened phase gap. Later, this was demonstrated for continuous length distributions [44–47]. Fractionation was also predicted for crystallization of polydisperse spheres [48]. Different crystal phases can split off with a narrower size distribution than the parent phase. A terminal polydispersity still holds for each crystal phase but the total system can have a higher polydispersity. The smectic and columnar phase have partial positional order and will probably fall in between the case of isotropic-nematic phase separation and crystallization, the smectic being particularly sensitive to the length distribution. In the context of small polydispersities the "universal law of fractionation" [of polydisperse particles partitioning over any two different coexisting phases] formulated by Evans *et al.* [49] might be usefully applied.

Since colloids are relatively large, sedimentation is also an important factor in these systems. It was shown that the occurrence of multiple phases of monodisperse particles in a single test tube [50] can partly be explained as a result of sedimentation [51]. Sedimentation also couples to fractionation, as was recently shown for polydisperse colloidal van der Waals fluids [52].

A smectic phase has been observed before in some dispersions of synthetic rodlike colloidal particles with a low polydispersity [15, 53–55]. Recently, it was shown that goethite particles can form a smectic phase in a highly (over 50%) polydisperse system [33]. This was attributed to an interplay of sedimentation, fractionation and Brownian motion. Furthermore, a columnar phase was found, together with the smectic phase, which might act as a "waste disposal" for ill-fitting particles. Because of new possibilities to make less polydisperse dispersions [34] it is now possible to study the effect of polydispersity on the phase behavior of goethite in greater detail. In this chapter the phase behavior of systems with different polydispersities is compared. A detailed measurement was performed by transmission electron microscopy (TEM) and in this way the real particle distributions at different heights in different phases could be determined.

2.2. Experimental

2.2.1. Synthesis

Different synthesis methods were used to obtain systems with a variety of polydispersities, as was published earlier by Thies-Weesie *et al.* [34]. The systems with a high polydispersity (g55 and g35) were obtained by hydrolysis of iron nitrate at high pH according to Lemaire *et al.* [29]. 1 M NaOH (Acros, reagent ACS, pellets, 97+%) was added dropwise, under stirring, to a 0.1 M iron nitrate (Fisher Scientific, p.a.) solution until a pH of 11–12 was reached. The precipitate was aged for 9 days after which the supernatant was removed and the sediment was washed two times with doubly distilled (dd) water and 3 M HNO_3 (Merck, p.a., 65%) to electrostatically charge the particles by proton adsorption. After centrifuging and redispersing in dd water for three times the particles were redispersed in dd water to obtain a stable dispersion in water at pH 3. The charge density at pH 3 is around 0.2 C m^{-2}. To obtain a lower polydispersity (g35) more centrifugation steps were used.

The system with the lowest polydispersity (g17) was obtained by a slightly adjusted forced hydrolysis method described by Krehula *et al.* [21]. 25 mL of 25% TMAH (tetramethyl ammonium hydroxide, Aldrich, 25% w/w in water) was added, under vigorous stirring, to 70 mL of 0.16 M iron nitrate. The solution was aged for 12 days at 100 °C. The obtained dispersion was centrifuged and stabilized as described above.

It is assumed that after many centrifugation steps the salt concentration is determined by the H^+ and charge-compensating NO_3^- concentrations. The Debye length is then 10 nm at most.

2.2.2. Characterization

Particle size distributions were determined by TEM using a Technai 10 and 12 (FEI company) electron microscope. The particles have a more or less rectangular boardlike

shape with three different dimensions: length L, width W, and thickness T. The length and width of about 500 particles was measured with iTEM imaging software to determine the average length $\langle L \rangle$ and width $\langle W \rangle$ and their standard deviation δ_L and δ_W. The length polydispersity is then defined as $\sigma_L = \delta_L / \langle L \rangle$. Also correlations between the length and width were determined by measuring the length and width of each particle together. The thickness was difficult to determine because most particles lay on their largest-area side on the TEM grid. For each sample about 10-20 particle thicknesses were measured.

Particle size distributions were also determined as a function of the height in the capillary. To this end, capillaries were cut into small pieces after first freezing them in liquid nitrogen. The pieces were put in small vials, after which water was added. The particles were homogeneously dispersed by ultrasonication and the different fractions were analyzed by TEM.

2.2.3. SAXS experiments

Samples with different volume fractions were prepared in flat glass capillaries (Vitro-Com RT3524) with internal dimensions of 0.2 $\times$4.0 $\times$ 100 mm^3. The capillaries were closed with two-component epoxy glue (Bison Kombi rapide) and kept in a vertical position to allow the establishment of the sedimentation equilibrium profile. The samples of the g55 system were made in November 2003, the ones of the g35 in January 2004 and of g17 in December 2004. To study the liquid crystalline phase behavior as a function of polydispersity and time, small-angle X-ray scattering (SAXS) measurements were performed. These measurements were conducted at the BM26 DUBBLE beamline of the European Synchrotron Radiation Facility (ESRF, Grenoble, France) [56] in February 2004 and November 2006. In 2006 the microradian resolution setup was used [57]. In this setup, diffraction of a 13 keV X-ray beam is registered at 8 m distance by a two-dimensional CCD detector (Photonic Science, 4008$\times$2671 pixels of 22 μm^2). To improve the resolution, the beam was focused by a set of compound refractive lenses (in this case 7 beryllium lenses) installed in front of the sample. The beam diameter at the sample position was about 0.5 mm. This setup allows achieving an angular resolution of the order of a few microradians, which is sufficient for collecting detailed information on periods of the order of the length of the particles used here.

To be able to calculate distances from the scattering patterns calibration samples were measured. In 2004 a dry rat tail collagen was used as the calibration sample and in 2006 a wet rat tail collagen and a 4.2 μm grid were used. The two calibration samples of 2006 gave nearly identical results and therefore the calibration of 2006 is taken as the most reliable. Comparing the same sample in 2004 and 2006 there is a difference of about 5-10%. For a better comparison the measurements of 2004 are scaled on the measurements of 2006 by using a scaling factor based on this average difference.

Table 2.1. Goethite particle dimensions

System	$\langle L \rangle$ (nm)	σ_L (%)	$\langle W \rangle$ (nm)	σ_W (%)	$\langle T \rangle$ (nm)	$\langle L \rangle / \langle W \rangle$
g55	216	55	35	48	∼16	6.2
g35	282	35	68	32	∼25	4.1
g17	220	17	62	29	∼23	3.5

2.3. Results and discussion

The particle dimensions of the systems used are shown in Table 2.1.

As was shown before [33,34], systems with a high polydispersity (g35, g55) show rich phase behavior. An isotropic (I), nematic (N), smectic A (SmA) and columnar (C) phase were found together in samples at a range of (initial) volume fractions (5-10% for g35 and 8-18% for g55). Here, we present a more detailed study of these systems.

In Figure 2.1a an example is shown of the SAXS pattern of coexisting smectic and columnar phases which are observed low in the samples. The sharp scattering at a small angle corresponds to the smectic periodicity and the broad scattering peak, originating from the liquidlike interactions within the smectic layers, can be seen as a broad shoulder under the sharper columnar peak around q = 0.08 nm^{-1}. The columnar phase is recognized by the powderlike sharp scattering rings. Because there are columnar domains with slightly different q-values, the integrated intensity profile shows broader peaks than expected for a columnar phase. In the inset of Figure 2.1c a sharper peak is shown originating from only one of the domains. These sharp peaks originate from a distorted-hexagonal intercolumnar structure (*c2mm* symmetry group) [31] and correspond here to distances of about 80 and 50 nm. This gives unit cell parameters of 100 × 133 nm with two particles per unit cell. Comparing this with the average width (68 nm) and thickness (25 nm) it is clear that there is a lot of free space between the columns, although the fact that the columnar phase exhibits a distorted hexagonal structure proves that the two smallest particle dimensions are not equivalent and that the particles are not able to rotate freely around their long axis in this columnar structure.

The occurrence of a smectic phase in highly polydisperse systems seems to be in contradiction with the terminal length polydispersity of 18% found for the smectic phase by simulations on hard spherocylinders [41]. The boardlike goethite particles are compared with spherocylinder models because there is hardly any literature on particles with this exact shape. The difference in shape does not seem to be too important in the case of a smectic phase where the length polydispersity should be dominant. The smectic phase found was rationalized earlier by the interplay between sedimentation and fractionation [33]. Furthermore, it is possible that particles that do not fit into the

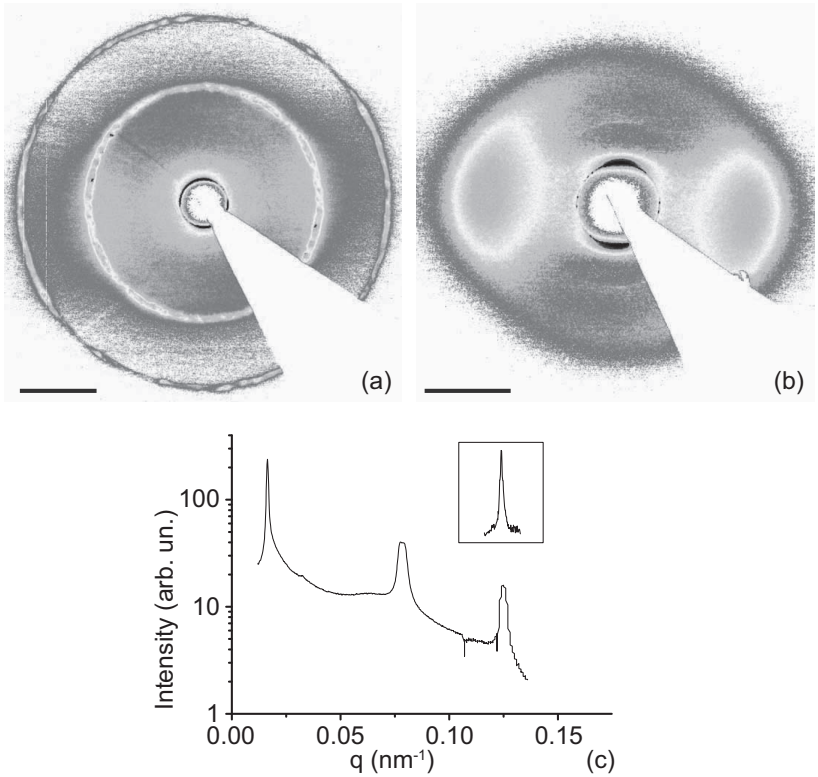

Figure 2.1. (a) SAXS pattern showing a coexisting smectic A and columnar phase (g35), (b) SAXS pattern of a single smectic A phase (g17), and (c) the integrated intensity profile of the pattern in (a) with a slice through one of the columnar domains shown in the inset. The scale bar is 0.05 nm^{-1}.

smectic phase are expelled and form a columnar phase, where particles with different lengths are allowed.

In the system with a low polydispersity (g17) only an isotropic, nematic and smectic A phase were found. The scattering pattern of the single smectic phase is shown in Figure 2.1b. No columnar phase was observed in any of the samples, at least up till a volume fraction of 14% and after standing for several years. In the highly polydisperse systems a columnar phase was already found at far lower volume fractions. This strengthens the idea of the columnar phase acting as a "waste disposal" for ill-fitting particles which is not needed for a system of low polydispersity. To gain deeper insight in this interesting phase behavior a more detailed analysis was done.

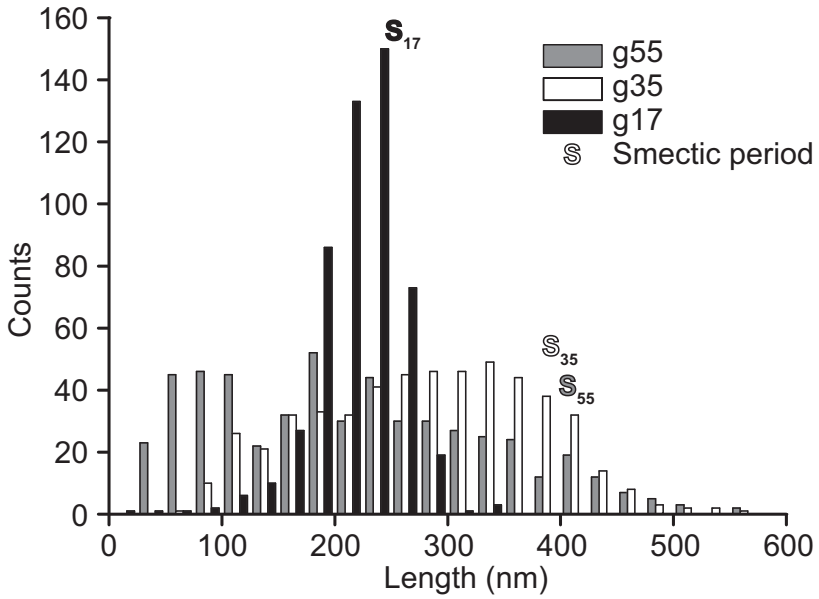

Figure 2.2. Length distributions of the parent suspensions of the g17, g35 and g55 systems. "S" indicates the period of the smectic phase as measured in 2006.

2.3.1. Fractionation

The small-angle smectic peaks originating from the periodicity of the layers give an indication of the length of the particles. This smectic periodicity is compared with the parent length distributions, measured by TEM, of the different systems, which can be seen in Figure 2.2. The periodicity lies in the large distance tail of the length distribution for the systems with a high polydispersity. The ratio of the smectic periodicity from SAXS and the average length measured by TEM gives an indication of the extent of the fractionation. This ratio reduces from 1.85 for the g55 system to 1.40 for the g35 system. For the system of lowest polydispersity (g17) the smectic periodicity is close to the average particle size (ratio of 1.14). Thus, for a more polydisperse system a stronger fractionation occurs.

Monte Carlo simulations of monodisperse hard spherocylinders have been done and the ratio between the periodicity of the smectic layers and the particle length which was found varied from 1.03 [58] to 1.27 [59]. A problem in calculating this ratio is the occurrence of particles in between the smectic layers with an orientation which is more or less perpendicular to the particles in the layers [58, 60]. Experiments on TMV found a factor of 1.12 [61]. The TMV particles are charged as are our particles. The ratio of the g17 system is close to that of the monodisperse TMV suggesting that hardly any

fractionation occurs.

High polydispersity. A more detailed analysis of the fractionation was done by TEM analysis of a capillary of the g55 system with an initial volume fraction of 8% instead of 16% which was used for the SAXS analysis. The average length and width, with their polydispersities, of fractions at different heights in the sample are shown in Table 2.2. It can be seen that the average length drastically increases to the bottom of the capillary, indicating fractionation during sedimentation.

As indicated before, fractionation has already been predicted theoretically for isotropic-nematic phase separation in rod dispersions [20, 42–47]. We find that the polydispersity of the nematic phase is substantially lower compared to the isotropic phase. It was observed before that the polydispersity of coexisting isotropic and nematic phases in dispersions of natural clay rods is lower than that of the original dispersion [62]. In our case additional smectic and columnar phases form from the large particles of the nematic phase mainly, thereby further decreasing the polydispersity of the nematic phase.

Interesting is the more or less constant particle length within the smectic region, while the polydispersity is lowest in the part where only a smectic phase occurs. The part where the smectic phase is coexisting with a columnar phase has a higher polydispersity, consistent with the notion that the columnar phase can accommodate particles that do not fit into the smectic layers. This can also be seen in the length distributions of some of the fractions, corresponding to different phases (Figure 2.3). The distribution of the fraction of the pure smectic phase is the narrowest, although it still contains quite some shorter particles. It can be seen that the largest difference between the pure smectic phase and the coexisting smectic and columnar phase is in the presence of very long ($\sim$600 nm) particles in the latter phase. Presumably, these largest particles cannot fit into the smectic layers but can be accommodated in the columnar phase.

The length polydispersity of 28% in the smectic phase still exceeds 18%, as was found in simulations [41]. There are some factors that might contribute to this. The breaking of the capillary is not very accurate, the breaking line was not always straight and precisely where it was supposed to be. In the 2.5 mm of the capillary which was used for the TEM analysis a change in the smectic periodicity of about 3% was found from SAXS. This of course increases the polydispersity found by TEM. Furthermore, the simulations were done for hard spherocylinders with infinite aspect ratio and these are soft-repulsive boardlike particles with an aspect ratio ($\langle L\rangle/\langle W\rangle$) of 6.2. Finally, in the simulations the distribution of the length of the particles is Gaussian and thus symmetric. It is clear from Figure 2.2 that the distribution of the g55 system is not symmetric and the smectic distribution (Figure 2.3) has a tail at small lengths, which would influence the simulation results.

Table 2.2. Average length and width of goethite particles as a function of height for the g55 system.

Fraction	Distance from the bottom (mm)	Phase	$\langle L \rangle$ (nm)	σ_L (%)	$\langle W \rangle$ (nm)	σ_W (%)	$\langle L \rangle / \langle W \rangle$
10	41.5 - 55.0	I	132	47	28	47	4.7
9	30.0 - 41.5	I	190	39	35	40	5.4
8	21.5 - 30.0	N	228	33	40	39	5.7
7	18.0 - 21.5	N	268	33	46	40	5.8
6	15.5 - 18.0	N	304	30	52	35	5.8
5	11.5 - 15.5	N	311	30	53	36	5.9
4	9.0 - 11.5	SmA + N	332	30	54	41	6.1
3	6.5 - 9.0	SmA	361	28	57	35	6.3
2	3.5 - 6.5	C+SmA	364	33	54	54	6.7
1	0 - 3.5	C+SmA	359	36	58	42	6.2

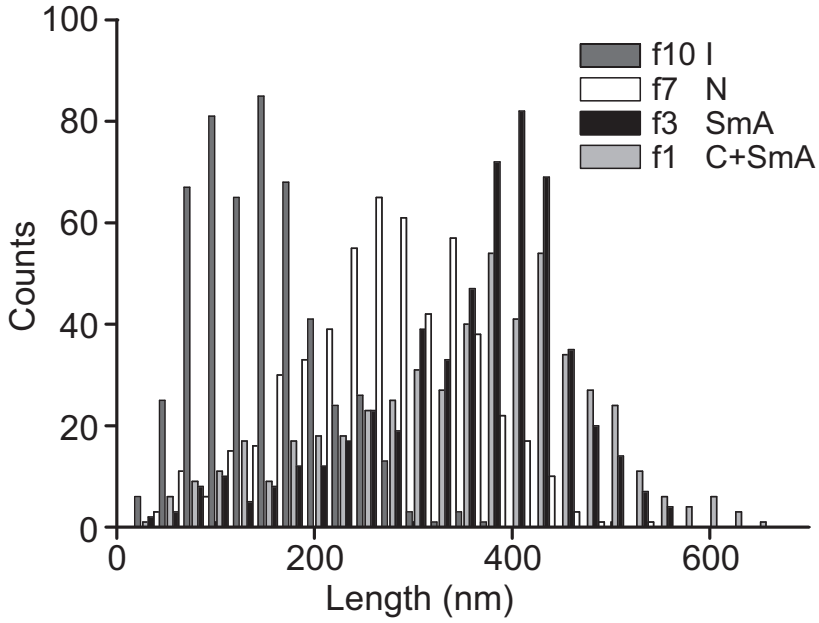

Figure 2.3. Length distributions of the fractions f1 (C+SmA), f3 (SmA), f7 (N) and f10 (I) of the g55 system.

For the average width the same trend was found as for the average length; the width increases going towards the bottom of the capillary. The lowest polydispersity is also found within the same range as for the length, although it is not expected to be important for the formation of a smectic phase. It seems that the length and width of the particles are strongly coupled - longer particles are also wider - although overall the fractionation in width is less pronounced than in length.

It is expected that the width polydispersity has a negative influence on the formation of a columnar phase, but this cannot be seen in these data. The columnar phase is always accompanied by a smectic phase and therefore it is not possible to know the width polydispersity in the columnar phase only. Furthermore, the particles are not rodlike but boardlike which makes the situation more complicated. Finally, a relatively large influence of the double layer can contribute to the accommodation of a higher width polydispersity.

To determine the thickness only about 10-20 particles could be measured so it is not possible to get good statistics out of it. A significant difference was only found for the two fractions in the isotropic phase: 8 and 13 nm compared to 20-24 nm for the other fractions. It is clear that there is a large difference in the volume of the particles going from the top to the bottom of the sample ($30 \cdot 10^3 - 500 \cdot 10^3$ nm^3). This corresponds to a variation of the gravitational length (l_g) from 4.3 mm to 0.26 mm. Here, we define l_g as

$$l_g = \frac{k_B T}{g \Delta\rho \langle L \rangle \langle W \rangle \langle T \rangle} \tag{2.1}$$

where $k_B T$ is the thermal energy, $\Delta\rho$ the mass density difference between goethite and water, and g the gravitational acceleration.

The aspect ratio ($\langle L \rangle / \langle W \rangle$) increases from 4.7 to 6.7 going down in the capillary with a more or less constant value in the nematic phase. In Figure 2.4a the individual aspect ratio (L/W) is shown as a function of the length of the particles for some of the fractions. It can be seen that the aspect ratio of the particles increases with the length of the particles. Fractionation can be clearly observed, the different fractions having a different average aspect ratio. Particles with a higher aspect ratio form more ordered phases. This is expected because they gain more free volume by aligning in ordered phases. Particles with a higher aspect ratio are also longer, so there is also fractionation in length.

A similar analysis of fractionation has been done for sepiolite clay [62]. Fractionation in the length of the particles was found in the coexisting isotropic and nematic phases, but no fractionation in width was observed. There are some differences between the sepiolite and goethite system that might explain this difference. Sepiolite is a natural clay as opposed to the synthetic goethite. The lengths and widths of the sepiolite particles appear to be uncorrelated which is not the case for the goethite particles (Figure 2.4a).

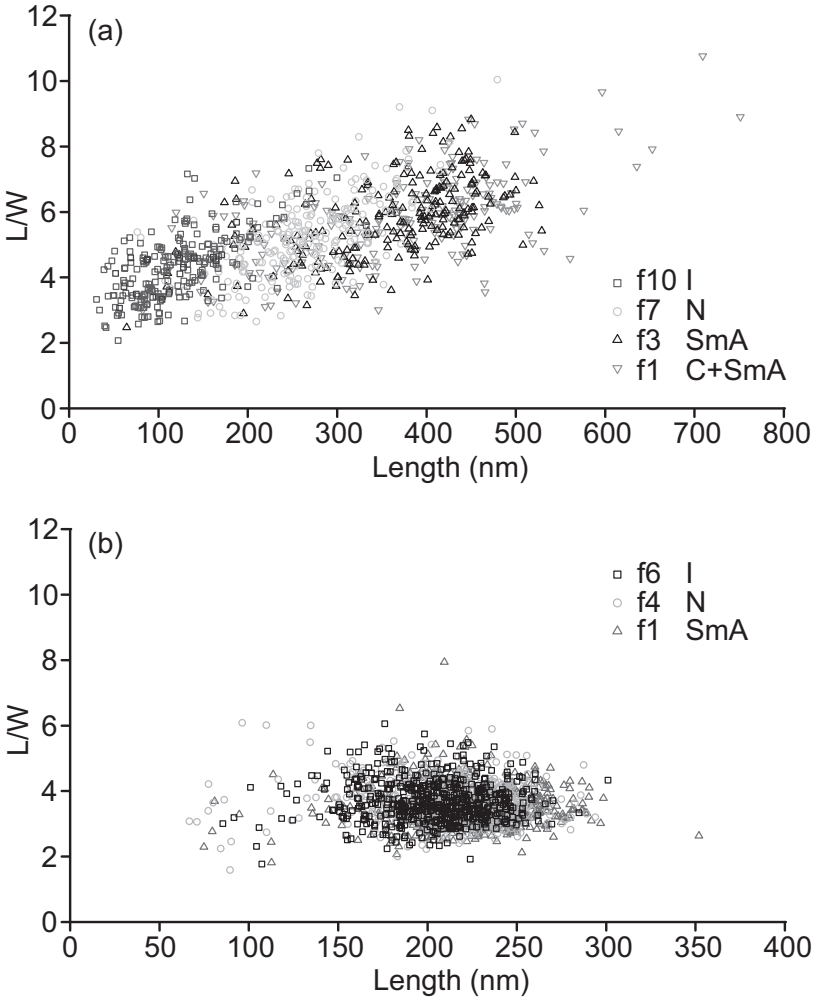

Figure 2.4. Aspect ratio (L/W) as a function of length of fractions of the g55 (a) and g17 (b) systems.

Furthermore, the width polydispersity of the sepiolite particles is small (15%) compared to that of the goethite particles studied here (48%).

Low polydispersity. The same TEM analysis was done for a capillary of the g17 system. It can be seen from Table 2.3 that there is a slight increase in the particle length going down the capillary, but there is no difference in the polydispersity. Figure 2.5 shows that the length distributions of the lowest and highest fraction have the same shape; they are only slightly shifted. For the g55 system the differences in length and length

Table 2.3. Average length of goethite particles as a function of height for the g17 system.

Fraction	Distance from the bottom (mm)	Phase	$\langle L \rangle$ (nm)	σ_L (%)	$\langle W \rangle$ (nm)	σ_W (%)	$\langle L \rangle / \langle W \rangle$
6	20.5 - 24	I	204	15	57	22	3.6
5	17.5 - 20.5	$I + N$	213	15	61	20	3.5
4	13.5 - 17.5	N	212	17	60	25	3.5
3	10.5 - 13.5	SmA	219	15	63	23	3.5
2	7.5 - 10.5	SmA	221	15	66	22	3.3
1	0 - 7.5	SmA	224	15	66	22	3.4

distribution were much larger (see Figure 2.3). This means that fractionation is much less pronounced for the goethite system of lowest polydispersity compared to highly polydisperse goethite.

It is important to point out that not only the width but also the symmetry of the parent length distribution plays a role here [49]. A wider parent distribution gives rise to a larger difference between the average values of the daughter distributions, which is the case for our systems. Furthermore, a more asymmetrical distribution gives rise to a larger difference between the widths of the daughter distributions. The system with the lowest polydispersity is also the most symmetrical one, and the daughter distributions indeed have the same polydispersity, in accordance with the "universal law of fractionation" proposed by Evans *et al.* [49].

For the width the same trend was found as for the length: a little increase in the average width going down the sample and a more or less constant polydispersity. The aspect ratio ($\langle L/W \rangle$) stays approximately the same over the whole sample. It can be seen in Figure 2.4b that the aspect ratio (L/W) is on average the same for all particles, so the small and large particles have the same shape. This is clearly different from the g55 system (Figure 2.4a).

2.3.2. Influence of time

The changes in time give valuable information about the process of phase separation. In the first few months after preparation already some changes could be seen. The lower initial volume fraction (∼10%) capillaries showed isotropic-nematic phase separation within a day, but it took several months to observe the development of a smectic and columnar phase. This indicates that particles slowly sediment and fractionate and then phase separate. The capillaries with a higher initial volume fraction (∼16%) showed a smectic and columnar phase already after a week. In this case it seems that fractionation and sedimentation-induced macroscopic separation, which are associated

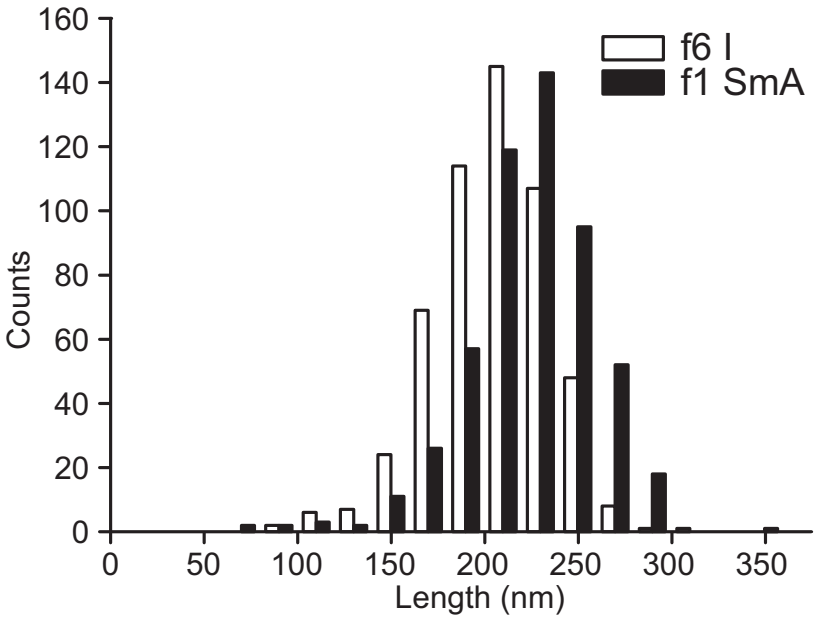

Figure 2.5. Length distributions of the fractions f1 (SmA) and f6 (I) of the g17 system.

with the isotropic-nematic phase transition, help to create circumstances to form a smectic phase within a week. It is clear that for both processes Brownian motion is important, which is facilitated by the electric double layer around the particles.

One of the g55 samples, with an initial volume fraction of 16%, has been measured by SAXS several times now. The first measurement of February 2004 (partly published in reference [33]) is compared with the measurement of November 2006. The smectic and nematic distances at a small angle, which give an indication of the particle length, are calculated from their q-values. The calibration of 2006 is taken as the most reliable one. Therefore the measurements of 2004 are scaled on the ones of 2006 as described in Section 2.2.3.

It can be seen in Figure 2.6 that in 2004, when the sample was 3 months old, there is a gradual increase in the distance going towards the bottom of the capillary. This is caused by a faster sedimentation of larger particles. In 2006, however, there are two regions with a more or less constant distance and a jump in the distance in between. This indicates a strong fractionation which makes it possible to form a much larger smectic phase. Down in the sample the smectic phase is accompanied by a columnar phase for the ill-fitting particles but higher in the sample even a pure smectic phase with a constant smectic periodicity has evolved at the height where previously a nematic phase was predominantly observed. This means that particles remain highly mobile

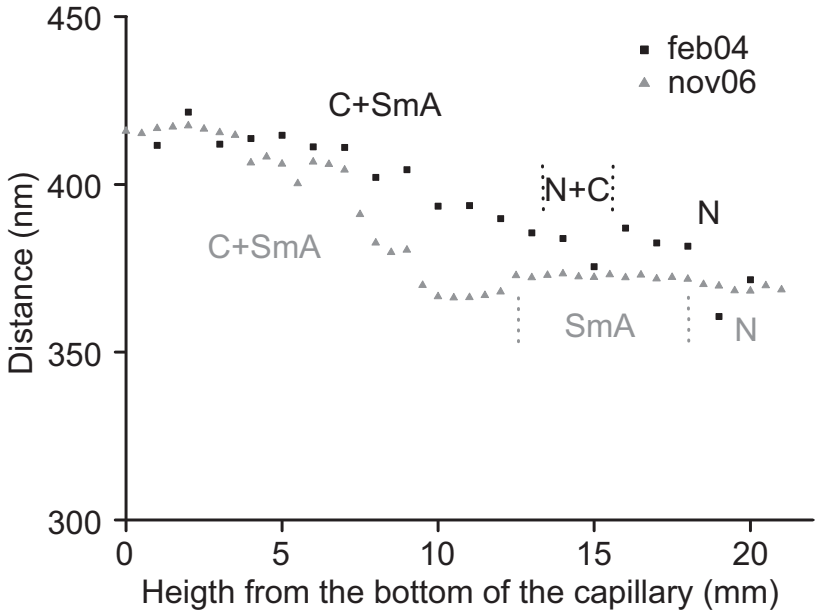

Figure 2.6. Small-angle peak distances of the g55 system.

so that in time continuous rearrangement of the particles occurs, causing a stronger fractionation and the growth of a pure smectic phase. The smectic phase might act as a kind of template for further growing this phase while retaining the same periodicity.

For the SAXS analysis described above, a capillary with an initial volume fraction of 16% was used which might not seem justified to be compared with the capillary used for the TEM analysis (initial volume fraction of 8%). Initially different liquid crystalline phases are observed, but in time similar behavior is observed. In both capillaries a smectic phase appears at a height where a nematic phase was observed before.

For the columnar distances in November 2006 there is also a small difference in the distances but it is less than for the smectic phase. The larger angle columnar peaks show a 4% increase in the distance going down in the capillary and the smaller angle peaks 8%, compared to 13% for the smectic phase. An explanation might be that the double layer of the particles is more important for the width and the thickness than for the length. Therefore, less influence of the differences in width and thickness of the particles is expected on the distances between the columns.

Small-angle distances were also measured in November 2006 for the g17 system (Figure 2.7). A more or less constant distance is found, in agreement with the constant particle length measured with TEM. The slight increase in distance going up in the

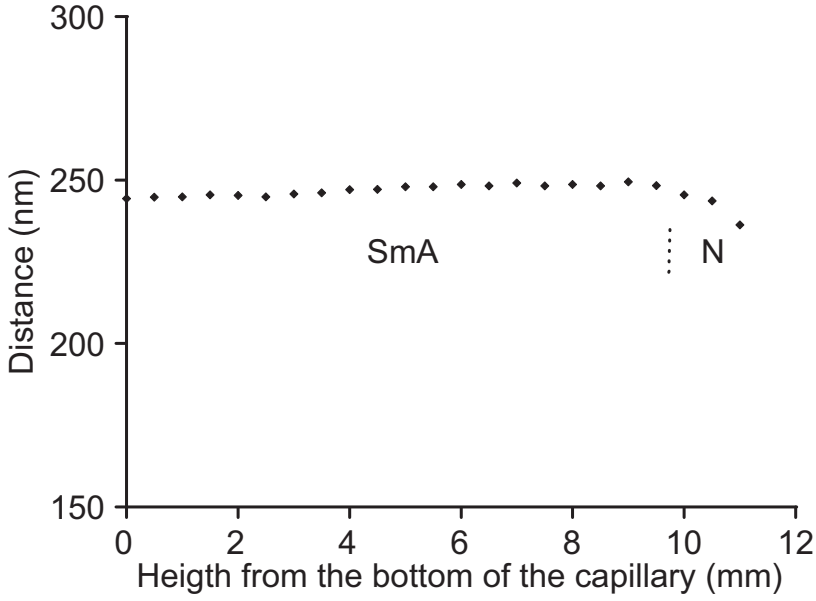

Figure 2.7. Small-angle peak distances of the g17 system.

sample might be counterintuitive because slightly smaller particles are expected there. This is probably caused by the higher osmotic pressure lower in the sample, which pushes the particles closer together, resulting in a smaller smectic periodicity.

2.4. Conclusions

Polydisperse (35% and 55%) dispersions of goethite form an isotropic, nematic, smectic *A* and columnar phase. The occurrence of a smectic phase is surprising because the terminal polydispersity to form a smectic phase was found to be 18% in simulations of hard spherocylinders. It was found by analysis of SAXS data and TEM measurements that sedimentation and fractionation play an important role. Regions within the sample were found with a length polydispersity almost twice as low as for the parent sample where the smectic phase was observed. Not only the average length increases going down the sample but also the aspect ratio. Furthermore, the width polydispersity does not hinder the formation of a columnar phase, presumably because of the double layers and unequal width and thickness of the particles.

It is remarkable that over a few years large changes occur in the samples. Fractionation is getting more pronounced in time and a pure smectic phase is evolving.

Brownian rearrangement of particles is happening for a long time which means that particles remain highly mobile due to the double layer surrounding the particles.

The development of a pure smectic phase with a constant periodicity over about 5 mm of the sample is also remarkable. It might be possible that the smectic phase itself acts as a template for the new layers that form on top of it, although the smectic phase is mostly oriented with the particles along the capillary and whole new layers can form on top of the old one. Therefore, at first sight there is no clear reason why the periodicity should remain constant over such a large distance.

In samples with a low polydispersity (17%) also isotropic, nematic and smectic A phases were found, but never a columnar phase. A columnar phase can accommodate particles with different lengths and therefore it is thought to act as a "waste disposal" for particles that do not fit into the smectic layers. This indicates that the smectic phase is the most stable phase and a columnar phase is only formed if the polydispersity does not allow the smectic phase to form.

A recently published new method for the synthesis of goethite nanotubes gives more monodisperse particles, with tunable dimensions [63]. This probably gives a nice model system for a further study of the phase behavior of monodisperse goethite.

Acknowledgements

Kristina Kvashnina and the other staff of the BM26 DUBBLE beamline at the ESRF are thanked for their support during SAXS measurements.

3

Biaxial liquid crystal phases

Abstract

Dispersions of boardlike goethite particles with short-range repulsive interaction form a versatile colloidal model system, showing a nematic, smectic A and columnar phase. In high magnetic fields a biaxial nematic phase is induced with the shortest dimension of the particles aligned along the field. Moreover, if particles have a shape almost exactly in between rodlike and platelike they can spontaneously, without external magnetic field, form biaxial nematic and biaxial smectic A phases, which is in accordance with theoretical predictions. The macroscopic domains were oriented by a magnetic field and their structure was revealed by small-angle X-ray scattering. Our results suggest that biaxial phases can be readily obtained by a proper choice of the particle shape.

3.1. Introduction

3.1.1. Biaxial phases

It is now 30 years ago that Yu and Saupe reported the first experimental observation of a biaxial nematic (N_b) phase, which was made in a micellar system [64]. The N_b phase is a modification of the usual (uniaxial) nematic (N_u) phase. In the N_u phase a spontaneous orientation of the main particle axis occurs: either the long particle axis in rodlike systems or the short particle axis in platelike systems. Biaxiality occurs if particles also orient along a second axis perpendicular to their main orientation, as is shown in Figure 3.1b and c. The N_b phase has potential advantages for the use in electro-optical applications, like flat-screen TV sets [65]. Currently, an N_u phase is used, which can be realigned using a small electric field. An N_b phase has the potential advantage that both molecular axes are aligned instead of one. If the long axis can be fixed, faster switching between different birefringent states is possible by rotating the short axes [66]. Interesting in this respect can also be a ferroelectric nematic liquid crystal, where the transverse dipoles of molecules can be aligned coherently to produce a large overall polarization [67–69].

Freiser was the first to predict the existence of an N_b phase in 1970 [70], and a few years later theoretical phase diagrams were published [71, 72]. From then on, a large amount of theoretical work and many computer simulations have been devoted to the N_b phase [73–79]. A simulated phase diagram is shown in Figure 3.2 [74]. It has been shown that a biaxial phase is expected to be found for molecules with a shape exactly in between rodlike and platelike, so when $L/W \simeq W/T$ (with L, W and T the length, width and thickness). A full phase diagram, including other (liquid) crystalline phases, was given by Taylor and Herzfeld and they found that the formation of a biaxial layerlike smectic phase strongly competes with the N_b phase [75]. Incorporating length polydispersity destabilizes the smectic phase and might reduce this effect [76].

Another possibility to obtain a biaxial nematic phase is by using a mixture of rodlike and platelike particles. This was already shown theoretically in 1973 [80] and has recently also been observed with computer simulations [81]. The difficulty here is the usually more favourable demixing into two uniaxial phases, one rich in rods and the other rich in plates [82–85].

For almost 40 years, there has been a search for biaxiality in liquid crystalline phases. The very few examples found so far are still debated and involve complicated interactions and complex (molecular) shapes [64,65,86–91]. For the classical lyotropic micellar system of Yu and Saupe [64] different suggestions have been raised about the nature of this biaxial phase. A difficulty is that micelles are adaptive systems where particle shape and phase symmetry mutually influence each other. At first it was thought that a mixture of rodlike and platelike micelles induced the N_b phase, but later it was

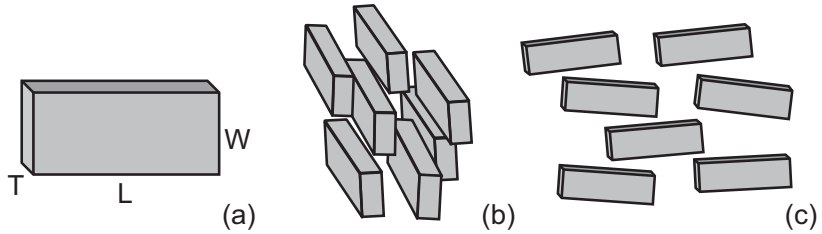

Figure 3.1. (a) Idealized shape of a goethite particle, (b) N_b phase oriented with the largest dimension (L) of the particles into the paper, (c) N_b phase oriented with the smallest dimension (T) of the particles into the paper.

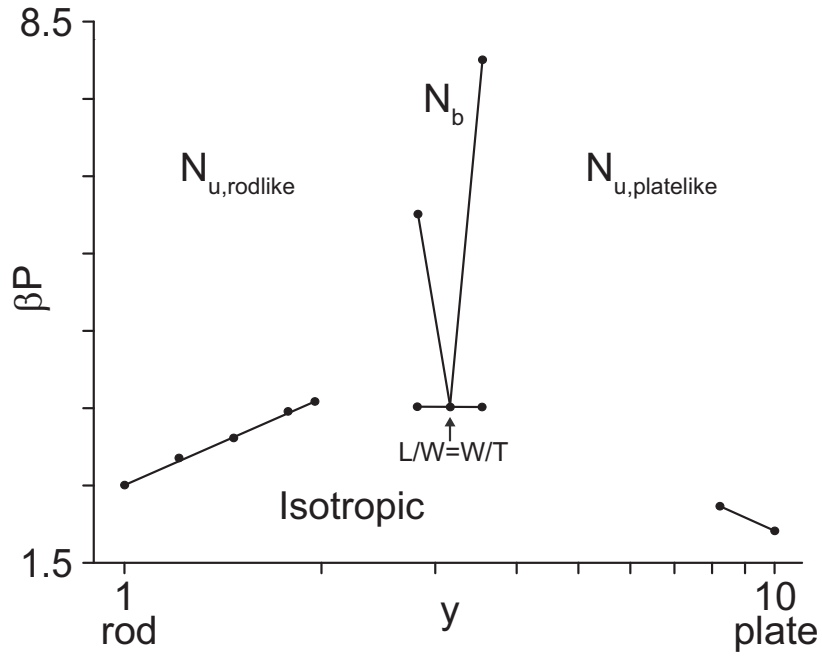

Figure 3.2. Simulated phase diagram of a hard fluid of biaxial ellipsoids, with $y = W/T$ and $L/T = 10$, redrawn from [74].

revealed that the micelles actually have a biaxial shape themselves [86]. It took until 2004 before seemingly conclusive evidence was found for the presence of an N_b phase in thermotropic liquid crystals [87, 88]. Yet, there is still an ongoing heated debate about this subject [65, 89–91], since it turns out to be very difficult to prove biaxiality. Recently, the existence of N_b phases in bent-core molecular systems was questioned again [92, 93]. In particular, it was suggested that the "biaxial nematic" X-ray patterns are actually caused by smectic C type fluctuations in the nematic phase.

A biaxial smectic A (SmA_b) phase was found for the first time in a side-chain polymer system that was aligned by a magnetic field [94]. Without alignment in an external field the phase was also found, for example using bent-core molecules in an anisotropic medium [95] and in a binary mixture of a boardlike metallomesogen with trinitrofluorenone [96].

3.1.2. Colloidal liquid crystals

Apart from the extensively studied molecular liquid crystals, anisometric colloids can also form lyotropic liquid crystal phases when dispersed in a liquid [10–12]. These systems have some advantages like their enhanced susceptibility to external fields [24, 26, 97–99]. Secondly, they are less sensitive to temperature changes and have a good thermal stability. Furthermore, they can be very cheap because some of them can even be found in a natural form. As a model system these particles are interesting because of their relatively large size, tunable shape and adjustable interactions.

In lyotropic systems a perfect anchoring is usually difficult to realize, making it hard to obtain large domains of a certain orientation. For some colloidal particles the magnetic properties can be used to overcome this problem, since already a small magnetic field can align the domains along the field direction.

Colloidal particles usually have a relatively high density, so that sedimentation effects play an important role in their phase behavior [51]. Leaving these dispersions in a vertical position, a sedimentation equilibrium profile will form and a density gradient is observed. Furthermore, fractionation will occur in these inherently polydisperse systems. These factors make it possible to have several liquid crystal phases within one sample, as was observed, for example, in gibbsite and goethite dispersions [33, 50, 100].

3.1.3. Colloidal biaxial phases

The examples of molecular biaxial phases mentioned previously have different types of interactions and either an ill-controlled or complex shape, making a comparison with theory rather difficult. Colloidal liquid crystalline particles are potentially interesting in this respect because they can be synthesized in different shapes and have short-range repulsive interactions. Although most attention has been paid to rodlike or platelike particles, boardlike colloids can also be obtained. These boardlike particles are promising because - as we have indicated - theory and simulations suggest that a biaxial nematic phase can be formed if particles have dimensions $L/W \simeq W/T$ [71, 72, 74].

In colloidal systems a biaxial nematic gel state was observed for vanadium pentoxide (V_2O_5) [101]. These fairly rigid particles have a ribbon structure which is closely related to that of bulk crystalline (orthorhombic) V_2O_5 [102]. The ribbons are well-defined bilayers of single V_2O_5 layers made of square pyramidal VO_5 units. These slabs are separated by water molecules and stack along the z-axis of a monoclinic unit cell. Particles of $250 \times 25 \times 1$ nm were used to study the biaxiality of the nematic phase.

A dispersion of these particles was studied in a Couette shear cell which produces an intrinsically biaxial shear. Small-angle X-ray scattering (SAXS) was used to study the organization of the ribbons, by sending X-rays either radially, through the centre of the cell, or tangentially, through the gap between the cylinders. The combination of these two perpendicular cuts in reciprocal space provided a complete description of the symmetry of the structure. At volume fractions larger than 4% both configurations led to anisotropic SAXS patterns, which demonstrates the biaxial nematic symmetry. When the shear flow was stopped the biaxial orientation did not relax within hours after stopping the shear. However, this nematic phase is a gel so the biaxial alignment of the ribbons may have been induced by the shear and then trapped in the gel.

Another good candidate to show a biaxial phase is goethite which is a versatile mineral liquid crystal, already known to readily form nematic, columnar and smectic phases [28, 31, 33]. These particles have a boardlike shape (Figure 3.1a) and by tuning the experimental conditions during synthesis we were able to make systems with a range of particle dimensions [34], one of them with $L/W = 3.1$ and $W/T = 3.0$. This is close to the condition $L/W \simeq W/T$ where biaxial phases are to be expected.

3.2. Experimental methods

3.2.1. Synthesis

The systems g17, g35 and g55 systems were obtained as described in Section 2.2.1. The biaxial system was obtained in almost the same way as the g35 and g55 systems. The aging time was 14 days and for centrifugation a larger volume was used [103].

Particle size distributions were determined TEM as described in Section 2.2.2. For the biaxial system 150 particle thicknesses were measured instead of only 20 for the other systems.

3.2.2. Small-angle X-ray scattering

Sample preparation is described in Section 2.2.3. Of the biaxial system, Capillary 1 (initial volume fraction of 7.5%) was made in December 2004 and Capillary 2 (initial volume fraction of 10.6%) was made in January 2006. Due to slow evaporation, the overall volume fractions had increased to 13.5% and 25.6%, respectively, at the time of the measurements.

To study the liquid crystalline phase behavior, SAXS measurements were performed. For thermotropic systems the main technique to prove biaxiality is NMR, but this technique cannot be used here because the system is sensitive even to low fields and at fields above 250 mT the system changes dramatically (see Section 3.3). The SAXS measurements were performed at the BM26 DUBBLE beamline [56], using the microradian resolution setup [57], and at the ID02 High Brilliance beamline of the European Synchrotron Radiation Facility (ESRF, Grenoble, France) [104]. A variable permanent

magnet (from the ID02 beamline) was used, which could reach a magnetic field of up to 1.5 T. Two stacks of NdFeB permanent magnets generated the field and the distance between them could be adjusted to reach the desired field strength. Different stacks were available, one set giving a field perpendicular to the X-ray beam and another set a field parallel to the X-ray beam. So, by changing the stacks the direction of the magnetic field could also be altered.

3.3. Magnetic properties and induced biaxiality

Besides their rich liquid crystalline phase behavior, goethite particles also have peculiar magnetic properties. A non-monotonic field-dependence of the birefringence in iron oxide dispersions containing goethite was already recognized by Majorana in 1902 [26] and further studied by Cotton and Mouton in 1907 [24]. The birefringence started positive, reached a maximum value, and then decreased to reach even negative values. It turned out that one of the components in their samples was goethite.

Bulk goethite is antiferromagnetic. The structure consists of double chains of octahedra occupied by iron atoms. Within a chain their spins are parallel, but there is an antiferromagnetic coupling between neighbouring chains. The Néel temperature depends on the size of the particles and varies between 325 and 400 K [29]. The magnetic easy axis of magnetic susceptibility tensor $\overleftrightarrow{\chi}$ lies along the shortest particle dimension. Besides that, goethite nanorods also have a weak permanent magnetic moment $\vec{\mu}$ along the long axis of the particles. This is presumably caused by non-compensated surface spins. The magnetic energy per particle in a magnetic field $\vec{B}$ is given by [29]

$$E_{\mathrm{m}} = -\vec{\mu} \cdot \vec{B} - \frac{V}{2\mu_0} \vec{B} \cdot \overleftrightarrow{\chi} \cdot \vec{B} \tag{3.1}$$

with V the particle volume [29]. The first term is the interaction between the particle dipole and the field and the second term is due to the induced magnetization.

In a small field, the first term dominates, which has a minimum when the particles are aligned along the field. On the contrary, the second term dominates at large fields when the energy reaches its minimum when the particles are aligned perpendicular to the field. Therefore, particles will align parallel to a small magnetic field, but perpendicular to a large magnetic field (> 300 mT).

These goethite particles have a Frederiks transition at very low fields. Samples held in 20 µm thick flat capillaries aligned beyond a field threshold of only 20 ± 5 mT [28]. This field intensity is 50 times lower than expected for tobacco mosaic virus (TMV) [105] or in V_2O_5 suspensions [97]. It is about 25 times lower than observed for usual thermotropic liquid crystals [106].

It was found that in large fields, when the particles are oriented perpendicular to the field, the nematic phase actually becomes biaxial [30]. This was found by birefringence measurements starting with a homeotropically aligned nematic sample. A field

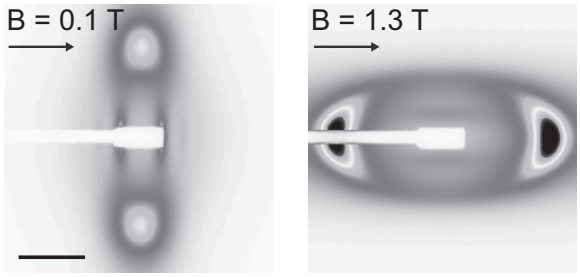

Figure 3.3. SAXS patterns of the nematic phase of goethite in a magnetic field. The scale bar is 0.05 nm^{-1}.

above the reorientation threshold was applied within the plane of the capillary. Large homeotropic domains grew and they displayed a weak birefringence that increased with the field intensity. If the nematic phase is uniaxial there should be no birefringence, which implies that this nematic phase is biaxial. It was shown that the thinnest dimension of the particles aligns along the field. This reveals that main component of $\overleftrightarrow{\chi}$ in Equation (3.1) is along the particle short axis.

The induced biaxial nematic phase was also observed with SAXS [107]. Going from a small to a large magnetic field, not only the peak orientations changed by 90 degrees because of particle reorientation, but also the peak positions changed. The liquidlike nematic peaks shifted to a larger angle (from 0.069 nm^{-1} to 0.086 nm^{-1}) going from a small to a large magnetic field (Figure 3.3). This indicates smaller distances in the direction of the field compared to the distances found for the uniaxial nematic phase in a small field. This confirms that the smallest dimension of the particles aligns along the field in large magnetic fields and that the phase is biaxial.

3.4. Biaxial correlations

Because of their boardlike shape, goethite particles are potential candidates to form biaxial phases even without an external magnetic field. In the g55 system (Table 3.1) there is a large difference between the L/W and W/T ratios and no biaxial phase was found in this system. The g35 has dimensions getting closer to $L/W \simeq W/T$, when a biaxial nematic phase would be expected (Table 3.1). The actual ratios are $L/W = 4.1$ and $W/T = 2.7$. This system has been studied in detail with SAXS.

Signs of possible biaxiality were found in the scattering patterns when the sample was 4.5 years old. SAXS patterns are given at different heights in the capillary, from 2–5 mm from the bottom of the capillary (Figure 3.4). In the lowest pattern sharp peaks can be observed originating from a columnar phase. The broad peaks arise from the liquidlike interactions in the nematic phase.

Table 3.1. Goethite particle dimensions.

System	$\langle L \rangle$ (nm)	σ_L (%)	$\langle W \rangle$ (nm)	σ_W (%)	$\langle T \rangle$ (nm)	$\langle L \rangle / \langle W \rangle$	$\langle W \rangle / \langle T \rangle$
g55	216	55	35	48	∼16	6.2	2.2
g35	282	35	68	32	∼25	4.1	2.7
g17	220	17	62	29	∼23	3.5	2.7
biaxial	254	25	83	25	28	3.1	3.0

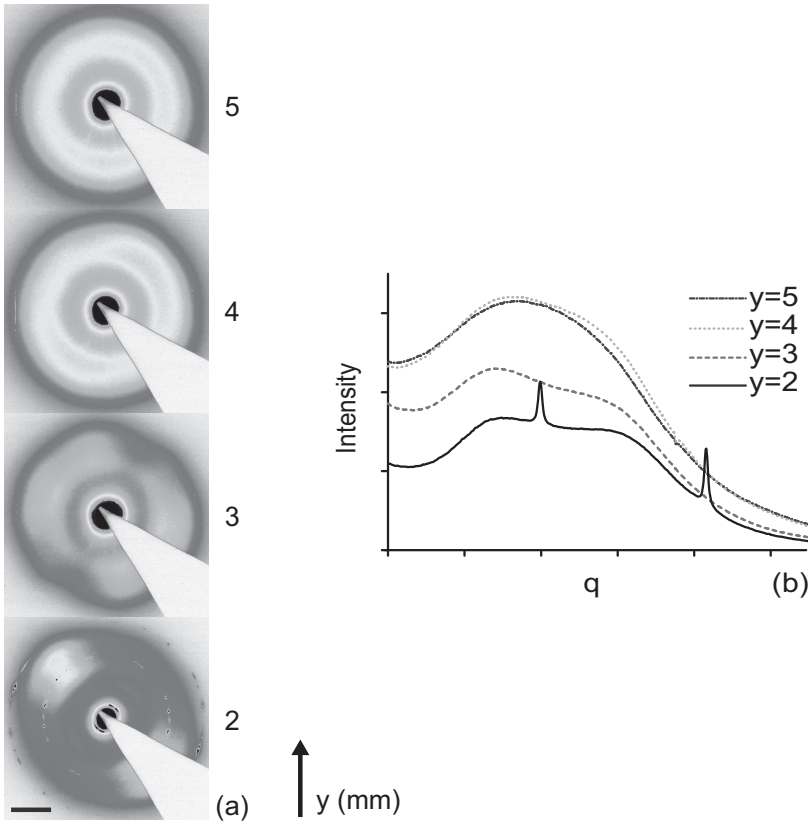

Figure 3.4. (a) SAXS patterns at different heights of a sample of the g35 system, with (b) the corresponding peak profiles. The scale bar is 0.05 nm^{-1}.

In the lower part of the nematic phase double-peaked scattering can be seen, which is clearer in the peak profiles shown in Figure 3.4b. Going up in the nematic phase the double peaks vanish and single peaks are observed. These double peaks can be an indication of biaxiality because it indicates two typical correlation distances, probably from the width and the thickness of the particles.

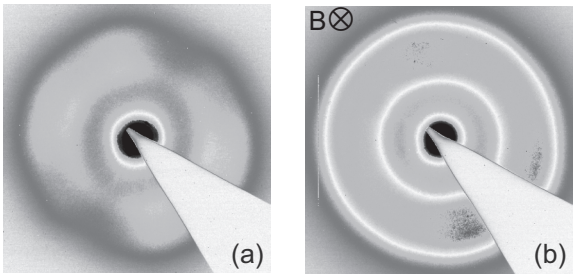

Figure 3.5. (a) SAXS pattern of the nematic phase without magnetic field and (b) in a magnetic field of 25 mT, along the X-ray beam.

To check the biaxiality the sample was put in a small magnetic field (25 mT) which was oriented along the X-ray beam. In that way the particles aligned along the field and also along the X-ray beam. If the nematic phase was really biaxial it should be observed as an anisotropic scattering pattern with two peaks at a different angle which are perpendicular to each other. This is because the width and thickness correlations should give a peak in orthogonal directions and at a different scattering angle. When we put this sample in the field it showed the pattern displayed in Figure 3.5b; the original pattern, without field, is shown in Figure 3.5a. It can be seen that the pattern actually becomes more isotropic when applying a field. This implies that the nematic phase is not biaxial as a whole, but it probably has some biaxial correlations on a local scale.

The g17 system seems to be closer to the biaxial condition $L/W \simeq W/T$ (Table 3.1), but we did not find any double peaks in the nematic phase of this system. There can be different reasons for this. First of all, these samples had been standing for a shorter time before doing the SAXS measurements and in the other system it took years before the signs of biaxial correlations were observed. Furthermore, in these systems the thickness of only 20 particles could be measured (see Section 3.2.1), so there is a large error in the average thickness giving also a large error in the W/T ratio.

3.5. Biaxial nematic phase

Another system studied has particles with average dimensions of $L \times W \times T = 254 \times 83 \times 28$ nm, with a polydispersity of 20–25% in all directions (see Table 3.1 and Figure 3.6) [103]. This gives $L/W = 3.1$ and $W/T = 3.0$ which is promising in view of finding an N_b phase. A schematic picture of the samples studied is given together with a polarization microscopy picture in Figure 3.7. Because of sedimentation a concentration profile developed and several liquid crystalline phases could be observed in one capillary. SAXS was used together with a small external magnetic field to determine the phases present in the system.

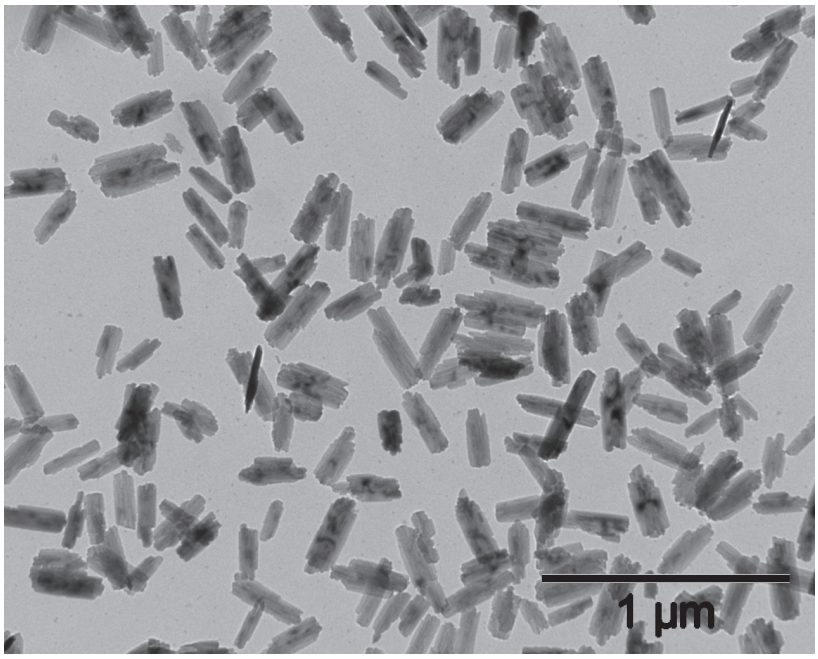

Figure 3.6. TEM picture of the goethite particles with $L/W \simeq W/T$.

Capillary 1 was first measured with the field aligned along the X-ray beam, so perpendicular to the paper. The magnetic poles were at maximum distance and gave a very small field of 3 mT. The SAXS pattern of the nematic phase is shown in Figure 3.8a. It is clear that the pattern is now anisotropic, which is different from the system described in the previous section (Figure 3.5b). Two orthogonal peaks at larger angles were observed corresponding to the width and thickness correlations; for the peak profiles in horizontal (solid line) and vertical (dashed line) direction see Figure 3.8d. In addition to the radial profiles, the azimuthal profiles of the scattering intensity along circles at q-values corresponding to the three main correlation peaks are show in Figure 3.9a. The q-values chosen are illustrated by circles in the scattering patterns. One can clearly see that different positional correlation peaks appear along directions orthogonal to each other. The fact that the peaks are perpendicular to each other indicates that the particles are orientationally ordered in three directions, as is illustrated in Figure 3.1b. This phase is clearly an N_b phase. It is also evident that an external field of as low as 3 mT is sufficient to orient the particles along the field because no peak was observed at a small angle corresponding to the length correlations.

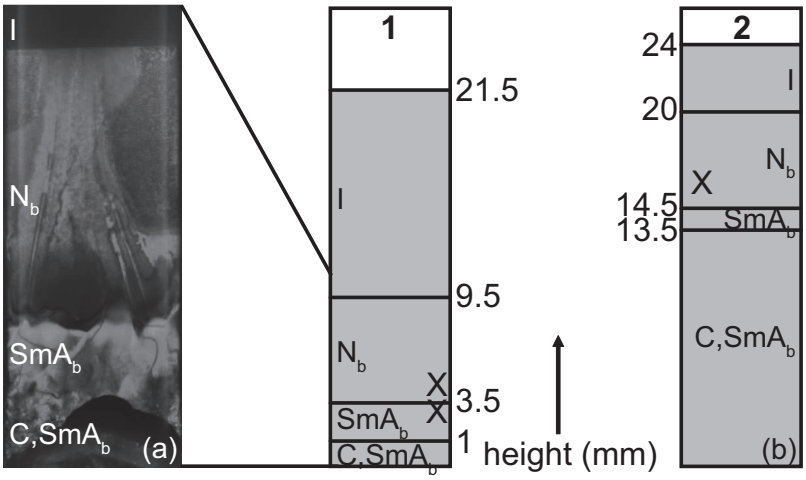

Figure 3.7. (a) Polarization microscopy picture of Capillary 1. (b) Schematic picture of the measured capillaries described in Sections 3.5 and 3.6, indicating the isotropic (I), biaxial nematic (N_b), biaxial smectic (SmA_b) and combination of columnar and smectic (C,SmA_b) phase. The $\times$'s correspond to the measurement positions discussed in this article.

Increasing the field to 40 mT (Figures 3.8b,e, 3.9b) the only change was a higher intensity of the peaks. This indicates that the particles were better aligned at this field strength. Subsequently, the field direction was changed from parallel to perpendicular to the X-ray beam by replacing the magnetic poles. After applying again 40 mT, peaks at small angles emerged in the field direction corresponding to correlations between the long axes of the particles (Figures 3.8c,f, 3.9c). The width correlations can now be seen in the vertical direction. In the same direction but at a larger angle there also appeared weak scattering corresponding to the thickness, presumably originating from a differently oriented domain caused by the reorientation process. The N_b phase changed orientation with the change of the magnetic field direction and was then predominantly like the situation depicted in Figure 3.1c. Table 3.2 summarizes the positions and the radial widths of the liquidlike correlation peaks in Figure 3.8e,f. One can see that the width of all the peaks, including the one in the horizontal direction in Figure 3.8f, is well beyond the instrument resolution, which was about 3×10^{-4} nm^{-1}. The normalized peak widths $\delta q/q_0$ are also comparable for the peaks originating from liquidlike interparticle correlations in the three orthogonal directions, which confirms the nematic nature of the phase.

Distances (d) were calculated from the scattering vector (q) of the three orthogonal peaks, observed in the scattering patterns measured with the different orientations

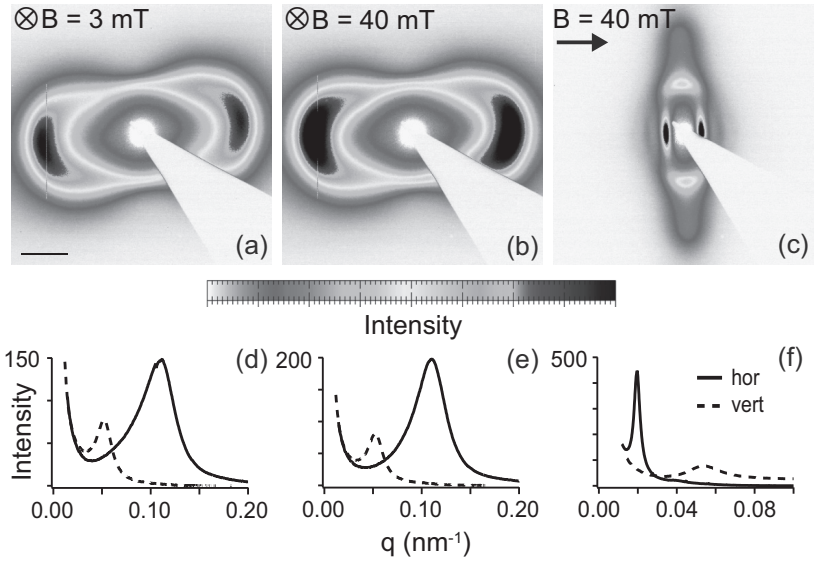

Figure 3.8. SAXS patterns of the N_b phase in Capillary 1 in a small magnetic field of (a) 3 mT and (b) 40 mT parallel (⊗) to the X-ray beam, and (c) of 40 mT perpendicular (→) to the X-ray beam, with the intensity profiles of a (d), b (e) and c (f) in the horizontal (solid line) and vertical (dashed line) direction. The scale bar is 0.05 nm^{-1}.

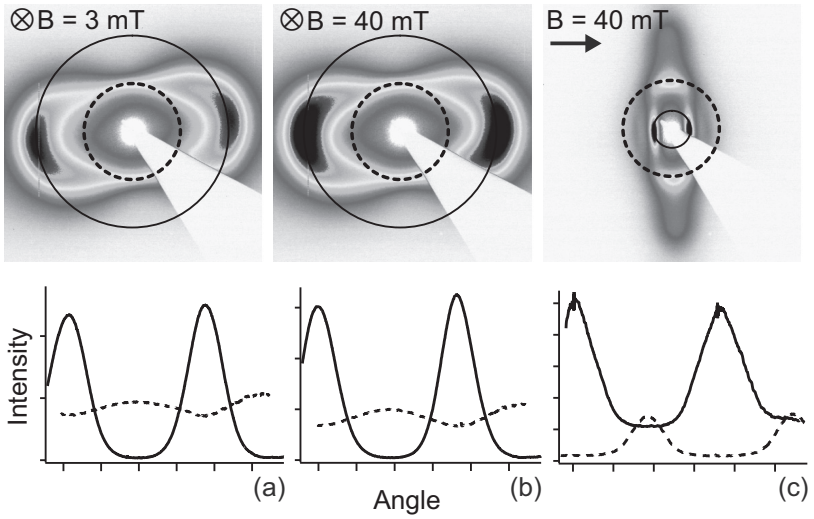

Figure 3.9. Plots of the intensity as a function of the angle at different q-values of the SAXS patterns shown in Figure 3.8.

Table 3.2. Position q_0 and radial width δq of the peaks seen in Figure 3.8e,f.

		q_0 (nm^{-1})	δq (nm^{-1})	$\delta q/q_0$
Figure 3.8e	vert	0.052	0.016	0.30
	hor	0.109	0.045	0.41
Figure 3.8f	vert	0.054	0.020	0.37
	hor	0.0195	0.0034	0.18

of the magnetic field, by applying $d \approx 2\pi/q$. Ensemble-averaged distances d_L, d_W and d_T were found of 320, 120 and 58 nm, which are slightly larger than the particle dimensions L, W and T of 254, 83 and 28 nm. The electric double layer around the charged particles is at least of the order of the Debye length (10 nm at most in this case). Taking this into account brings the dimensions already close to the distances measured. Furthermore, polydispersity causes fractionation in the system and therefore mainly the longer particles are expected to be in the lower part of the capillary (where these measurements were done, see Figure 3.7) [108]. The measured d_L/d_W and d_W/d_T ratios are 2.7 and 2.1, while the actual particle ratios are $L/W = 3.1$ and $W/T = 3.0$. However, including the Debye length gives $L_{eff}/W_{eff} = 2.7$ and $W_{eff}/T_{eff} = 2.1$, which now correspond well to the peak ratios measured. Together with the SAXS patterns these values give convincing evidence that an N_b phase was indeed found.

To be sure that the N_b phase is not field induced, measurements were performed without any magnetic field. Therefore, Capillary 2 (Figure 3.7) was used, which had not been in a magnetic field before, and was first measured without any field. The observed SAXS pattern of the nematic phase is presented in Figure 3.10a. It shows peaks at a small angle corresponding to the length correlations and perpendicular to that peaks at a larger angle from the width correlations. No peak is observed at a larger angle which would correspond to distances of the order of the thickness of the particles. This implies that the smallest dimension of the particles is aligned along the X-ray beam and that the three different dimensions of the particles are oriented orthogonal to each other. It is concluded that an N_b phase was also present without field and is not induced by the magnetic field. Furthermore, the domain of the N_b phase is larger than the X-ray beam, which is about 0.5–1 mm in diameter at the sample position.

At 40 mT, the N_b phase aligned along the field as was observed before (Figure 3.10b). After the field was reduced to 3 mT for one hour, it was seen that the N_b phase slowly relaxed into the direction of its original orientation (Figure 3.10c).

Interestingly, a direct transition from the I to the N_b phase was observed in both capillaries without an N_u phase in between. An intermediate N_u is already expected if the L/W and W/T ratios are slightly different (Figure 3.2) [71–74]. It might be that polydispersity has a stabilizing effect for the N_b phase compared to the N_u phase, which

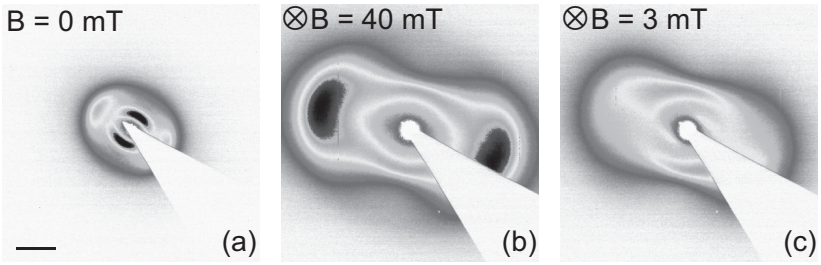

Figure 3.10. SAXS patterns of (a) the N_b phase in Capillary 2 in 0 mT, (b) in 40 mT (parallel $\otimes$ to the X-ray beam) and (c) the relaxation of the N_b phase shown at 3 mT. The scale bar is 0.05 nm^{-1}.

has been shown to be the case for the N_u phase compared to the I phase [42, 44, 47]. Another aspect can be a possible electrostatic heterogeneity of the particles.

It was attempted to perform additional birefringence measurements on the N_b phase. Therefore, it was tried to align the particles along the optical axis, using a small field along this optical axis, to obtain a homeotropic sample. The measured birefringence could then be compared with values measured for the induced biaxial phase of goethite [30]. Unfortunately, the capillaries used (0.2 x 4.0 x 100 mm^3) were too thick to be able to observe anything optically. The problem is that goethite is a pigment and absorbs a lot of light.

3.6. Biaxial smectic A phase

A smectic A phase was also found in the same system. The same measurements were done for this phase, using Capillary 1. It did not align along the field of 3 mT (parallel to the X-ray beam, that is perpendicular to the paper), as can be seen from the small-angle peaks originating from the length correlations (Figure 3.11a). The pattern is similar to the one observed for the N_b phase in zero field (Figure 3.10a), but with much sharper small-angle peaks. These very sharp and intense peaks, oversaturated in this picture, are characteristic for the periodicity of the smectic phase. Perpendicular to them, at larger angles, liquidlike peaks were observed corresponding to distances comparable to the width of the particles. However, no peaks were observed at even larger angles, so the smallest dimension of the particles was oriented along the X-ray beam. This implies that again the three different dimensions of the particles were oriented orthogonally to each other and an SmA_b phase was observed (Figure 3.11d).

By increasing the field to 40 mT, peaks appeared at larger angles, while the peaks at small angles vanished (Figure 3.11b). The observed SAXS pattern was then similar to the aligned N_b phase (Figure 3.8a,b), indicating that the smectic phase was now also aligned along the field and the widths and thicknesses of the particles were perpendicular

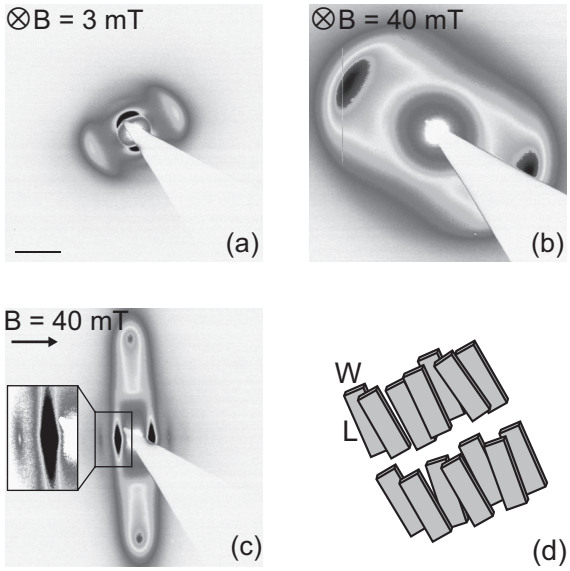

Figure 3.11. SAXS patterns of the SmA_b phase in Capillary 1 in a small magnetic field of (a) 3 mT and (b) 40 mT parallel (⊗) to the X-ray beam, and (c) of 40 mT perpendicular (→) to the X-ray beam (including zoom). The scale bar is 0.05 nm^{-1}. (d) The structure of the biaxial smectic phase, corresponding to (a).

to the field and perpendicular to each other. This shows that also the smectic phase is clearly biaxial. After rotating the field direction from parallel to perpendicular to the X-ray beam, sharp peaks from the length correlations (oversaturated in this picture) returned at small angles (Figure 3.11c). Second order peaks were observed (Figure 3.11c, zoom), suggesting a well aligned smectic phase. The distances corresponding to the three different peak angles were calculated from the different SAXS patterns and found to be $d_L = 327$, $d_W = 120$ and $d_T = 56$ nm, comparable to the distances found in the N_b phase. The d_L/d_W and d_W/d_T ratios measured are again 2.7 and 2.1.

Finally, we would like to stress that the observed biaxiality cannot be induced by artefacts such as anchoring at the capillary walls. The results shown in Figure 3.8a,b, Figure 3.10b and Figure 3.11b are obtained from domains with the particle's long axis normal to the capillary walls. In that case there can be no (biaxial) anchoring effect of the capillary walls. Moreover, the biaxiality is not induced by the magnetic field since the biaxial structure was also observed without applying a magnetic field and it remains after removal of the field.

3.7. Conclusions

In high fields goethite particles form a biaxial nematic phase. Without magnetic field, in goethite dispersions with particle ratios L/W larger than W/T by at least a factor of 1.3, some biaxial correlations have been observed in one system but no real biaxial phase. However, in a dispersion of particles with $L/W \simeq W/T$ we clearly show the existence of a biaxial nematic and biaxial smectic phase. The magnetic properties of the particles have been used to align the domains in different directions during SAXS measurements, which allowed to construct a complete picture of the biaxial phases. The macroscopically large domains are also observed without alignment by a magnetic field. Surprisingly, the N_b phase is stable over a large concentration range and no N_u phase was found. These results suggest that the biaxial nematic and biaxial smectic phases can be readily obtained by a proper choice of the particle dimensions, which for the first time confirms earlier theoretical work. Compared to the work of Yu and Saupe [64], our particles have a fixed and well-defined shape. This system can be a model for smaller nanoparticles that could be useful for applications.

Acknowledgements

Patrick Davidson is thanked for enlightening discussions and for his help, together with Ivan Dozov, with the birefringence measurements. We also thank the staff of the BM26 and ID02 beamlines of the ESRF for their excellent support and Theyencheri Narayanan for sharing the magnet.

4

Sliding undulation fluctuations in the smectic A phase

Abstract

The spontaneous formation of a highly ordered smectic A phase of goethite particles is demonstrated. The observation of a fifth order smectic X-ray reflection, which is still instrument limited, indicates a very small value of the Caillé parameter $\eta_c \ll 0.05$. An unusual peak shape was observed with highly anisotropic tails in the transverse direction (perpendicular to the smectic periodicity). The peak shape is rationalized in terms of sliding undulations, in which the director stays fixed while the layers undulate by sliding the particles along each other.

4.1. Introduction

The effect of any type of disorder in crystals and liquid crystals on their properties is still an intriguing and challenging problem. For these studies, the static structure is often distinguished from the dynamic properties. For (liquid) crystals the term static usually refers to the average structure. Dynamics is about the (thermally-induced) time-dependent fluctuations of the building blocks (atoms, molecules, colloidal particles) from their average position.

In fact, the static and dynamic properties are closely related and they determine each other. For atomic (e.g., ionic) crystals the bonding is very strong, $\gg k_{\mathrm{B}}T$, so that the dynamic fluctuations are only a minor deviation from the average lattice positions. Thermal fluctuations (and the corresponding entropy contributions) become crucial if soft matter systems, such as macromolecular and colloidal crystals, are considered. Thermotropic and lyotropic liquid crystals are also examples where the fluctuations play a very significant role.

A conceptually important example is the role of fluctuations in smectic liquid crystals. Most crystals possess so-called long-range positional order. It means that in perfect 3D crystals (i.e. crystals without non-equilibrium defects) the thermal fluctuations of the atoms around their equilibrium positions do not destroy the positional correlations over macroscopic distances. In smectics with 1D periodicity, however, the mean square fluctuations diverge logarithmically with the distance, which is known as the Landau-Peierls instability.

These fluctuations have been studied in thermotropic [109–111], lyotropic [112–118] and polymeric [119–121] liquid crystals using X-ray and neutron diffraction. In the diffraction domain no real (δ-like) Bragg peaks are observed, but cusp singularities with anisotropic power-law decays. This has mostly been studied in multidomain samples, but there are also examples of single domain studies [115, 120]. With these single domains it is possible to study the decay in the parallel and perpendicular direction. In the diffraction data there might also be an influence of the mosaic spread.

Goethite particles are able to form a variety of liquid crystalline phases as well, including the smectic A phase (see Chapter 2) [33]. The scattering peaks observed during small-angle X-ray scattering (SAXS) experiments are analyzed to study the fluctuations present in the smectic phase of this system.

4.2. Landau-Peierls instability in the smectic A phase

The smectic A phase has a layer structure with 1D positional order within which the particles are oriented normal to the layers. The fluctuation spectrum of the smectic structure depends on the elastic properties, which determine the energy costs for variations from the average positions. Of importance are the deviations in the direction

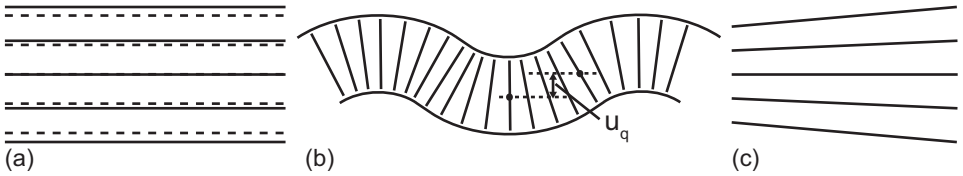

Figure 4.1. Sketch of (a) compression, (b) splay and (c) bend distortion in a smectic A phase. Panel (a) illustrates that a systematic variation of the layer coordinate in the longitudinal direction, $\nabla_\parallel u \neq 0$ leads to a change of the smectic period. Panel (b) outlines a layer undulation mode with an amplitude u_q associated with the splay distortion of the director. Bend (panel c) and twist (not shown) distortions are usually neglected.

normal to the layers, which can be described using the coordinate variable u. In the long-wavelength limit, i.e. for slow-varying fluctuations, the most important part of the elastic free energy can be written as

$$F_{\rm el} = \frac{1}{2}\int \left[B(\nabla_\parallel u)^2 + K_1(\nabla_\perp^2 u)^2)\right] d^3r, \tag{4.1}$$

where B measures the energy cost associated with compressing or stretching the layers (Figure 4.1a) and K_1 is the splay elastic constant [122]. The splay distortion is shown in Figure 4.1b; it can be produced at a constant layer spacing which is energetically favorable. More costly are twist and bend (Figure 4.1c) distortions where the layer spacing is not constant and their elastic constants are not included in the free energy.

According to the equipartion theorem, the mean-square amplitudes of the fluctuation modes $u(\mathbf{q})$ are given by

$$\left\langle |u(\mathbf{q})|^2 \right\rangle = \frac{k_{\rm B}T}{Bq_\parallel^2 + K_1 q_\perp^4}. \tag{4.2}$$

One can see that the amplitude of the mode with $q_\parallel = 0$, which describes the undulations of the layers, becomes anomalously large in the long-wavelength limit, $q_\perp \to 0$. This is the mode, which is responsible for the Landau-Peierls instability.

This instability will have a consequence for diffraction experiments. No true Bragg peaks will be observed, but only power-law singularities. In the vicinity of an $n-$th order quasi-Bragg peak the intensity can be described by

$$I(\mathbf{q} - n\mathbf{q}_0) \propto \begin{cases} (q_\parallel - nq_0)^{-2+n^2\eta_c} & \text{if } q_\perp = 0, \\ q_\perp^{-4+2n^2\eta_c} & \text{if } q_\parallel = 0, \end{cases} \tag{4.3}$$

where

$$\eta_{\rm c} = \frac{q_0^2 k_{\rm B} T}{8\pi (K_1 B)^{1/2}} \tag{4.4}$$

is the Caillé parameter.

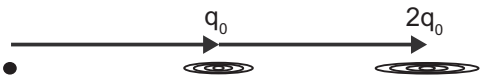

Figure 4.2. Effect of the Landau-Peierls instability on the appearence of the smectic reflections.

There are some important points to stress here. The tails are very much extended along the $\mathbf{q}_0$ direction, while the decay in the perpendicular direction is much faster. Furthermore, the effect of the Landau-Peierls instability grows quickly for higher-order reflections, due to the factor n^2. These effects are schematically illustrated in Figure 4.2.

4.3. Experimental

A sample of the g35 system of which the synthesis is described in Section 2.2.1 was used in this study.

SAXS measurements were performed at the DUBBLE beamline of the ESRF in May 2009. The sample was rotated in steps of 0.2° between -5° and 5° to obtain profiles of the full smectic peak. A home-made variable permanent magnet was used to align the sample. The scattering pattern shown in Figure 4.3 was obtained during a measurement session in September 2008. All scattering data are corrected for the detector offset and the background scattering. Here, the magnet of the ID02 beamline was used (see Section 3.2.2).

4.4. Results

In Figure 4.3 a 2D diffraction pattern of the smectic A phase of goethite, measured in a magnetic field of 60 mT, is shown. A zoom of the 5th order peak is presented as well. It was observed that the longitudinal peak width is still comparable to the resolution. After the measurements were performed, the field was switched off and the 5th order peak remained visible. The fact that the width this 5th order peak is still instrument limited suggests that the parameter η_c, Equation (4.4), must have an extremely low value: $5^2\eta_c \ll 2$, i.e. $\eta_c \ll 0.05$.

The smectic phase of this system has a large periodicity, much larger than in usual thermotropic systems (hundreds of nm versus a few nm). Therefore, q_0 has a value that is about two orders of magnitude smaller leading to a decrease of η_c by about 4 orders of magnitude. However, we do not possess a reliable estimate of the values of the elastic constants B and K_1. In any case, the diffraction data clearly indicate that the reduction of q_0 is not sufficiently compensated by a reduction of the elastic constants B and K_1.

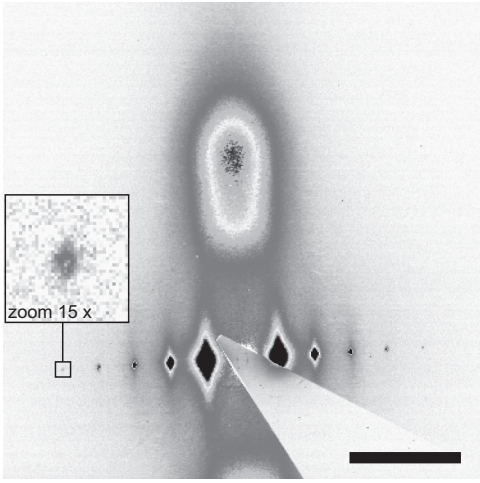

Figure 4.3. SAXS pattern of the smectic A phase of goethite with a zoom of the 5th order peak. The scale bar is 0.05 nm^{-1}.

A truly surprising result here is the observation of highly anisotropic tails of the quasi-Bragg peaks in the perpendicular direction instead of along $\mathbf{q}_0$. This is opposite to the usual theory summarized in Section 4.2.

Figure 4.4 shows examples of the peak profiles in the vertical direction q_x, measured in a field of 100 mT for different sample orientations (Figure 4.5). In this measurement the sample is tilted by $\omega = \pm 5°$ around the vertical axis in steps of 0.2°. The profiles were acquired by integrating the scattering intensity along $q_\parallel$ within a narrow slice containing the smectic (100) reflection. The intensities up to about 100 units were evaluated using the data measured with an exposure time of 10 seconds. For higher intensities the data measured with exposure times of 1 s and 100 ms were used to avoid detector saturation effects. Profiles as a function of q_x at different $q_y = q_0 \tan\omega$ were obtained in this way, where $q_x^2 + q_y^2 = q_\perp^2$. Lorentzian-like tails were observed with a q^{-2} decay of the scattering intensity instead of a q^{-4}, as would be expected from the theory described above.

A very similar peak shape has been observed in the smectic phase of a block copolymer by Ŝtêpánek *et al.* [120]. Comparable to goethite, the smectic reflections in the block copolymer are significantly spread in the direction orthogonal to the wavevector of the smectic periodicity and a very clear Lorentzian lineshape is observed along $q_\perp$. The authors of Ref. [120] interpreted the broadening in the "wrong direction" as an effect of the so called mosaic spread (i.e. the sample contained domains with close but not identical orientations according to Ŝtêpánek *et al.*). However, the mosaic spread

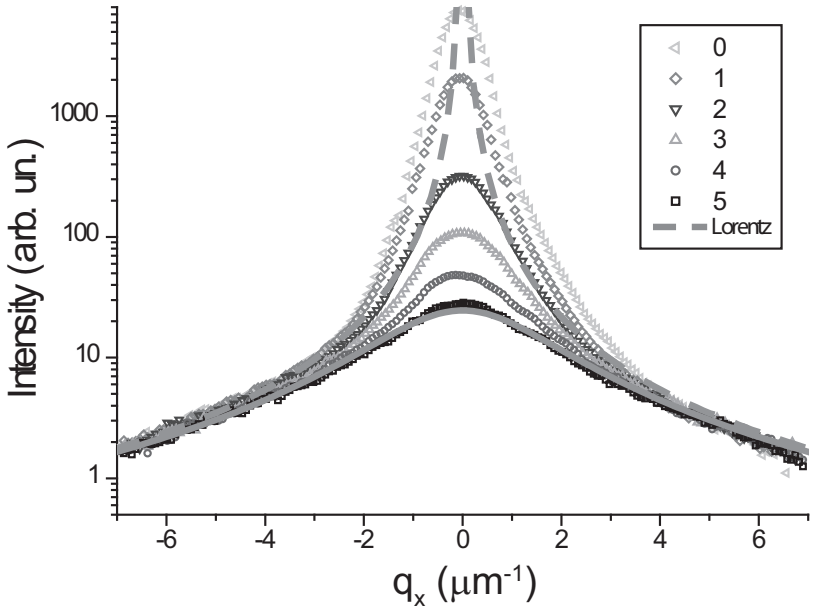

Figure 4.4. Profiles of the X-ray scattering intensity along the vertical q_x direction for different sample orientations. The X-ray beam is parallel to the smectic layers (0), and makes an angle of $\omega = 1°$ (1), $2°$ (2), $3°$ (3), $4°$ (4) and $5°$ (5). The gray lines show the Lorentzian profiles, Equation (4.12), with $q_y = 0$ (dashed) and $q_y \neq 0$ (solid).

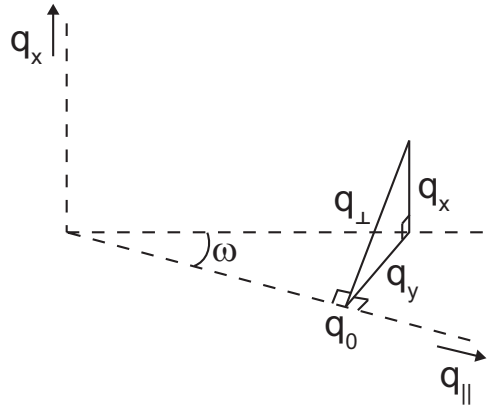

Figure 4.5. Overview of the components of the diffraction $\mathbf{q}$. The q_y component is determined by the rotation angle ω.

cannot explain the Lorenzian tails of the smectic reflections. One would rather expect a Gaussian-like decay due to the central limit theorem.

4.5. Discussion

A re-examination of the theory is needed to understand our results. A more general form of the elastic free energy, Equation (4.1), is [122]

$$\begin{aligned} F_{\mathrm{el}} &= \frac{1}{2}\int \left[B(\nabla_{\parallel}u)^2 + D(\nabla_{\perp}u + \delta\mathbf{n})^2)\right] d^3r \\ &\quad + \frac{1}{2}\int \left[K_1(\nabla\cdot\mathbf{n})^2 + K_2\left(\mathbf{n}\cdot(\nabla\times\mathbf{n})\right)^2 + K_3\left(\mathbf{n}\times(\nabla\times\mathbf{n})\right)^2\right] d^3r, \end{aligned} \tag{4.5}$$

where the D term describes the energy penalty for smectic C-type fluctuations, i.e. fluctuations of the director $\mathbf{n}$ (locally averaged particle orientations) and the layer normal $\mathbf{N}$ away from each other. Furthermore, we have explicitly spelled out not only the splay distortions (the K_1 term), but also the bend (K_2) and the twist (K_3) distortions. The latter two usually correspond to higher-energy excitations since they are associated with a variation of the layer spacing. The bend and twist excitations are therefore usually expelled from smectic liquid crystals and the corresponding K_2 and K_3 terms are neglected.

The usual approach is then to minimize first the elastic energy, assuming that the average director $\mathbf{n}$ and the layer normal $\mathbf{N}$ are the same. This leads to $\delta n = -\nabla_{\perp}u$ for small deviations. The D term disappears and Equation (4.1) is obtained. In the following, however, we do not neglect the D term.

4.5.1. Interpretation

For further analysis, sliding fluctuations, as shown in Figure 4.6, are taken into account. When sliding fluctuations occur there are parts of the smectic A phase that are actually smectic C-like. In a smectic C phase $\mathbf{n}$ and $\mathbf{N}$ are not parallel to each other. In this case $\delta n \neq -\nabla_{\perp}u$ and the D term will not disappear. The elastic free energy will then be given by

$$\begin{aligned} F_{\mathrm{el}} &= \frac{1}{2}\int \left[B(\nabla_{\parallel}u)^2 + D(\nabla_{\perp}u + \delta\mathbf{n})^2)\right] d^3r \\ &\quad + \frac{1}{2}\int K_1(\nabla\cdot\mathbf{n})^2 d^3r. \end{aligned} \tag{4.6}$$

In this case the layer coordinate u and the director $\mathbf{n}$ are not linked to each other anymore and can fluctuate independently. In other words, two different types of fluctuations can now co-exist in the system. The coordinate u is written as a sum of two terms

$$u(\mathbf{r}) = u_1(\mathbf{r}) + u_2(\mathbf{r}), \tag{4.7}$$

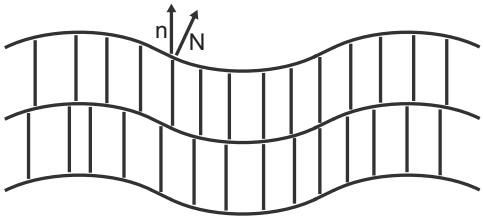

Figure 4.6. Sliding fluctuations in the smectic phase with **n** the director and **N** the layer normal.

where the first contribution corresponds to the splay undulations satisfying

$$\nabla_\perp u_1(\mathbf{r}) = -(\delta \mathbf{n}) \tag{4.8}$$

while the second contribution $u_2(\mathbf{r})$ can be assigned to the sliding undulations. The elastic energy associated with modes varying in space with a wavevector $\mathbf{q}$, now simplifies to

$$F_\mathbf{q} = \frac{1}{2}\left[Bq_\parallel^2 |u_{1\mathbf{q}} + u_{2\mathbf{q}}|^2 + Dq_\perp^2 u_{2\mathbf{q}}^2 + K_1 q_\perp^4 u_{1\mathbf{q}}^2\right]. \tag{4.9}$$

In the long-wavelength limit, $q \to 0$, the u_1 fluctuations correspond to the lowest-energy excitation because of the $q_\perp^4$ prefactor in the K_1 term. These splay fluctuations will therefore have the highest amplitude. Upon increasing the $q_\perp$ value, however, the u_2 mode will become increasingly important. At $q_\perp$ larger than a critical value $q_c = \sqrt{D/K_1}$ the u_2 mode has the lowest energy. On the scale much smaller than $2\pi/q_c$, the sliding u_2 mode will dominate the undulation fluctuations in the system. To illustrate this, let us consider a simple model.

4.5.2. Simple model

It is assumed that all the elastic constants K_i are very large so that, on the scale of interest, the director can hardly fluctuate, i.e. $u_1 = 0$. Therefore, there will be no splay distortion, but sliding fluctuations are taken into account. All K terms will vanish and the elastic free energy (Equation (4.5)) can be reduced to

$$F_{\text{el}} = \frac{1}{2}\int \left[B(\nabla_\parallel u)^2 + D(\nabla_\perp u)^2)\right] d^3r. \tag{4.10}$$

The mean-square amplitudes of the fluctuation modes $u(q)$ are then given by

$$\left\langle |u(\mathbf{q})|^2 \right\rangle = \frac{k_\text{B}T}{Bq_\parallel^2 + Dq_\perp^2}. \tag{4.11}$$

It can be seen that now the amplitudes of the long-wavelength modes diverge only as $q_\parallel^{-2}$, and $q_\perp^{-2}$. This removes the divergence in the amplitudes of the particle displacements. The Landau-Peierls instability is gone and the structure becomes long-range ordered. The true Bragg reflections should then appear in the diffraction domain.

The presence of the fluctuation modes (Equation (4.11)) will lead to the appearance of tails of the Bragg peaks, which can be described by [123]

$$I_n(\mathbf{q}) \propto \frac{1}{B(q_\parallel - nq_0)^2 + Dq_\perp^2} \tag{4.12}$$

in the vicinity of the nth-order smectic reflection. These tails are similar to the phonon-induced tails in ordinary crystals. On the other hand, since the intensity decay in the two orthogonal directions is determined by the different elastic constants B and D, the tails can become highly anisotropic.

The result of this simple model closely matches our experimental findings. The fact that the tails are spread in the perpendicular direction suggests that the elastic constant D, corresponding to the sliding fluctuations, should be much smaller than the compressibility constant B. We do not possess estimates of the elastic constants relevant for our system. We note, however, that for hard particles one can indeed expect that $D \ll B$. The B term is related to the variation of the interlayer distance leading to a reduction of the free space between the particles, which should result in a significant entropy loss. The D term, however, is related to particles sliding along each other, which can be done much easier by the hard particles.

In the $q_\parallel$ direction there is little intensity in the tails, simply because of $B \gg D$. To explain the intensity profile in the $q_\perp$ direction, the experimental results from Figure 4.4 are replotted on a log-log scale in Figure 4.7. For comparison, the direct beam profile is also shown. Two contributions can be distinguished in the peak profiles. One is instrument-limited, which can be clearly seen in the $\omega = 0°$ curve for $q < 2.5\mu\text{m}^{-1}$. This contribution quickly decays as a function of ω. Furthermore, there is a quadratically decaying contribution, which dominates for $\omega = 5°$. The scattering intensity profile closely follows a Lorentzian lineshape in accordance with Equation (4.12). This is also observed for the, not instrument-limited, tails of the other curves. The sliding mode u_2 apparently dominates the layer undulations in the q-range beyond the instrument resolution.

The shape of the tails of the diffraction peaks can also be qualitatively explained, as is shown in Figure 4.8. When sliding fluctuations occur the layer periodicity is not constant. The smectic periodicity is controlled by the particle length L and a fluctuation will decrease the periodicity. A rotation of the layer normal by an angle α will reduce the layer periodicity to $L\cos\alpha$. This piece of the sample will then effectively scatter the X-rays into a different direction with an increased q-value of $2\pi/(L\cos\alpha)$. The horizontal component $[2\pi/(L\cos\alpha)]\cos\alpha = 2\pi/L$ of this wavevector is independent of α, therefore, this scattering will be distributed along a vertical line normal to the wavevector of the smectic order $\mathbf{q}_0$. This simple consideration shows that the D term and the sliding fluctuations can be responsible for the observed shape of the reflections.

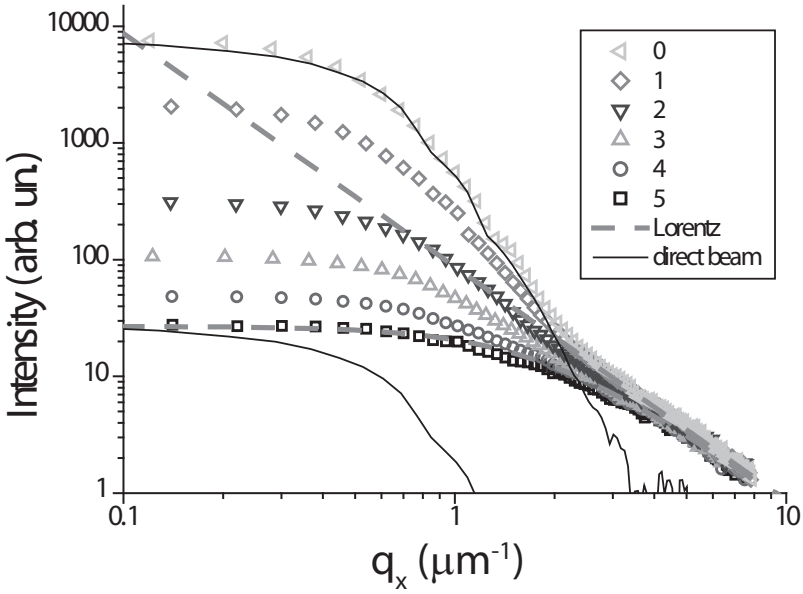

Figure 4.7. The curves from Figure 4.4 plotted on a log-log scale. The direct beam profile is also shown; the same profile is plotted two times on a different intensity scale.

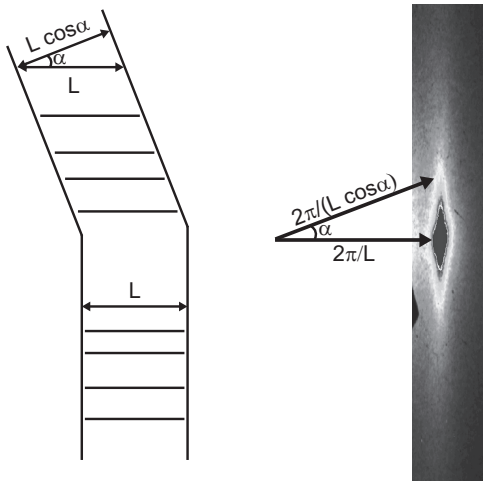

Figure 4.8. Qualitative explanation of the shape of the tails of the smectic peaks.

4.6. Concluding remarks

In goethite, smectic peaks with long streaks are observed. These are clearly not arcs, as a mosaic spread would yield. The unusual peak shape is rationalized in terms of sliding undulations, in which the director stays fixed while the layers undulate by sliding the particles along each other. These kind of fluctuations in smectic phases have been visualized before in different colloidal systems using scanning electron microscopy [53] and also light microscopy [54], but they were not studied in detail. We believe that the present results are able to shed light on the observations in copolymers [120]. Moreover, these findings might also re-new the interest in the important fundamental problem of the role of the Landau-Peierls instability in other smectics. According to Patrick Davidson, apart from goethite and co-polymers, similar behavior in the diffraction domain is observed in thermotropic molecular liquid crystals [124].

Acknowledgements

The staff of the BM26 DUBBLE beamline at the ESRF and Dmytro Byelov, Anatoly Snigirev and Roelof van Silfhout are thanked for their support during SAXS measurements. Patrick Davidson, Wim de Jeu and Dmytro Byelov are acknowledged for helpful discussions.

Part 2

Goethite in an external magnetic field

5

General phase behavior in an external magnetic field

Abstract

The behavior of the different liquid crystalline phases observed in a colloidal dispersion of goethite, with a polydispersity of 35%, has been studied by small-angle X-ray scattering. The particles align parallel to a small magnetic field and perpendicular to a large magnetic field, which was observed in the isotropic and nematic phase. The smectic phase also aligned parallel to a small magnetic field but it formed an aligned columnar phase with a distorted hexagonal structure in higher magnetic fields. The columnar phase mainly aligned in higher magnetic fields.

5.1. Introduction

Dispersions of boardlike goethite (α-FeOOH) particles are an intriguing example of mineral liquid crystals. A non-monotonic field-dependence of the birefringence in iron oxide dispersions containing goethite was already recognized by Majorana in 1902 and Cotton and Mouton in 1907, who studied aqueous colloidal suspensions of mixed iron oxides [24, 26]. The birefringence started positive, reached a maximum value, and then decreased to reach even negative values. One of the components appeared to be goethite. Lemaire *et al.* [28] further revealed that the goethite particles have a permanent magnetic moment along their long axis L, presumably due to uncompensated spins within their anti-ferromagnetic crystal structure. In contrast, their magnetic easy axis is along the shortest particle dimension T. The interplay between them leads to the peculiar reorientation from parallel to a small magnetic field to perpendicular to a large magnetic field.

Furthermore, goethite dispersions show a rich phase behavior as is shown in Chapter 2. Smectic A and columnar phases have been found even in very (55%) polydisperse systems (Chapter 2) [33, 34]. Sedimentation and fractionation play an important role in the formation of these phases. All different phases of goethite were studied by small-angle X-ray scattering (SAXS) in a magnetic field.

5.2. Experimental

The goethite dispersion used in this chapter is g35 from Chapter 2, the synthesis of which is described in Section 2.2.1.

TEM analysis was performed as in Section 2.2.2.

Samples were made as in Section 2.2.3. The sample had been standing for about 3.5 years before doing these measurements. SAXS measurements were performed at the ID02 high brilliance beamline of the European Synchrotron Radiation Facility (ESRF, Grenoble, France) [104]. The variable permanent magnet described in Section 3.2.2 was used.

5.3. Results and discussion

The particle dimensions of the system used (g35) are $282 \times 68 \times 25$ nm with a length polydispersity of 35%. This system shows rich phase behavior as was explained before (Chapter 2). It forms an isotropic (I), nematic (N), smectic A (SmA) and columnar (C) phase in a sample with an initial volume fraction of 5.8%. The structure of the different phases can be seen in Figure 5.1. This sample had been standing for a long time and therefore sedimentation and fractionation contributed to the formation of the higher order phases [33]. A polarization microscopy picture is shown in Figure 5.2. The lowest phase is a combined smectic and columnar phase (C+SmA) of which the upper

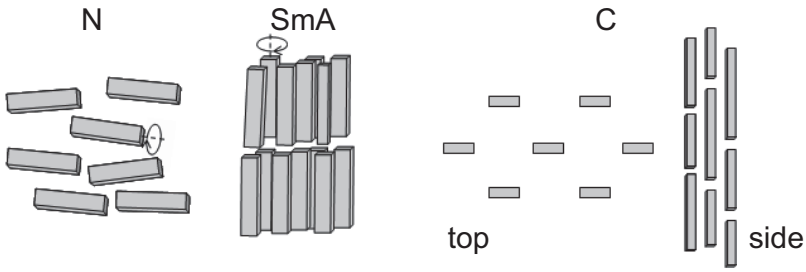

Figure 5.1. Structure of the nematic (N), smectic A (SmA) and columnar (C) phase of goethite. For the columnar phase a top and a side view are shown. The particles are drawn in one orientation but in the nematic and smectic phase they can rotate around their long axis.

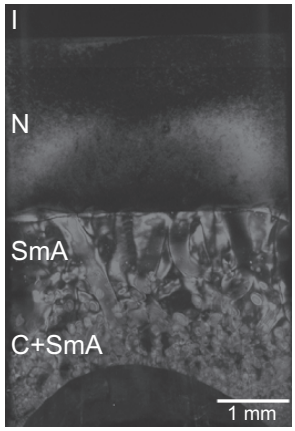

Figure 5.2. Liquid crystalline phases observed between crossed polarizers in a goethite sample.

part is purely smectic. On top of this phase a nematic phase can be seen and the upper phase is isotropic. The dark part at the bottom of the picture is the glue which was used to close the capillary.

An estimate of the volume fraction at the phase boundaries has been made from the sample absorption measured during the SAXS experiments. The volume fraction at the I-N phase boundary is approximately 7.3%, at N-SmA 10% and at SmA-(C+SmA) 11%. No clear jumps in the concentration profile were observed at the phase boundaries. All different phases were studied with SAXS in an external magnetic field.

5.3.1. Nematic phase

Lemaire *et al.* [28] already found that goethite particles align parallel to a small magnetic field and perpendicular to a large magnetic field. This is also shown in Figure 5.3

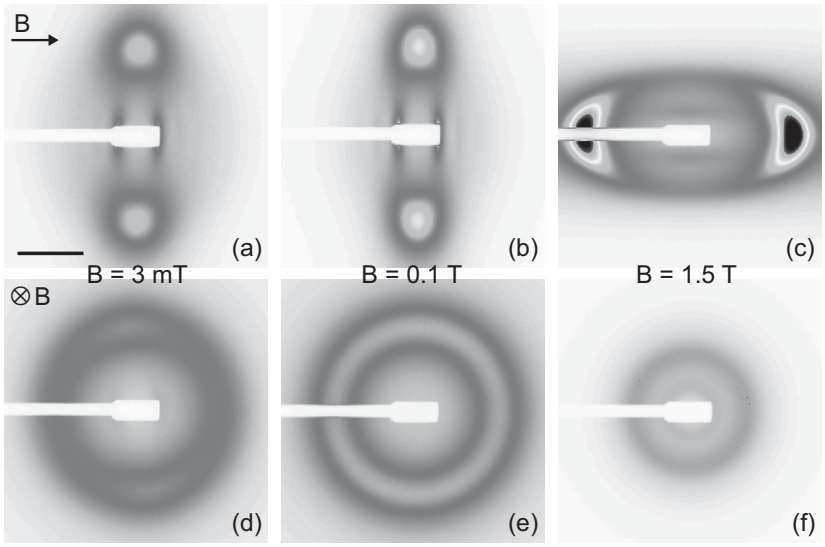

FIGURE 5.3. Nematic phase of goethite in a magnetic field. Upper pictures with the magnetic field perpendicular to the beam (in the horizontal direction), lower pictures with the field parallel to the beam. The scale bar is 0.05 nm^{-1}.

for the nematic phase. In the upper part of the figure (a-c) the magnetic field is perpendicular to the X-ray beam (in the horizontal direction) and in the lower part of the figure (d-f) the magnetic field is parallel to the X-ray beam. All measurements with the field perpendicular to the beam were performed before the measurements with the field parallel to the beam.

It can be seen that in a magnetic field of 3 mT the nematic phase is already mostly oriented in one domain (Figure 5.3a, the orientation is similar to Figure 5.1 N). The diffuse peaks at a large angle originate from the liquidlike order perpendicular to the direction of orientation in the nematic phase. At a small angle there are also peaks visible (partly screened by the beamstop) indicating positional correlations on distances of the order of the length of the particles. However, these peaks are quite broad and cannot originate from a smectic phase. So, in this system there are already strong length correlations in the nematic phase.

In a magnetic field of 0.1 T the particles in the nematic phase are clearly better aligned parallel to the field (Figure 5.3b). The SAXS pattern with the field parallel to the beam (e) shows an isotropic ring meaning that the shortest two axes of the particles do not have a preferred orientation.

At 1.5 T the particles have changed orientation and are now aligned perpendicular to the field (c). In the patterns c and f weak scattering can be observed at a small

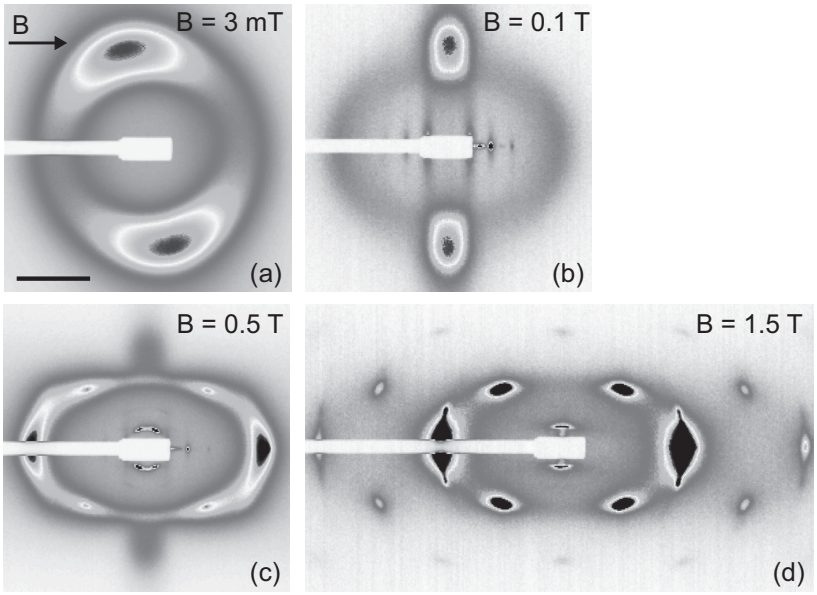

Figure 5.4. Smectic phase of goethite in a magnetic field. The scale bar is 0.05 nm^{-1}.

angle, perpendicular to the field. This means that length correlations are present perpendicular to the magnetic field. In the picture with the field parallel to the beam (f) it can be seen that the isotropic ring is now at significantly smaller angle than in a small magnetic field. The q-value corresponds to 136 nm compared to 91 nm in a small magnetic field. This means that within a plane perpendicular to the field the particles are further apart from each other. In contrast, from the picture with the field perpendicular to the beam (c) a distance of 73 nm along the field can be calculated which is smaller than the 91 nm in small fields, so now shorter distances are present along the field. This means that the particles are mainly oriented with their shortest dimension along the field and their two larger dimensions perpendicular to the field.

5.3.2. Smectic phase

The behavior of the smectic phase in a magnetic field is shown in Figure 5.4. In a magnetic field of 3 mT the typical sharp peaks at a small angle, corresponding to the smectic periodicity of the layers, are not observed (a). At the same time, optical Bragg reflections were observed in the sample at this height. The apparent discrepancy can be understood on the basis of the orientations of the smectic domains present in the sample. To observe the smectic periodicity in a SAXS pattern the X-ray beam must be parallel to the smectic layers. A slight tilt of the layers is already enough to let the small-angle peaks disappear.

In a small magnetic field of 0.1 T the smectic phase aligns with the particles along the magnetic field (b). The small-angle peaks corresponding to the periodicity of the layers can now be seen, even up to the third order. The broad peaks originate from the liquidlike interactions within the smectic layers. They are now less spread out in the azimuthal direction than in the very small field of 3 mT, indicating alignment with the field. At a field strength of 0.5 T the smectic phase starts to transform into a columnar phase with a distorted hexagonal structure (c, structure like Figure 5.1 C), as was earlier observed for a nematic phase in a magnetic field [31]. At a small angle there are smectic peaks that are oriented in multiple directions indicating that this is not an equilibrium structure yet. At the highest field strength of 1.5 T the columnar structure is nicely ordered (d), second order peaks can be observed (even third order peaks were observed with a very small intensity). Higher order peaks are mainly observed in the direction of the field. This is because the structure is formed in all perpendicular directions. The off-axis diffraction spots are actually cross sections through scattering rings around the field direction. The peaks at a small angle suggest that there are still remnants of the smectic phase present, now oriented with its layer normal perpendicular to the field.

More about the behavior of the smectic *A* phase in a magnetic field can be found in Chapter 6.

5.3.3. Columnar phase

No pure columnar phase was found in this system, so the columnar phase was studied together with the smectic phase. The behavior in a magnetic field of those two phases together can be seen in Figure 5.5. The powderlike scattering rings are typical for a columnar phase (Figure 5.1 C) with a lot of differently oriented domains. The much broader liquidlike peak of the smectic phase lies in between the columnar rings. Hardly any change of the diffraction pattern was observed in a small magnetic field. At 0.5 T (b) it can be seen that the long axis of the particles is mainly oriented perpendicular to the field. The domains tend to orient in the field but still some of the powderlike peaks can be observed and at a small angle the smectic peaks are in some intermediate state. At 1.5 T (c) the structure is more ordered but it is clear that it is not as nice as the columnar structure developed from the smectic phase discussed before (see Figure 5.4d). It seems that this part of the sample, which is almost at the bottom of the capillary, cannot rearrange that easily. It is probably more restricted because of the higher osmotic pressure.

5.4. Conclusions

Goethite liquid crystalline phases show interesting behavior in a magnetic field. The nematic phase aligns parallel to the field at a low field strength and perpendicular to a large magnetic field, with the shortest axis of the particles mainly oriented along the

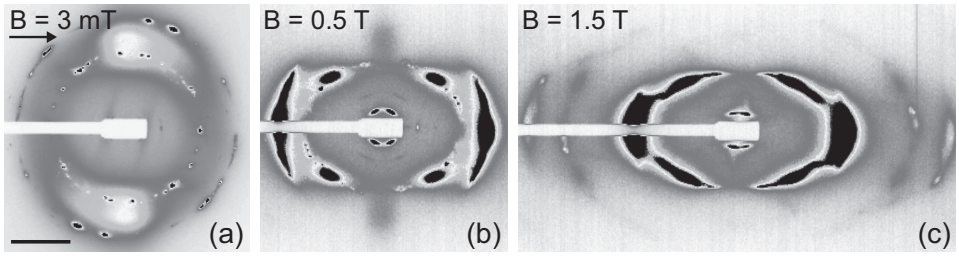

Figure 5.5. Combined columnar and smectic phase of goethite in a magnetic field. The scale bar is 0.05 nm^{-1}.

field. The smectic phase also aligns parallel to a small magnetic field but it forms a columnar phase with a distorted hexagonal structure in a higher magnetic field. The behavior of the columnar phase could only be studied together with a smectic phase. This combination has also the tendency to form an oriented columnar phase in a magnetic field but it reacts more slowly, probably because the particles seem to be more restricted at a higher osmotic pressure.

Acknowledgements

Pierre Panine and the staff of the ID2 beamline at ESRF are acknowledged for giving the opportunity to measure at their beamline and for their excellent support.

6

Behavior of the smectic A phase in a magnetic field

Abstract

The behavior of the smectic A phase in a magnetic field has been studied using small-angle X-ray scattering. It was found that in systems with a high polydispersity the smectic phase aligns parallel to a small field and it transforms into a columnar phase in high fields. In these systems a columnar phase is already present at higher concentrations without field. It apparently becomes more stable in a large magnetic field, when the particles orient perpendicular to the field. In systems with a low polydispersity the smectic phase aligns along a small magnetic field as well, but in high fields it reorients perpendicular to the field. The results suggest that the reorientation process follows a rather complex pathway. The particle orientation and the orientation of the layers seem to be able to decouple leading to smectic C-type deviations. No columnar phase is found in these systems without field nor does it form in a magnetic field.

6.1. Introduction

Goethite particles show a rich liquid crystalline phase behavior, which depends on the dimensions and polydispersity of the particles (Chapter 2) [33, 34, 108]. These particle properties can be tuned by varying the exact synthesis conditions [34]. For systems with a low polydispersity a nematic and smectic A phase have been observed. Systems with a high polydispersity also show nematic and smectic A phases, and even a columnar phase going down in the sample. A smectic phase is not expected to form if particles have a high polydispersity, but because of sedimentation and fractionation a smectic phase can form in which the polydispersity is much lower than that of the total system [108]. The columnar phase seems to act as a "waste disposal" for the particles whose length does not fit into the smectic layers. In a dispersion with specific particle dimensions ($L/W \simeq W/T$ with L, W and T the length, width and thickness) even a biaxial nematic and biaxial smectic A phase were found (Chapter 3) [103, 125].

It was shown before that all these phases can be manipulated by applying an external magnetic field [28–34, 107]. For example, a magnetic-field-induced nematic-to-columnar phase transition has been observed [31, 32] and a transition from one type of columnar phase (simple rectangular) to another (centered rectangular) (Chapter 10) [126]. In this work we focus on the behavior of the smectic A phase in a magnetic field in systems with different polydispersities. Earlier studies on thermotropic liquid crystals have shown a complex reorientation behavior of the smectic A phase in a magnetic field that depends on several factors, like the temperature or surface treatment [127–130].

6.2. Experimental

6.2.1. Synthesis

The synthesis of systems g17 and g35 is discussed in Section 2.2.1. g14 was made in a similar way as g17, but now 125 mL of 25% TMAH was added to 370 mL of 0.18 M iron nitrate (Acros Organics, p.a.). The solution was aged for 5 days at 85 °C.

Particle characterization by TEM is described in Section 2.2.2.

6.2.2. SAXS experiments

Sample preparation is discussed in Section 2.2.3. The g14 samples were flame sealed instead of using glue and were made in August 2008. The samples had a volume fraction of 13.5% (g14), 13.6% (g17) and 12.4% (g35). SAXS measurements were conducted at the BM26 DUBBLE beamline of the European Synchrotron Radiation Facility (ESRF, Grenoble, France) during different measurement sessions in 2007, 2008 and 2009. The microradian resolution setup was used [57].

The variable permanent magnet described in Section 3.2.2 was used.

Table 6.1. Goethite particle dimensions.

System	$\langle L \rangle$ (nm)	σ_L (%)	$\langle W \rangle$ (nm)	σ_W (%)	$\langle T \rangle$ (nm)	$\langle L \rangle / \langle W \rangle$
g14	189	14	57	25	∼17	3.5
g17	220	17	62	29	∼23	3.5
g35	282	35	68	32	∼25	4.1

6.2.3. X-ray microscopy

X-ray microscopy [131] experiments were performed at the ID06 beamline of the ESRF. The X-rays were generated with an undulator with a source size of about 20 μm. The distance from the source to the sample was 56m and an energy of 12 keV was selected with a double crystal monochromator using Si (111) crystals. Two sets of compound refractive lenses (CRLs) [132–134] were used as a condenser and an objective in the microscopy setup. The condenser consisted of 19 Be CRLs with a diameter of 200 μm and it was placed at a distance of 54.3 m from the source; the objective of 50 Be CRLs with a diameter of 50 μm was placed at a distance of 56.2 m from the source. The sample was placed two meters after the condenser and the magnification of the setup was around 22. A CCD detector with a pixel size of about 0.65 μm^2 was used to record the images.

6.3. Results and discussion

The particle dimensions of the systems described in this chapter are shown in Table 6.1.

6.3.1. Smectic A to columnar phase transition in systems with a high polydispersity

In samples with a high polydispersity not only a smectic A phase but also a columnar phase was observed below the nematic and isotropic phase, as was explained before (Chapter 2) [33, 108]. In such a system (g35, see Table 6.1), we studied the behavior of the smectic A phase in a magnetic field (also described in Chapter 5).

In a small field of 60 mT, the smectic A phase aligned with the particles along the magnetic field (Figure 6.1a). This phase is characterized by the very sharp and intense scattering at small angles. These sharp peaks originate from the layerlike ordering. Perpendicular to these and at a larger angle a broad scattering peak is observed from the liquidlike interactions between the particles within the smectic layers. In this case the alignment was well developed because the sample had been in a magnetic field for about 4 hours. Here, we were able to observe peaks, originating from the smectic periodicity, up to the fifth order. The periodicity is 390 nm, which is large compared to the average length of the particles (282 nm). This difference can be explained by

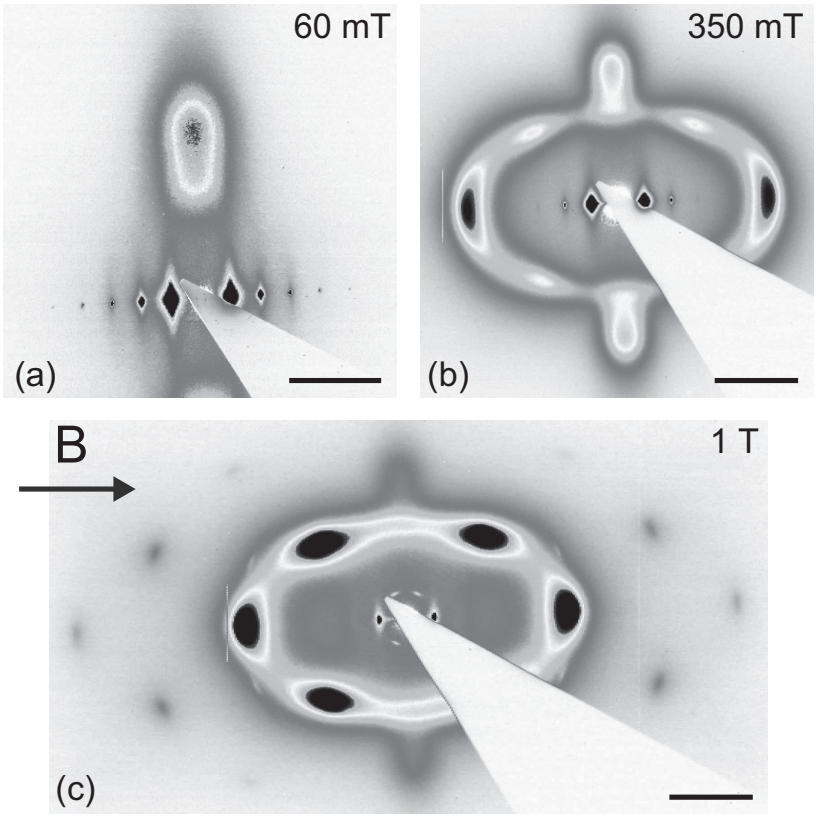

Figure 6.1. SAXS patterns of the smectic phase of g35 in a magnetic field of: (a) 60 mT, (b) 350 mT, (c) 1 T. The scale bar is 0.05 nm^{-1}.

sedimentation and fractionation and the fact that in a polydisperse system the smectic period is determined by the larger particles [33, 108].

At a field strength of 350 mT, when it is expected that the particles rotate from parallel to perpendicular to the field, peaks appeared at large angles that do not correspond to the smectic phase (Figure 6.1b). The smectic phase started to transform into a columnar phase with a centered rectangular structure, as was observed before for the nematic phase in a magnetic field [31]. The smectic phase, which is still partly present, was not rotated yet as can be seen from the small-angle peaks.

The columnar structure becomes nicely ordered in a field of 1 T (Figure 6.1c). Higher order peaks can be observed mainly in the direction of the field. This is because the structure is formed in all directions perpendicular to the field and the diffraction spots are cross sections through scattering rings around the field direction. The less intense peaks at a small angle suggest that there are still remnants of the smectic phase present

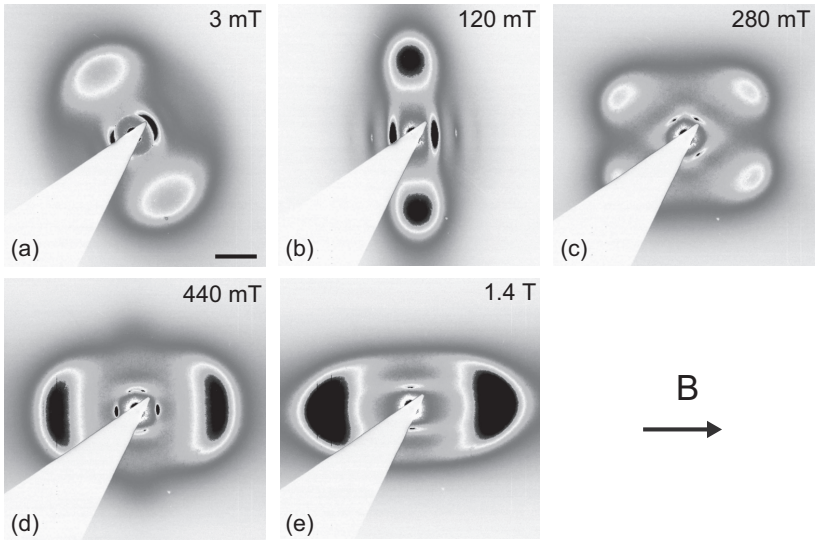

Figure 6.2. SAXS patterns of the smectic phase of g17 in a magnetic field of (a) 3 mT, (b) 120 mT, (c) 280 mT, (d) 440 mT, (e) 1.4 T. The scale bar is 0.05 nm^{-1}.

that now have different orientations. After removal of the field the system goes back to the smectic phase.

A cause of the increased stability of the columnar compared to the smectic A phase in a magnetic field, above the critical field, can be the induced orientation of the particles. In the columnar phase the particles already have a specific orientation of the short axes of the particles as is indicated by the centered columnar structure; in the smectic phase the particles are free to rotate along the long axis. When a large magnetic field is applied the particles will align with their shortest axis along the field. This decreases the orientational entropy in the smectic phase but not in the columnar phase; there it was already lower.

6.3.2. Reorientation of the smectic A phase in systems with a low polydispersity

As was shown earlier (Chapter 2) [34, 108], in a system with a low polydispersity (g17) a smectic A phase was found without the presence of a columnar phase. The SAXS pattern of this smectic phase, in a very small magnetic field of 3 mT, is shown in Figure 6.2a. 3 mT was used because that is the minimum magnetic field that could be reached with the magnetic poles at their maximum distance. The periodicity of the smectic phase is around 250 nm, which is now close to the average particle length of 220 nm.

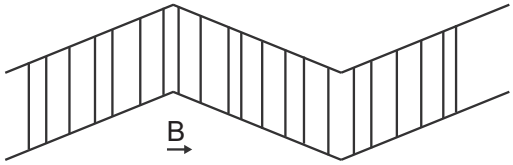

Figure 6.3. Schematic picture of the zig-zag undulations in the smectic phase.

When a magnetic field of 120 mT was applied, the smectic phase aligned with the particles along the field direction (Figure 6.2b), as for the highly polydisperse system (Figure 6.1a). The peaks at a small angle became more intense and more localized at one position. The second order peaks can now be clearly seen and when looking carefully even the third order peaks could be observed. At a magnetic field of 280 mT, which is around the critical field strength where the particles rotate from parallel to perpendicular to the field, two (intermediate) orientations of the smectic phase were observed at the same angle to the field (Figure 6.2c). At 440 mT the particles rotated further, in the direction perpendicular to the field, as can be seen from the scattering pattern (Figure 6.2d). The peaks at a larger scattering angle merged into one broad peak in the horizontal direction. In contrast, the smaller angle peaks were not yet perpendicular to the field, although they were already closer to the vertical in comparison to panel (c). Such a pattern can occur if the particles themselves are pretty well aligned but the layers still show many undulations, probably with smectic C type domains. A schematic picture is given in Figure 6.3.

Furthermore, sharp peaks at a small angle reappeared at the original – horizontal – position, where they were observed in a small magnetic field. Although these peaks are rather intense, the corresponding wide-angle broad peaks in the vertical direction were not clearly observed for this part of the smectic phase. This is because the observed scattering peaks are actually cross sections through scattering rings around the field direction and the intensity is spread over this ring. For the same reason, the small-angle peaks in the direction orthogonal to the field have a smaller intensity compared to the ones that are along the field.

Apparently, at 440 mT, the smectic phase partly aligned along the magnetic field again, while most of it was already aligning perpendicular to the field. This type of behavior was also observed with X-ray microscopy, which showed parallel domains together with perpendicular domains with many undulations (Figure 6.4a) [135]. These pictures were taken from another system (g35) but the scattering pattern (Figure 6.4b) is similar (ignoring the columnar part), so it probably gives a good illustration. The Fourier transform (Figure 6.4c) of the microscopy picture corresponds well to the actual scattering pattern.

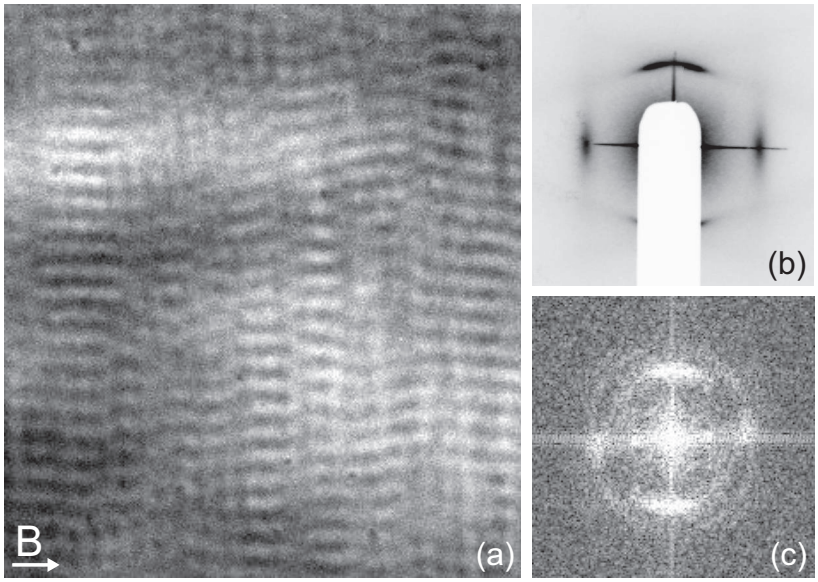

Figure 6.4. (a) X-ray microscopy picture of the smectic phase of g35 in a magnetic field of 400 mT, with (b) the corresponding scattering pattern and (c) the Fourier transform of the microscopy picture.

At the highest applied field of 1.4 T the smectic phase was fully aligned perpendicular to the field and it seems to be completely smectic A again (Figure 6.2e).

6.3.3. Reorientation behavior

To have a closer look at the reorientation behavior around the critical field strength, a sample of the g14 system was studied over time in a field of 280 mT. The SAXS pattern of the smectic phase, immediately after applying a field of 280 mT, but after a stepwise increase of the field from 0 to 280 mT within about half an hour, is shown in Figure 6.5a. This pattern is similar to the one shown in Figure 6.2c, although in this case the small-angle peaks are already closer to the vertical position, while the wide-angle peaks are at a comparable angle as the previous sample. Here, the small- and wide-angle peaks are not perpendicular to each other which indicates that the particles are not oriented exactly perpendicular to the layer periodicity. It implies the presence of smectic C type domains.

This behavior is sometimes observed during rotation in these kind of samples, probably depending on the exact measurement pathway. It suggests that the layers themselves actually rotate faster than the particles within the layers, which is counterintuitive. Another explanation for the discrepancy between the small- and wide-angle peaks might be that they correspond to different domains. The observed peaks are from cuts through

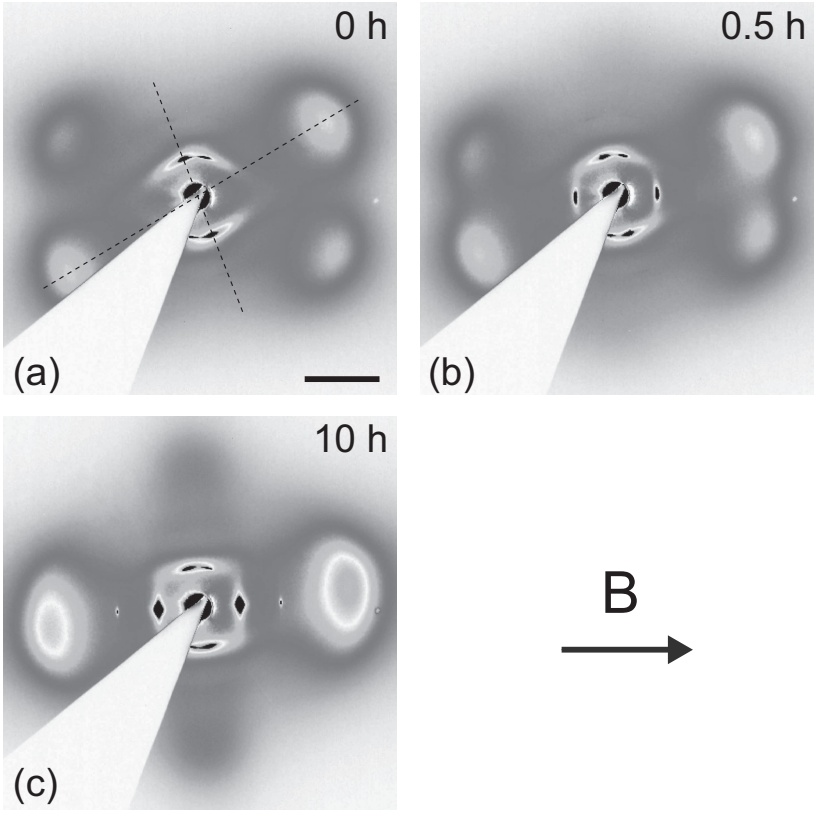

Figure 6.5. SAXS patterns of the smectic phase of g14 in a magnetic field of 280 mT: (a) t = 0, (b) t = 0.5 h, (c) t = 10 h. The scale bar is 0.05 nm^{-1}.

the Ewald sphere and it is easy to miss the sharp smectic peaks. If there is a distribution of domain orientations it is possible that the observed small-angle peaks belong to another domain than the observed wide-angle peaks.

Because of multiple observations of these non-perpendicular small- and wide-angle peaks, it can also have an origin in the reorientation behavior. The exact cause may depend on the pathway of the transformation. For example, the smectic phase might split up in many small domains. Particle reorientation is a collective effect of these domains which is a slow process compared to the translations that the individual particles can perform within the domain. A kinetic decoupling of the particle and layer reorientation will then take place. The smectic structure can reappear before the full rotation is complete. The director of the particles could then be not exactly parallel to the layer normal, thus kinetically forming smectic C like domains.

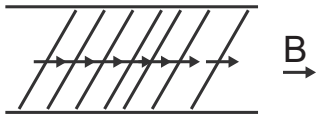

Figure 6.6. Schematic picture of the possible influence of dipole-dipole interactions during the reorientation process.

Dipole-dipole interactions between the particles could be a possible cause for the preferred particle and layer orientations. At this field strength the effective magnetic-field-induced dipole will not be exactly along the shortest particle axis but will have a certain angle to that. Therefore, particles prefer to be at an angle to the magnetic field. It is then easy to shift the particles a little to arrange the particles in a more favorable orientation with respect to each other so that they have a stronger dipole-dipole interaction (Figure 6.6). The layer normal will then be at a smaller angle to the field than the particle director. In this way smectic C like domains are formed and it will take more time to rotate the particles further to go to the thermodynamically preferred smectic A phase.

After about half an hour the wide-angle peaks have rotated further which means that the particles are moving toward an alignment perpendicular to the field and the structure is now going to a smectic A phase again. Besides that, it can be seen that small-angle peaks reappear at the position where they were in a smaller field, when the particles were all aligned parallel to the field (Figure 6.5b). Apparently, after the initial rotation, domains with an orientation parallel to the field formed again. After 10 hours it was seen that the parallel alignment even became stronger, showing second order peaks (Figure 6.5c). The more perpendicularly oriented domains also became better aligned, indicated by the broad peaks that are at the horizontal position now. So, in the end there are two types of domains, one with its particles parallel and the other one with its particles perpendicular to the field which has smectic C type undulations as in Figure 6.3.

A possible explanation is that the smectic phase first rotates as domains following the average of the orientations favored by the particles. However, because of polydispersity in particle size and magnetic properties of the particles, they will not all show the same behavior in a field. After a certain time particles that intrinsically prefer another orientation, in this case parallel to the magnetic field, can separate and form new domains. The parallel domains will get better aligned in time, while in other domains the particles go to the perpendicular orientation. In this way two domains form with

orthogonal orientations, which is more favorable than having all kinds of intermediate orientations (*cf.* nematic-nematic phase separation in Chapter 7). The q-values of the small-angle smectic peaks of the perpendicular domains are slightly (2%) smaller than that of the parallel domains which can be an indication that the larger particles prefer the perpendicular orientation. Also in molecular systems reorientation of the smectic A phase can follow complicated behavior [129]. Compared to that work we have some extra information because we can also observe the liquidlike peak which is still at a reasonably small angle.

6.4. Conclusions

The behavior of the smectic A phase of goethite in a magnetic field was found to depend on the properties of the system. In systems with a high polydispersity a columnar phase is present below the smectic A, nematic and isotropic phase. The smectic phase in these systems aligns parallel to a small magnetic field, but it transforms into a columnar phase in high fields. It seems that the columnar phase becomes more stable in high fields.

In systems with a low polydispersity a smectic A phase is present together with a nematic and isotropic phase, but without columnar phase. The smectic phase in these systems aligns parallel to a small magnetic field but perpendicular to a large magnetic field. This reflects the behavior of single particles, although the exact reorientation process is complicated and not fully understood yet. It seems that domains with different orientations form and that smectic C type undulations are present during the process. The particles appear to orient more or less collectively in domains after which a splitting occurs between domains with particles parallel and perpendicular to the field. Finally, all particles will align perpendicular at a large magnetic field.

Acknowledgements

Dmytro Byelov and the staff of the BM26 DUBBLE beamline at the ESRF are thanked for their support during SAXS measurements. Dmytro Byelov is also thanked for X-ray microscopy measurements, together with Anatoly Snigirev.

7

Magnetic-field-induced nematic-nematic phase separation

Abstract

We found, using polarization microscopy and small-angle X-ray scattering, that for goethite a low polydispersity suffices to form two separate nematic phases, while previous theory showed that this is only possible for mixtures of particles with extremely different lengths or diameters. Applying a critical magnetic field, which induces some of the goethite nanorods to rotate, leads to sufficient excluded volume between the particles to cause macroscopic phase separation between two orthogonal nematic phases. The larger the polydispersity of the system, the broader the range of field strengths where nematic-nematic phase separation occurs. This is a new phase separation mechanism which is expected to lead to interesting interfacial phenomena.

7.1. Introduction and theory

Sixty years ago, Onsager published his seminal paper on the first purely entropy-driven phase transition [20]. He described the transition from the disordered isotropic (I) phase to the orientationally ordered nematic (N) phase in terms of the excluded volumes between anisometric particles. Another, much more rare, effect is N-N phase separation in systems with extremely different lengths or diameters where to leading order the excluded volume does not play a role [136–145].

Onsager formulated a simple virial expansion of the free energy for dispersions of both rodlike and platelike particles. The expansion can be truncated after the second virial term for infinitely thin, hard rods. The free energy F per particle, in units of the thermal energy kT, is then given by [20, 146]

$$\frac{\Delta F}{NkT} \simeq constant + \langle \ln(\rho f) \rangle + \frac{1}{2}\rho \langle\langle v_{\text{excl}} \rangle\rangle \tag{7.1}$$

where $\rho \equiv N/V$ is the number density of rods and $\langle \ln(\rho f) \rangle$ is a combination of the ideal translational and orientational entropy. Each pair of triangular brackets denotes an average in terms of the relevant particle angles described by orientational distribution function f. The packing entropy is proportional to the excluded volume (v_{excl}), asymptotically given by

$$v_{\text{excl}} \sim 2DL^2 |\sin\gamma| \tag{7.2}$$

with γ the angle between two thin rods of diameter D and length L. The I-N phase transition is explained as a shifting balance between the orientational and packing entropy (Figure 7.1). At a certain concentration the gain in packing entropy will exceed the loss in orientational entropy and the system undergoes an I-N transition. Remarkably, within the nematic phase the average excluded volume between particles is found to be

$$\langle\langle v_{\text{excl}} \rangle\rangle \sim 4/\rho. \tag{7.3}$$

At higher concentrations the particles spontaneously align more strongly, thus reducing the excluded volume so that the last term in Equation (7.1) remains constant.

Comparing these theoretical results with experiments, polydispersity is an important factor. Interestingly, equations 7.1 and 7.3 remain valid if the triangular brackets now also include (number-)averaging over the different particle dimensions and the excluded volume is generalized to include different lengths and diameters [147]. The first numerical results on bidisperse systems were presented by Lekkerkerker *et al.* showing strong fractionation effects and widening of the biphasic I-N gap [42].

Another remarkable effect found in bidisperse systems is the occurrence of N-N phase separation [136–145]. To better understand this phenomenon an analytical theory was used [138–140]. Surprisingly, the excluded volume does not play a role here – since the last term of Equation (7.1) remains constant within the nematic phase – instead the

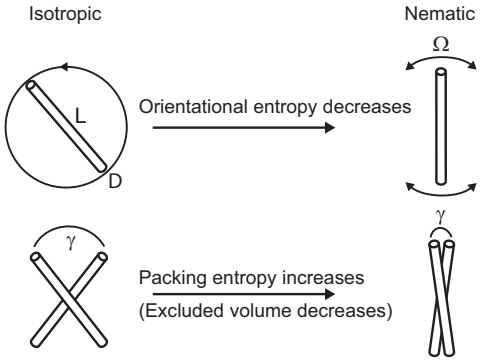

Figure 7.1. Isotropic to nematic phase transition.

phenomenon involves the balance between the orientational entropy and the entropy of mixing. The long particles induce a too strong alignment of the short particles, whose orientational entropy favors demixing. Typically, a large length ratio of at least 3.2 or diameter ratio of 4.3 is needed to get N-N phase separation [142]. Later, it was shown that N-N phase separation can also be obtained in a polydisperse system [45–47] and for more realistic L/D ratios [143–145]. Experimentally, this effect has been observed in bidisperse [148], bimodal [149] and polydisperse systems [16].

The I-N phase transition in a magnetic field has been studied before [32, 150, 151]. In this work, the nematic phase itself is studied in a magnetic field. We use repulsive goethite particles, which are boardlike (in between rod- and platelike). When dispersed in water their surface charge leads to somewhat larger effective particle dimensions. More concentrated goethite dispersions readily show nematic, smectic and columnar phases [28, 31, 33]. The magnetic properties of these particles are very intriguing [28]. They have a permanent magnetic moment $\vec{\mu}$ along their longest axis L, presumably because of uncompensated surface spins within their anti-ferromagnetic crystal structure. In contrast, the magnetic easy axis of magnetic susceptibility tensor $\overleftrightarrow{\chi}$ lies along the shortest particle dimension T. Therefore, the particles align parallel to a weak and perpendicular to a stronger magnetic field.

The magnetic energy (E_m) per particle in a magnetic field $\vec{B}$ is given by [29]

$$E_\mathrm{m} = -\vec{\mu} \cdot \vec{B} - \frac{V}{2\mu_0} \vec{B} \cdot \overleftrightarrow{\chi} \cdot \vec{B} \tag{7.4}$$

with V the particle volume. In dilute systems this gives a Boltzmann distribution with E_m in the exponent [29], so that an orientational distribution function can be externally imposed. Near the I-N phase boundary the magnetic energy (Equation (7.4)) should be added (in units of kT) to the free energy (Equation (7.1)) [152].

7.2. Experimental

7.2.1. Synthesis

The synthesis of the g55 system is described in Section 2.2.1, that of the g14 system is similar to the g17 synthesis mentioned in the same section. It was done on a 5 times larger scale and aging took place for 5 days at 85 °C.

The g29 system was obtained in a similar way as the g55 but some changes were made, the exact synthesis is described below. 800 mL of a 0.1 M $Fe(NO_3)_3$ solution (Acros, p.a.) was mixed with 1 M NaOH (Merck, p.a.), while stirring, until pH 11 was reached. As the NaOH was added to the $Fe(NO_3)_3$ solution, a dark-brown precipitate formed. The mixture was then centrifuged for 30 min (Beckman Coulter Avanti J-20XP, rotor JLA-8.1000, 6000g), the supernatant was removed and the particles were redispersed in 800 mL millipore (mp) water. 1 M NaOH was added to bring the solution at pH 12 and the suspension was put into the oven, for a day, at 70 °C. The solution was taken out from the oven and the supernatant was removed. The particles were redispersed in 750 mL mp water and centrifuged at 6000g for 30 min. The centrifuging procedure was followed twice. After the last centrifugation step, the particles were redispersed in 250 ml of 3 M HNO_3 (Merck, 65%). The solution was centrifuged again at 6000g for 30 min and redispersed in 750 mL mp water. The procedure was performed three times. Following the third centrifugation step, the particles were redispersed in 250 mL mp water of pH 3 (prepared with HNO_3).

Particle size distributions were determined by TEM as described in Section 2.2.2.

7.2.2. Polarization microscopy

Capillaries of $0.1 \times 2.0 \times 100$ mm and $0.05 \times 1.0 \times 100$ mm (VitroCom) were filled with goethite dispersions with volume fractions (ϕ) ranging from $7 - 13\%$ and flame sealed at both ends. They were kept in a vertical position to establish a sedimentation equilibrium profile. *I-N* phase separation was observed within a day after preparation.

Phase separated samples were studied in a magnetic field using polarized light microscopy. A Bruker BE25v electromagnet with large flat poles was used to produce a homogeneous magnetic field. On one side of the magnet there was a light source and a polarizer and on the other side a microscope (head of a Zeiss Axiolab microscope) with an analyzer and a 10× objective (Edmund Optics HR), connected to a CCD camera (QImaging MicroPublisher 5.0 RTV). The microscope was rotated 90° to be able to study the sample in a vertical position and observe gravity effects.

Birefringence measurements were performed at the "Laboratoire de Physique des Solides" in Orsay, France. Birefringence values were obtained using an optical compensator. A small variable permanent magnet was attached to the microscope, which was also rotated 90°.

Capillaries of 1 mm wide are shown in the figures, unless stated otherwise.

7.2.3. SAXS

Small-angle X-ray scattering (SAXS) measurements were performed in June 2009 at the BM26 DUBBLE beamline of the European Synchrotron Radiation Facility (ESRF, Grenoble, France) [56], using the microradian resolution setup [57]. The beam size was about 0.5–1 mm. Note that there is slight asymmetry in all SAXS patterns. The intensities in the right and the bottom parts of the detector seem to be somewhat higher. Presumably, this (unphysical) effect is caused by the detector. The variable permanent magnet described in Section 3.2.2 was used. The measurements were performed on samples which had never been exposed to a magnetic field before. A simple usb polarized light microscope (dnt DigiMicro 1.3) was used to observe the samples stored within a home-made variable permanent magnet (VPM) in between the SAXS measurements.

7.3. Results and discussion

7.3.1. Polarization microscopy

We prepared vertical samples of the g29 system (Table 7.1) showing I-N phase separation (Figure 7.2a), focusing our studies on the nematic phase. Polarization microscopy was used to study its behavior in a magnetic field. Without magnetic field, the nematic phase showed domains with different orientations (Figure 7.2a). When a small magnetic field (a few mT up to 180 mT) was applied, the particles aligned parallel to the field and a homogeneous nematic phase was observed (Figure 7.2b). Increasing to the critical field strength (300 mT), where particles change their orientation from parallel to perpendicular to the field, a fine texture was formed immediately (Figure 7.2c). The fine texture consisted of small droplets of apparently different phases. The droplets readily coalesced and grew over time (Figure 7.2d). Two types of droplets formed: one kind moved upwards and the other downwards (Figure 7.2e). After about a day macroscopic phase separation was reached and an interface was formed between the two nematic phases (Figure 7.2f). Besides that, a rise of the level of the I-N interface was observed, which will be discussed in the next chapter. A schematic picture of the changes in phase behavior going from 0 to 300 mT is shown in Figure 7.3. Interestingly, previous measurements seem to indicate an alternative escape mechanism where a striped pattern of different domains of a single phase at oblique angles to the magnetic field is being formed [30].

7.3.2. SAXS

To determine the nature of the different nematic phases SAXS was performed. Before applying a magnetic field, nematic domains with different orientations were observed. Immediately after applying a field of 270 mT, perpendicular to the X-ray beam, two orthogonal orientations were recognized everywhere in the nematic phase (Figure 7.4a). The sample was kept in this field for about a day and was studied with polarized light

Table 7.1. Goethite particle dimensions.

System	$\langle L \rangle$ (nm)	σ_L (%)	$\langle W \rangle$ (nm)	σ_W (%)	$\langle T \rangle$ (nm)	$\langle L \rangle / \langle W \rangle$
g55	216	55	35	48	∼16	6.2
g29	242	29	49	30	∼17	4.9
g14	189	14	57	25	∼17	3.5

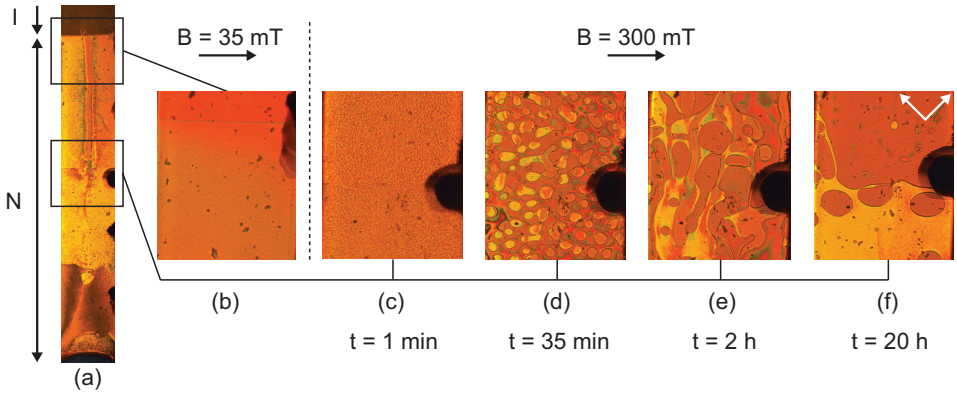

Figure 7.2. Polarized light microscopy pictures of: (a) an I-N phase separated sample (g29, $\phi = 9\%$) without magnetic field, (b) alignment in a field of 35 mT, (c) the nematic phase with a fine texture in a magnetic field of 300 mT at t = 1 min, (d) growing droplets at t = 35 min, (e) droplets moving at t = 2 h, and (f) phase separation at t = 20 h. The black areas are marks to recognize the position in the sample.

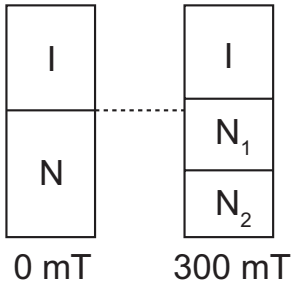

Figure 7.3. Schematic picture of the behavior of an I-N phase separated sample without field and in a field of 300 mT.

microscopy. During this day phase separation within the nematic phase was again observed (Figure 7.4b). SAXS patterns at different heights within the nematic phase are shown in Figure 7.4c-g. It can be seen that above the interface (c,d) the particles

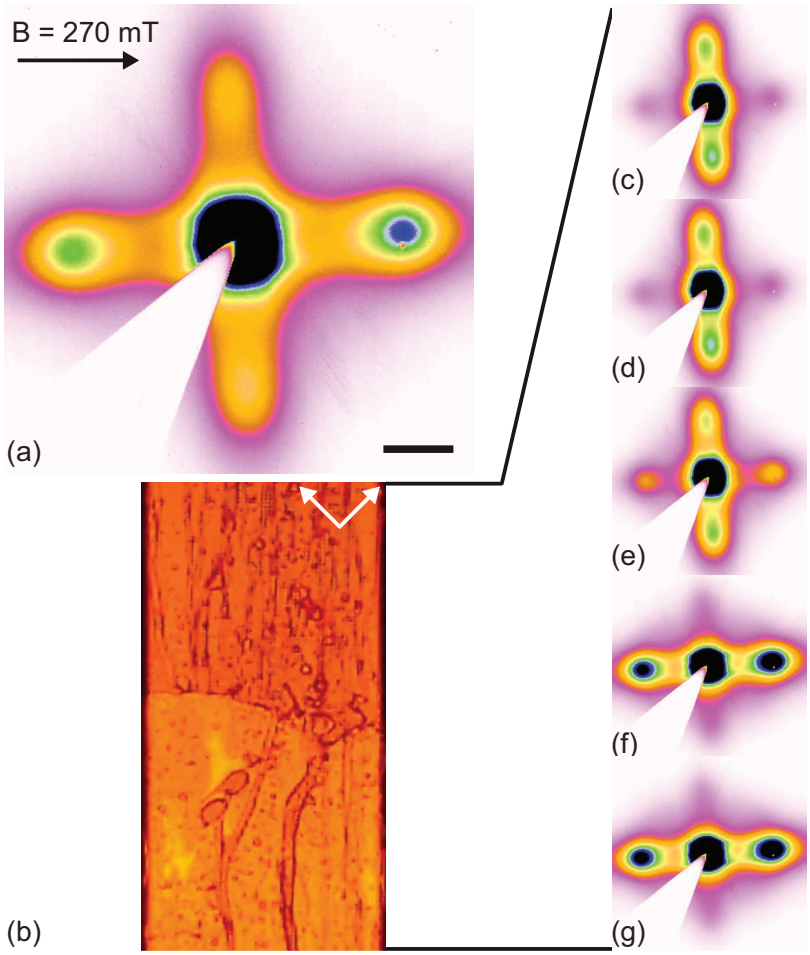

Figure 7.4. SAXS patterns of the nematic phase in a magnetic field of 270 mT, perpendicular to the X-ray beam, (a) just after applying the field and (c,d) after one day above the formed interface, (e) at the interface and (f,g) below the interface. The scale bar is 0.05 nm^{-1}. (b) The (low resolution) polarized light microscopy picture corresponding to (c-g). The width of the capillary is 2 mm (g29, $\phi = 11.5\%$).

were oriented parallel to the field; the broad peaks originate from the correlations between the smaller particle dimensions. Below the interface (f,g) the particles were aligned perpendicular to the field. At the interface (e) both particle orientations were observed, since the beam hits both nematic phases.

Subsequently, a 270 mT field was applied along the X-ray beam (Figure 7.5), thereby realigning the particles. In the upper nematic phase the particles immediately aligned

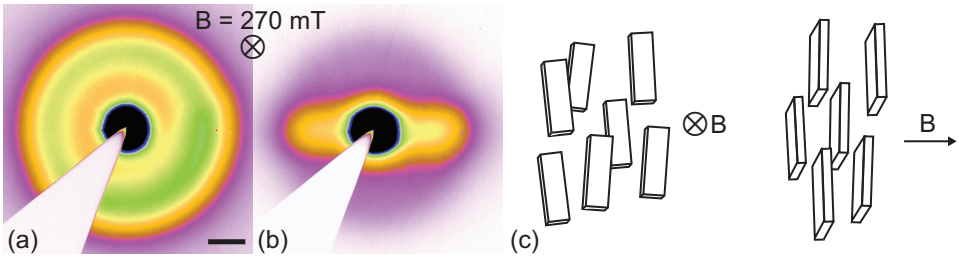

Figure 7.5. SAXS patterns of the nematic phase in a magnetic field of 270 mT, parallel to the X-ray beam, (a) after one day above the formed interface and (b) below the formed interface. The scale bar is 0.05 nm^{-1}. (c) Schematic picture of the lower nematic phase with two directions of the magnetic field.

along the new direction of the field, so one looks on top of the particles with the X-ray beam. A uniform scattering ring was obtained (Figure 7.5a) implying that this nematic phase was uniaxial. In the lower nematic phase the long axis of the particles aligned perpendicular to the field. The observed scattering peaks are due to the correlations between the two smallest particle dimensions. The scattering patterns with the field perpendicular to the beam (Figure 7.4f,g) have their peaks at a larger angle or smaller correlation distance than the pattern with the field parallel to the X-ray beam (Figure 7.5b). This implies that the smallest correlation distance is along the field direction in accordance with an easy axis of magnetization along T (for a schematic picture see Figure 7.5c). The lower phase is therefore a biaxial nematic phase.

It can be concluded that the phase separation within the initially uniform nematic phase is based on perpendicular particle orientations which are imposed by an external field. Within the critical magnetic field range, some particles already start to orient perpendicular to the field, while other particles are still aligned parallel to the field. In this way these two extreme types of particles experience a maximum excluded volume ($\gamma = 90°$, see Figure 7.1 and Equation (7.2)) and will therefore gain a lot of packing entropy by phase separating into two nematic phases with different orientations. Particles with an intermediate orientation seem to end up in either one of the two orthogonal phases. A different mechanism is causing this N-N phase separation than what was found before [16, 148, 149]; in those examples the excluded volume did not play a large role.

7.3.3. Birefringence

A closer look at the different nematic phases was taken by determining their birefringence. Without doing quantitative measurements, interference colors observed during polarization microscopy can already give valuable information about the birefringence. Bright interference colors indicate a small birefringence, a decreasing intensity of the

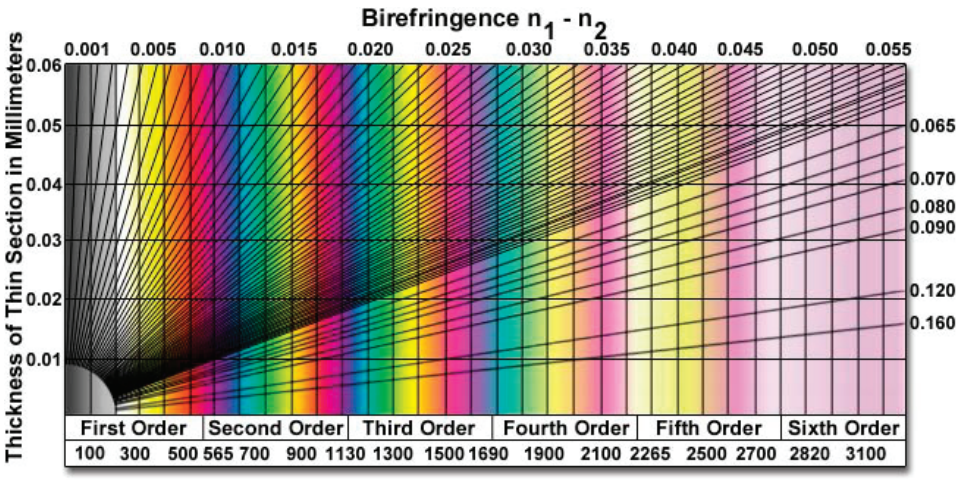

Figure 7.6. Michel-Levy birefringence chart.

color bands indicates an increasing birefringence as can be seen in Figure 7.6. Within a uniaxial nematic phase the birefringence (Δn) increases with the volume fraction (ϕ) and the nematic order parameter (S_2) according to

$$\Delta n = \Delta n_{\text{sat}} \phi S_2 \tag{7.5}$$

where Δn_{sat} is the specific birefringence (the birefringence limit when ϕ and S_2 are both 1).

In an N-N phase separated sample, the lower, biaxial nematic phase (N_b^-) has an orientation perpendicular to the field. In the configuration used here, the field was applied along the width of the capillaries (Figure 7.7). Therefore, the particles that are aligned perpendicular to the field can be aligned not only with their long axis along the wall (a), but also perpendicular to the wall ((b), homeotropic) and all orientations in between. This is different from the upper nematic phase (N^+) which is aligned along the field and therefore the particles will always have their long axis along the capillary wall.

In Equation (7.5), S_2 can be used for the parallel, uniaxial nematic phase because the two smaller dimensions of the particles have no preferred orientation. For the perpendicular, biaxial nematic phase the situation is more complicated and S_2 is not the correct order parameter to use. Furthermore, there are two different Δn's involved here. The extreme cases that might occur in the situation of alignment perpendicular to the field can be seen in Figure 7.7. If the particles are aligned along the wall of the capillary (a) the difference in refraction along the length and thickness is important and a different order parameter should be used here. However, around the critical field

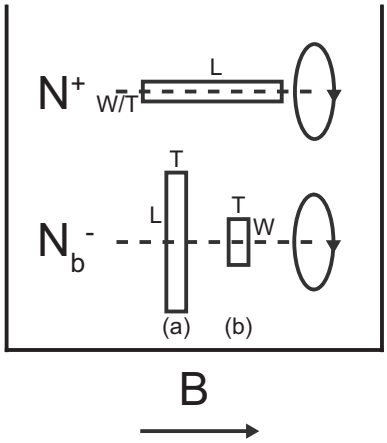

Figure 7.7. Schematic picture of the possible particle orientations in an N-N phase separated sample.

strength, where the measurements in this chapter are done, the biaxial order is still small and the situation is probably close to the uniaxial nematic phase.

The particles can also be homeotropically aligned (Figure 7.7b), then the orientation of the width and thickness is important. Clearly, another order parameter and Δn_{sat} will be important here. If a complete alignment along the long axis is assumed, the birefringence can be given as

$$\Delta n = \Delta n_{\mathrm{sat}} \phi \langle \cos 2\varphi \rangle \tag{7.6}$$

with φ the azimuthal angle describing the particle orientation in the plane perpendicular to the nematic director. In this case, Δn_{sat} is defined by the index of refraction along the width and thickness of the particles, while for the uniaxial case (Equation (7.5)) all three refractive indices specify Δn_{sat}.

If the order is high, a significant birefringence is expected for the situation in Figure 7.7b. However, around the critical field strength the biaxiality is not well developed yet and there will be a low order causing a small birefringence. This has been observed before using homeotropic samples for birefringence measurements in a magnetic field [30]. A small negative birefringence (-0.002) was observed around the critical field strength and it increased by increasing the field. In a field of 1 T it was still lower than that of a uniaxial nematic phase which was aligned parallel to a small field (-0.02 compared to 0.06).

An example of the lower part of an N-N phase separated sample, in a field of 250 mT, can be seen in Figure 7.8. The upper, parallel, nematic phase did not show interference colors; it had a good alignment along the field. The lower, perpendicular and biaxial, nematic phase showed intense interference colors indicating a small birefringence. After

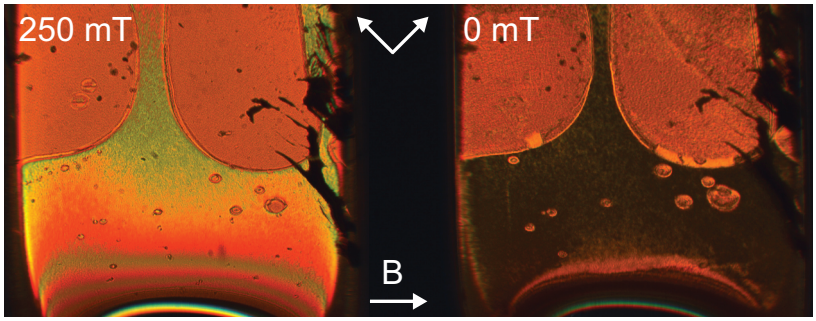

Figure 7.8. Polarization microscopy pictures of an N-N phase separated sample (g29, $\phi = 9\%$) in a field of 250 mT and immediately after switching off the field.

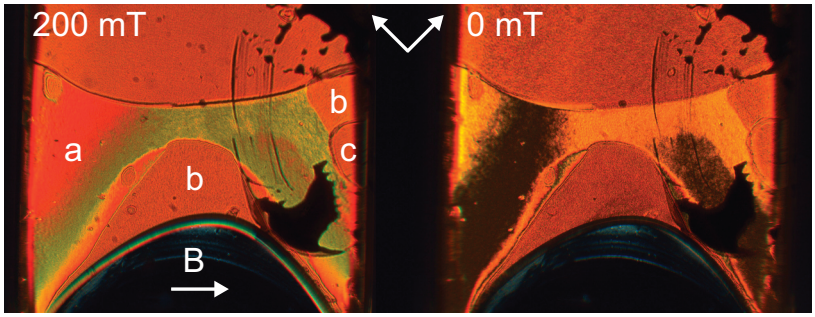

Figure 7.9. Polarization microscopy pictures of an N-N phase separated sample (g29, $\phi = 9\%$) in a field of 200 mT and immediately after switching off the field.

switching off the field, this part of the nematic was observed as a dark region. This suggests that the particles had a homeotropic alignment, which indeed gives a smaller birefringence than alignment along the wall.

In another sample, measured in a field of 200 mT, different regions were observed within the lower, perpendicular nematic phase (Figure 7.9). In region a again interference colors were observed; this region became partly black after the field was switched off and it partly showed some yellow color. This region apparently has particle orientations perpendicular to the wall or at least close to that. Regions b did not show interference colors and seemed to be similar to the upper nematic phase. However, it was clearly different from that concluding from the much smoother interface between b and a than between a or b and the upper nematic phase. So, regions b probably had an orientation perpendicular to the field, but with the long axis along the capillary wall. Region c was still a droplet of the parallel nematic phase as could be seen from the more pronounced interface around this region.

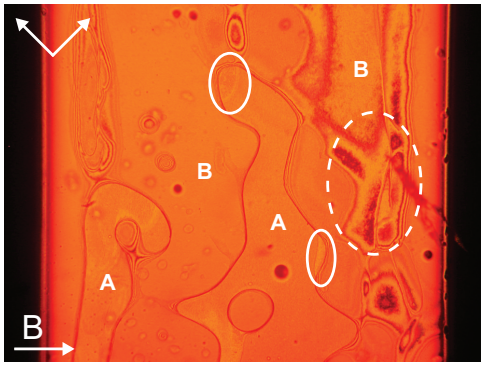

Figure 7.10. Polarization microscopy picture of an N-N phase separated sample (g29, $\phi = 10\%$).

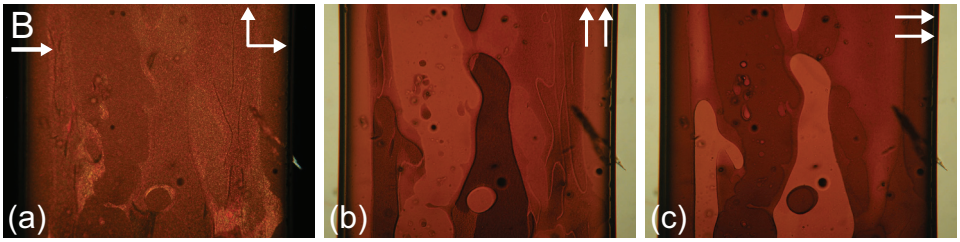

Figure 7.11. Polarization microscopy pictures of an N-N phase separated sample with different orientations of the polarizers.

It was expected that the capillary walls would have an influence on the particle orientation, preferring the particles to be aligned with their long axis along the wall. Apparently, the influence is not that large because large regions with other orientations were observed.

For a more detailed analysis of the birefringence, a 50 μm thick capillary with an I-N phase separated sample was studied in a field of about 270 mT (perpendicular to the optical axis). N-N phase separation occurred and the sample was left standing over night (Figure 7.10). The parallel and perpendicular orientations of the different regions were confirmed using an optical compensator. In this case, the particles mostly had an orientation parallel to the wall. Within the perpendicular area (A) there were some regions (e.g. inside the solid ellipses) that showed interference colors (not very clear in the picture), indicating a smaller birefringence. These are areas where the particle orientation was tilted compared to the orientation along the wall.

Within the parallel area (B) also some regions were observed that showed interference colors and had a smaller birefringence (e.g. inside the dashed ellipse). So, also here there were some regions with a tilt compared to the perfect alignment. This was not

expected because, in this configuration, parallel to the field would always be parallel to the wall as well. It seems that if a droplet with the perpendicular orientation passes a parallel area it leaves a flow-induced trace where the particles are tilted away from the ideal alignment. It was seen that this area was slowly getting better aligned in time and finally got homogeneous.

The birefringence was measured in areas A and B and the obtained values of -0.08 and 0.1 respectively were a bit higher than the measurements of Lemaire *et al.* who found a value of 0.064 for the aligned nematic phase [29]. This can partly be ascribed to the slightly higher volume fraction of the nematic phase in our sample (about 11% compared to 8.5%). Furthermore, it has to be mentioned that there can be a pretty large error in the values because of the thickness of the capillaries; 50 μm seems to be still too thick. Important factors playing a role here are absorption, scattering and dichroism. The values measured seemed to be overestimations of the real values. In the solid and dashed ellipses the measured birefringence was -0.03 and 0.03 respectively, which is clearly smaller than that of the more homogeneous part of these regions. This indicates an orientation away from parallel to the wall in the solid ellipses and a distortion of the alignment in the dashed ellipse.

The same sample was also studied with different orientations of the polarizers. With the polarizer and analyzer vertical and horizontal respectively, the full capillary became dark as is expected if the particles are aligned in the vertical and horizontal direction (Figure 7.11a). The interface between different regions and the area with more defects were still visible, because there were some intermediate orientations present. Furthermore, it was noticed that the contrast with parallel polarizers was actually very good. The parallel region became bright with vertical polarizers (Figure 7.11b) and the perpendicular region with horizontal polarizers (Figure 7.11c). This indicates a clear difference in absorption along the different particle axes, i.e. dichroism.

7.3.4. Effect of polydispersity

In calculations for monodisperse particles field-induced N-N phase separation could not be identified [152, 153], so polydispersity might play an important role in the process. First of all, larger particles tend to align perpendicular at a lower field strength compared to smaller particles, since the permanent and induced moments depend on the particle size in a different manner. Furthermore, a polydispersity in the permanent magnetic moment is even expected for monodisperse particles, because the number of uncompensated surface spins within the antiferromagnetic structure is not necessarily the same for every particle.

To determine the effect of polydispersity on N-N phase separation, systems with different size polydispersities have been studied. The particle dimensions of the systems

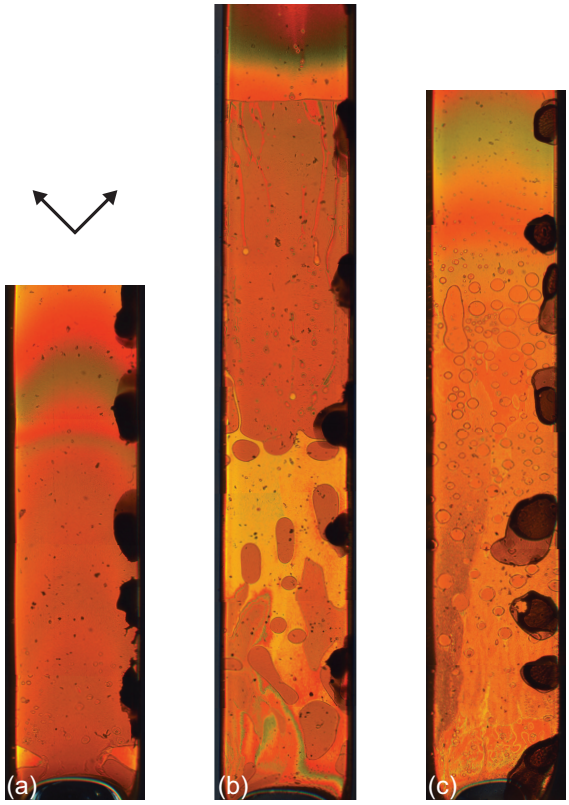

Figure 7.12. Polarization microscopy pictures of N-N phase separated samples of the g29 system at a) 185 mT, b) 300 mT and c) 500 mT (ϕ = 9.5%, 9% and 10% respectively). The width of the capillaries is 1 mm.

studied can be found in Table 7.1. The behavior of the nematic phase of these systems was studied within a range of field strengths using polarized light microscopy.

For the g29 system, the first signs of phase separation were observed at a field strength of 185 mT, as can be seen from the small areas of a different phase at the bottom of the capillary in Figure 7.12a. In the first stage of the phase separation process droplets started to form at the bottom of the capillary. This is already an indication that the larger particles rotate at this small field, because larger particles will be mainly present at the bottom of the capillary due to sedimentation.

The larger the field, the larger the lower phase with the orientation of the particles perpendicular to the field, as can be observed in Figure 7.12b and c. At 300 mT (b) almost half of the nematic phase has the perpendicular orientation and at 500 mT there are only some droplets with the parallel orientation left which are slowly moving

Table 7.2. Critical field measurements.

System	σ_L (%)	σ_W (%)	B_c (mT)	B_{limit} (mT)	$\frac{B_c - B_{limit}}{B_c}$ (%)
g55	55	48	285	140	51
g29	29	30	285	185	35
g14	14	25	180	140	22

upwards within the nematic phase. This is expected because by increasing the field more particles will start to orient perpendicular to the field.

To make a comparison between the systems with different polydispersities, first the critical field (B_c) of the isotropic phase (fresh samples with a volume fraction of 5%) was determined. This was done by finding the field where the isotropic phase became dark again (between crossed polarizers) after first becoming bright at lower fields. The value for the g14 system is much lower than for the other systems. It is not clear why, but perhaps the synthesis method has an influence on the magnetic properties of the systems.

Then, for I-N phase separated samples the field was established where the first signs of N-N phase separation were observed (B_{limit}). The data obtained are shown in Table 7.2. The difference between the two values ($B_c - B_{limit}$) is a measure for the range of field strengths where N-N phase separation takes place. Measuring this directly was not possible because smectic and/or columnar phases formed before a full nematic phase was reached, which changed the composition of the nematic phase (see Chapter 2). The ratio $\frac{B_c - B_{limit}}{B_c}$ is compared with the polydispersity in Table 7.2. There is a clear relation between this ratio and the polydispersity of the systems; the values are even comparable. This indicates that the polydispersity of the particles has a large influence on the N-N phase separation process.

7.4. Conclusions

We showed that phase separation takes place inside the nematic phase of colloidal goethite dispersions within the critical field range where individual particles change orientation. SAXS measurements proved that the two resulting nematic phases have orthogonal orientations, a uniaxial nematic with particles parallel to the field and a biaxial nematic with particles perpendicular to the field. The occurrence of N-N phase separation in this system is remarkable, because it was previously found that a large length ratio between particles is needed to get N-N phase separation [142]. In our case a different mechanism is causing the phase separation because an external magnetic field causes the orientational distribution function to broaden and even leads to orthogonal orientations. The phase separation is then rationalized by the large excluded volume between these perpendicularly oriented particles.

Polydispersity is an important factor for N-N phase separation, since the magnetic properties of the particles depend on their size. It was found that the larger the polydispersity of the system, the broader the range of field strengths where N-N phase separation occurs.

The interface formed between these phases is extremely interesting, since the two orthogonal orientations have to join there. As can be observed from Figure 7.2 the interfacial tension between the phases seems to be remarkably low (cf. [154]) and droplets are not spindle-shaped as often observed with I-N interfaces. Different kinds of coalescence events are observed during phase separation which is subject of further studies.

Acknowledgements

Andreea Lupascu and Mihai Diaconeasa are acknowledged for their experimental work, Andreea's work was supported by a Schlumberger grant. Bonny Kuipers is thanked for the magnet setups and Emile Bakelaar for the software of the VPM. We thank Patrick Davidson for enlightening discussions and for his help, together with Ivan Dozov, with the birefringence measurements. We also thank the staff of the BM26 DUBBLE beamline at the ESRF for their excellent support and Theyencheri Narayanan for sharing the magnet.

8

The isotropic-nematic interface in an external magnetic field

Abstract

Polarization microscopy was used to study the behavior around the isotropic-nematic interface in a magnetic field. In small fields (< 180 mT) both the isotropic (or then paranematic) and nematic phase aligned and the interface between them faded, but did not change position. At a bit higher fields the interface lowered, while nematic-nematic phase separation occurred lower in the sample. From about 250 mT droplets were observed within the paranematic phase that sedimented to the nematic phase, thereby increasing the level of the paranematic-nematic interface. Within the paranematic phase regions with different orientations formed. The lower part had an orientation perpendicular to the field, going up in the sample a region with a spread of orientations existed and above that a parallel part (at the smaller fields). At 300 mT the paranematic-nematic interface became unstable and the perpendicular paranematic phase connected with the perpendicular biaxial nematic phase down in the sample. The full paranematic phase was perpendicular in a field of 400 mT and the paranematic-nematic interface became vague.

8.1. Introduction

Anisometric mineral particles can form liquid crystalline phases depending on their concentration in suspension. Since these particles also have a large susceptibility to external fields, they can easily be manipulated [11, 12].

The isotropic (I) to nematic (N) phase transition was already described by Onsager in 1949, who developed an entropy-based theory [20]. It has long been predicted that an external field, which aligns the particles, will facilitate a phase transition from the isotropic to the nematic phase [155] and phase diagrams based on the Onsager theory were given by Khokhlov and Semenov [156]. Experimental evidence was found in *fd* virus suspensions [150] and later also in gibbsite dispersions [151]. For the virus particles very large fields of about 20 T were needed to achieve this transition, for the mineral gibbsite much lower fields of a few tesla were needed to observe an increase in the amount of nematic phase.

Colloidal goethite particles are very sensitive to external fields and show peculiar behavior [28]. The situation of goethite is difficult because the particles possess a permanent magnetic moment along their long axis, but also an enhanced susceptibility along their short axes. This induces an alignment along the field in low fields (up to about 250 mT) and an alignment perpendicular to higher fields. An idealized theoretical model for this behavior was developed by Wensink and Vroege [152]. Goethite particles were represented by monodisperse, charged spherocylinders; the calculated phase diagram can be seen in Figure 8.1. The aligned isotropic phase is called a paranematic (pN) phase, since it is not longer really isotropic. The dashed line in the paranematic region represents the field where the order parameter is zero. The dotted lines show the second order phase transitions from the uniaxial (para)nematic phase to the biaxial nematic phase. The phase diagram shows indeed the reorientation from parallel to perpendicular to the field and also the transition from the uniaxial to biaxial nematic phase. Furthermore, the nematic phase is favored over the paranematic phase in a magnetic field. A tricritical point exists where the pN^--N_b^- transition becomes second order. Other scenarios are possible depending on the magnetic properties of the system.

In this chapter mainly the behavior of goethite around the I-N interface in a magnetic field will be discussed. Polarization microscopy was used to study this.

8.2. Experimental

The system used in this chapter is the g29 system of Chapter 7. In Section 7.2 the synthesis is described and also the details of the polarization microscopy setup. Capillaries of $0.05 \times 1.0 \times 100$ mm (VitroCom) have been used. The microscopy pictures shown are composed of several microscopy pictures joint together.

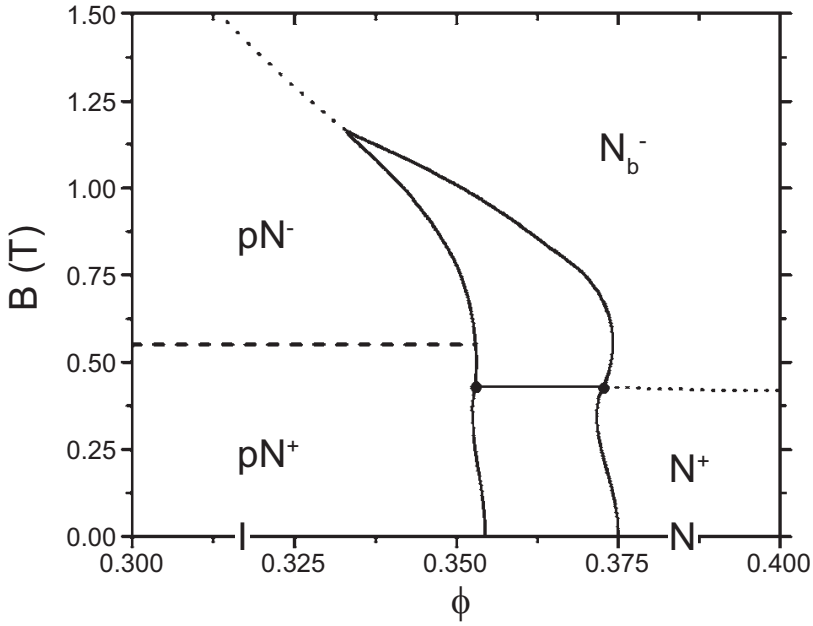

Figure 8.1. Theoretical phase diagram for goethite in a magnetic field, showing a paranematic phase with parallel (pN^+) and perpendicular (pN^-) alignment, a nematic phase with parallel alignment (N^+) and a biaxial nematic phase with perpendicular alignment (N_b^-) [152].

8.3. Results and discussion

I-*N* phase separated samples were studied at different magnetic field strengths, now focusing on the behavior around the *I*-*N* interface. The first measurements were performed at fields below the critical field strength. The behavior in a field of 100 mT can be seen in Figure 8.2. The isotropic and nematic phase were aligned parallel to the field. The interface was first visible as a red line but it slowly became vague; the red line turned into a wider band. The nematic phase was homogeneous in this field, but in the paranematic phase interference colors could be observed. The different color bands are caused by a gradient in the birefringence as is presented in the Michel-Levy birefringence chart shown in the previous chapter (Figure 7.6). The birefringence (Δn) increases with the volume fraction (ϕ) and the nematic order parameter (S_2) (see Equation (7.5)). Since goethite has a large density (4.26 g/mL) and the particles are relatively large, there is a large concentration gradient in the sample, which causes the gradient in the birefringence.

In the nematic phase interference colors were not observed. Here, the order parameter is much larger than in the paranematic phase (typically 0.95 compared to 0.05 [29,30]).

Therefore, the interference colors will be much lighter in color (see the higher orders in Figure 7.6) and cannot be seen in the strongly absorbing goethite.

After switching off the field, the initial situation came back within seconds, except for the exact domain structure within the nematic phase. The pictures in Figure 8.2c were taken two minutes after switching off the field. Right below the I-N interface, interference colors were visible just after switching off the field, which indicates that there is still a gradual transition from the isotropic to the nematic phase. Within hours after switching off the field, the interference colors disappeared and a sharp I-N interface was formed.

At fields where N-N phase separation takes place (see Chapter 7) the behavior starts to be more complicated. In Figure 8.3 the behavior in a field of 200 mT can be seen. Interference colors were again observed in the paranematic phase, but around the original I-N interface the color bands were narrower than in a field of 100 mT, indicating a larger gradient in the birefringence. The paranematic phase is probably already getting less well ordered because the critical field is being approached, while the nematic phase still has a large order parameter.

Furthermore, the bands gradually moved downwards over time in the field. This implies that the order just below the original I-N interface was decreasing. The field was switched off after 7 days and it can be seen in Figure 8.3c that the I-N interface changed its position; it reformed lower than it initially was. This confirms the lower order observed from the interference bands while it was still in the field. Besides the behavior around the I-N interface, it can be seen that N-N phase separation has taken place. The newly formed, biaxial nematic phase is apparently denser than the original nematic phase. Because of the formation of this denser phase the total volume of nematic phase has decreased and the level of the I-N interface lowered. Nevertheless, the decrease in the height of the I-N interface seems to be too large to be accounted for just by the denser lower nematic phase which is still very small. This would suggest that the parallel nematic phase might also be denser than the non-aligned nematic phase.

An interesting change in the paranematic phase was observed in a field of 250 mT (Figure 8.4). First, small droplets formed in the paranematic phase and larger droplets in the nematic phase (8 min) and the interface between the paranematic and nematic phase was not clear for a while (1 h). Then, a new interface was formed, at a bit higher position, and droplets were still sedimenting from the paranematic to the nematic phase (3.5 h). The movement of these droplets induced a wiggly black band which could be clearly observed after 10 hours. Above and below this band, interference colors were observed. The black color indicates a region of zero birefringence and thus a spread of particle orientations. Below this black band the particles were probably oriented perpendicular to the field (in a sample measured in a field of 270 mT the paranematic phase, just above the pN-N interface, was confirmed to have an orientation

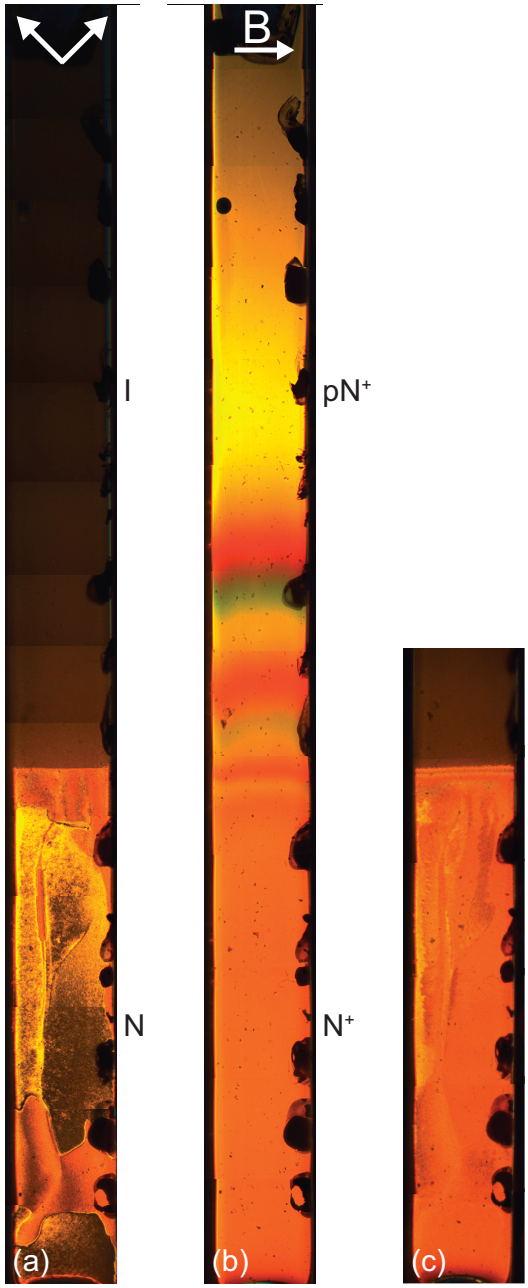

Figure 8.2. Polarization microscopy picture of an I-N phase separated sample ($\phi = 9.5\%$), (a) before applying the field, (b) in a 100 mT field for 1.7 days and (c) just after switching off the field.

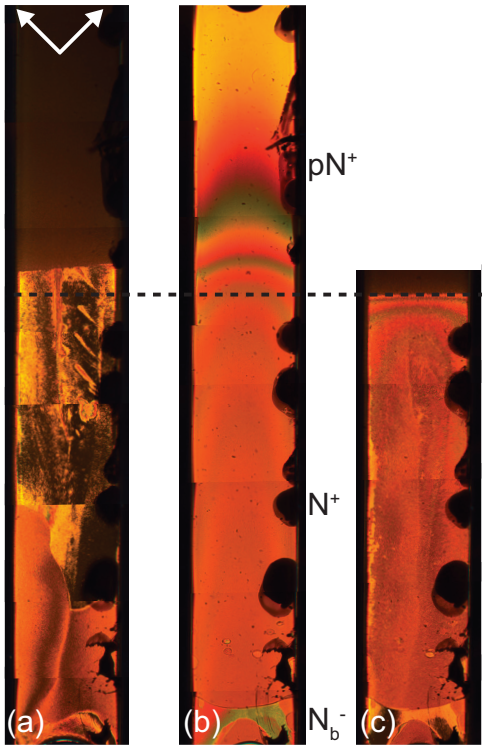

Figure 8.3. Polarization microscopy picture of an I-N phase separated sample ($\phi = 9\%$), (a) before applying the field, (b) in a 200 mT field for 7 days and (c) just after switching off the field.

perpendicular to the field above which also a black region with zero birefringence was observed). Above the black band the orientation is expected to be parallel to the field. From this upper region nematic droplets sedimented to the nematic phase with the same orientation. After 3.5 days the interface between the parallel nematic phase and perpendicular paranematic phase was well developed. Within the paranematic phase the interference bands were also better developed and the black band can be clearly seen.

A more complete study of this rich behavior was performed at 270 mT (Figure 8.5). In the paranematic phase similar behavior was observed as in the nematic phase. Droplets formed in a large part of the sample, where the droplets were smaller in the paranematic phase compared to in the nematic phase as can be seen from the picture taken after 40 minutes. The droplets formed in the paranematic phase were nematic and they sedimented to the nematic phase, thereby increasing the level of the pN-N interface, as could be seen after two hours in the field. Just below this interface interference colors

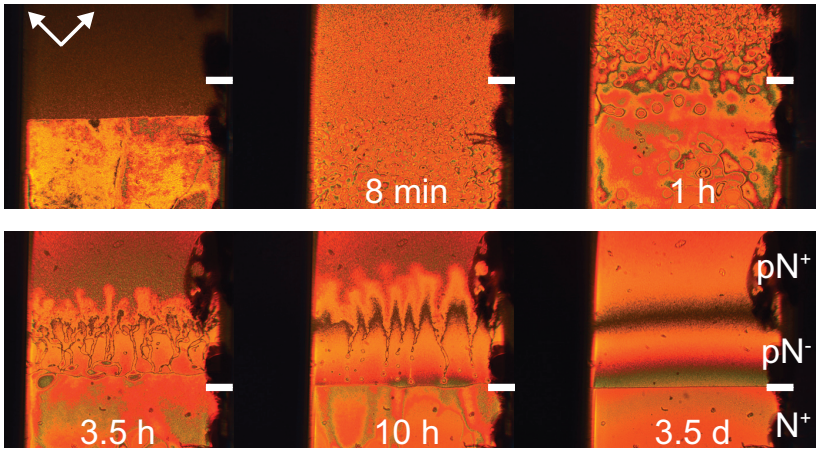

Figure 8.4. Polarization microscopy pictures of an I-N phase separated sample ($\phi = 9\%$) in a 250 mT field. The white mark indicates one specific position in the capillary.

were observed indicating that the parallel alignment was still distorted by droplets and the pN-N interface was not clear yet. There seemed to be a flow from the nematic to the paranematic phase as well and after 5 days the level of the interface had lowered a bit. However, it was still clearly higher than the initial position, even though a nematic phase which seems to be denser had formed. The nematic phase is stabilized in the field, which confirms theoretical predictions [152, 155, 156] and earlier experiments [150, 151]. Compared to the other experiments the process can be followed more directly in our case. In the work of Tang and Fraden [150] droplets that formed a network were observed when a magnetic field was applied to an initially fully isotropic sample, but no formation of a macroscopic nematic phase was seen. Van der Beek *et al.* [151] observed a rise of the I-N interface only when letting homogenized samples phase separate in a magnetic field, but no formation of droplets in the isotropic phase was observed when increasing the field.

In the paranematic phase some interference colors were observed after 5 days in 270 mT and there was a large area more or less black. This implies that there was a small part with some (perpendicular) alignment, but in the largest part there was hardly any order and probably all orientations were present within the paranematic phase. The field is clearly close to the critical field where a spread in orientations is expected in the paranematic phase.

Just after switching off the field, the I-N interface formed at the same position as it was in the field. After one hour, it could already be seen that the interface position was clearly going down and it was then close to the situation before a field

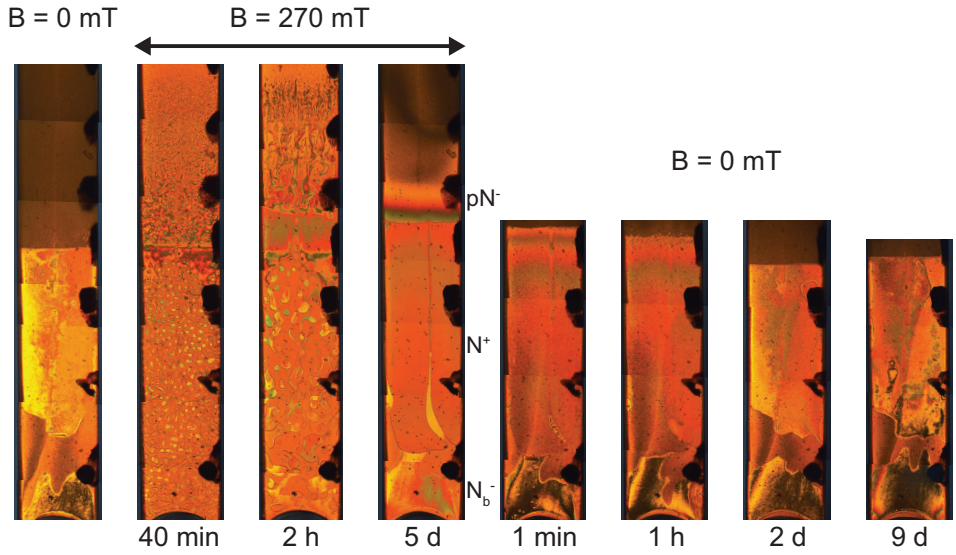

Figure 8.5. Polarization microscopy pictures of an I-N phase separated sample ($\phi = 9\%$); before applying the field, in a 270 mT field and after switching off the field.

was applied. Therefore, it was expected that equilibrium was reached soon after that. However, the interface dropped even further and after two days it was clearly lower than it was initially. This was attributed to the denser perpendicular nematic phase which was still present at the bottom of the capillary. The dynamics in the isotropic phase is faster than in the nematic phase, so while equilibrium is reached around the I-N interface, the nematic phase is still changing. Particles have to diffuse within the nematic phase, especially from the denser biaxial nematic phase which formed in the field. This diffusion is a slow process. After 9 days, it could be seen that the interface was rising and the nematic phase was probably getting less dense again.

The slow diffusion can also be seen when repeating the experiment in a field of 270 mT, 9 days after the previous experiment. In Figure 8.6 the behavior after two hours in a field can be seen. Compared to the situation in Figure 8.5 after two hours, it was observed that N-N phase separation was much more localized to the bottom of the capillary in the second experiment. It is clear that the composition of the nematic phase was still very different from the initial situation. The behavior around the I-N interface was similar in the first and second experiment indicating that the I-N region reached the equilibrium situation in zero field faster than the lower region of the nematic phase.

In a field of 300 mT, droplets were again forming in a large part of the sample (Figure 8.7), except for the upper part of the isotropic phase which remained more or less dark. The droplets in the paranematic phase were still small after 10 minutes, but

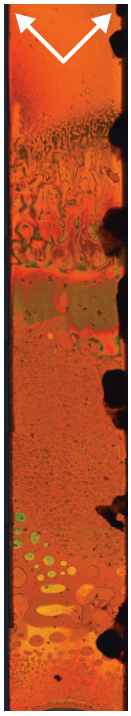

Figure 8.6. Polarization microscopy picture of an I-N phase separated sample after two hours in a 270 mT field, 9 days after the experiment in Figure 8.5.

they grew over time as can be seen from the pictures taken after one hour. After one day, a new interface has formed between the paranematic and nematic phase, which was a bit higher than the I-N interface at zero field, even with the large dense nematic phase formed at the bottom of the capillary. From the paranematic phase still some droplets sedimented to the nematic phase.

After 5 days, the interface had lowered its position and it became unstable. Droplets from the paranematic phase were falling through the interface and channels were being formed. At the left side of the capillary a channel connecting the paranematic and the lower nematic phase can be seen. This lower nematic phase had the same orientation of the particles as the paranematic phase just above the pN-N interface; they were both oriented perpendicular to the field. Apparently, these phases had a small density difference and were very similar; channels connecting the two phases were made through the upper nematic phase with a parallel orientation.

In a field of 400mT, most particles had an orientation perpendicular to the field. As can be seen in Figure 8.8 (2.5 h) some small droplets still formed in the paranematic

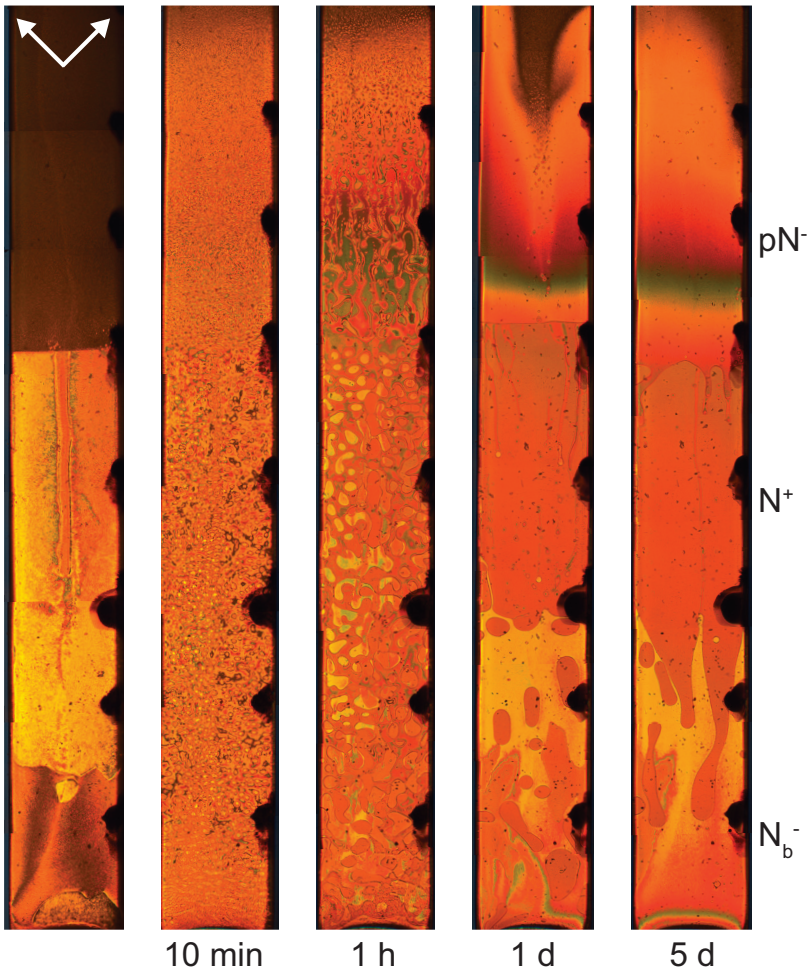

Figure 8.7. Polarization microscopy pictures of an I-N phase separated sample ($\phi = 9\%$); before applying the field and in a 300 mT field over time.

phase. These droplets had a parallel alignment as could be concluded from the observation that they coalesced with the nematic droplets with a parallel alignment. After 7 hours, hardly any droplets were observed in the paranematic phase anymore. The position of the I-N interface does not seem to have changed, but it was not easy to determine since there was no sharp interface present.

After 6 days, the amount of paranematic phase seemed to have increased, based on the change of the position of the interference bands and of the areas of parallel nematic phase. Probably, the perpendicular, biaxial nematic phase increased in density. Within

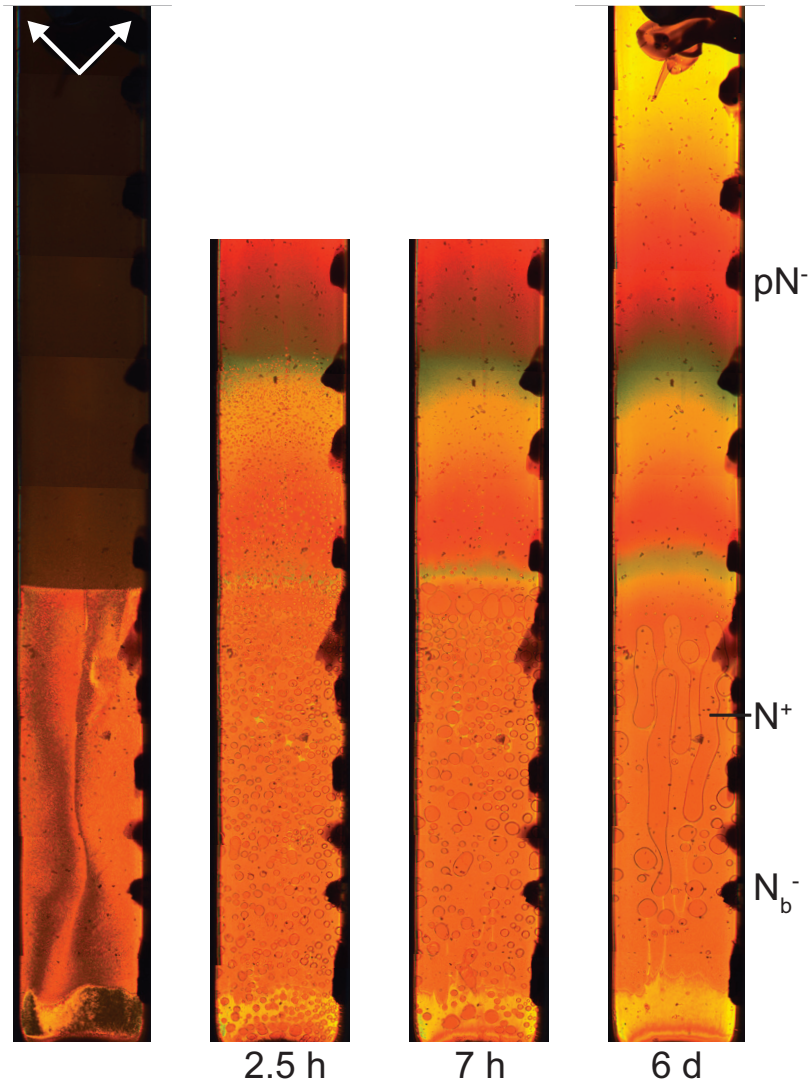

Figure 8.8. Polarization microscopy pictures of an I-N phase separated sample ($\phi = 10\%$); before applying the field and in a 400 mT field over time.

the parallel nematic phase there was apparently a density gradient, since the areas were stretched over a large part of the capillary.

The paranematic phase was aligned perpendicular to the field; no dark areas were observed which would indicate a spread in the orientations of the particles. This phase was clearly better aligned than at 300 mT, as can be seen from the interference colors that were now less intense.

Higher fields were not studied in detail here. At least more than 600 mT is needed to see no N-N phase separation anymore. The paranematic phase becomes better aligned and the interface with the nematic phase fades. It was observed by Lemaire *et al.* that the difference between the paranematic and nematic phase vanishes at a certain field strength, in their case they used 1 T [32].

8.4. Conclusions

The behavior of the region around the I-N interface in a magnetic field was studied using polarization microscopy. In a small magnetic field (up to 180 mT) the paranematic and nematic phase align parallel to the field. In time, the interface between the paranematic and nematic phase fades, but the difference is still clear from the interference colors observed in the paranematic phase. After the field is switched off, the I-N interface is still in the same position.

In fields where N-N phase separation occurs (above 180 mT), there are two effects affecting the position of the I-N interface. Firstly, at least the lower, biaxial nematic phase that forms has a higher density and perhaps the upper, parallel nematic phase as well. Therefore, it reduces the total volume of the nematic phase and it lowers the position of the I-N interface. Secondly, nematic droplets form in the paranematic phase which sediment to the nematic phase, thereby increasing the height of the I-N interface. Which of the two factors wins over the other depends on the field strength. In small fields no droplets are formed in the paranematic phase yet and the interface drops. Increasing the field, droplets start to form and the interface rises.

At fields above around 300 mT the I-N interface starts to go down again, probably because of the large denser nematic phase. Furthermore, the interface starts to get unstable. Within the paranematic phase there are also regions with different orientations as in the nematic phase. The lower part of the paranematic phase has a perpendicular alignment like has the lower nematic phase. In high fields these two phases connect and form channels through the parallel nematic phase. At fields above about 600 mT there is no N-N phase separation anymore and the interface between the paranematic and nematic phase starts to fade.

The dynamics in the isotropic phase was observed to be much faster than in the nematic phase. The I-N interface restores within a day, but the composition of the nematic phase was found to be still much different from the initial situation 9 days after switching off the field.

Acknowledgements

Andreea Lupascu is acknowledged for her preliminary experimental work, her work was supported by a Schlumberger grant. Bonny Kuipers is thanked for the magnet setup and we thank Patrick Davidson for enlightening discussions.

Part 3

Modified goethite

9

Modified goethite in an external magnetic field

Abstract

Goethite particles were successfully modified with chromium, aluminum and cobalt. The behavior of the different liquid crystalline phases, observed in colloidal dispersions of this modified goethite, has been studied by small-angle X-ray scattering and was compared with unmodified systems. All these systems show similar behavior with and without field. On the other hand, the magnetic properties of the normal and modified systems are different: the relative importance of the permanent and induced magnetic moment was found to have changed. Magnetic-field-induced nematic-nematic phase separation was observed in a mixture of normal and aluminum-modified goethite.

9.1. Introduction

Goethite particles have the opposing tendencies to align with their permanent moment parallel to the field at low magnetic field strengths and to orient perpendicular to a larger magnetic field due to their induced moments. By tuning the relative importance of the permanent and induced moments different phase diagrams can be expected [152]. When the permanent magnetic moment is relatively unimportant compared to the susceptibility anisotropy, the first-order isotropic-nematic phase transition changes into a second-order transition in a large magnetic field. In the other situation where the permanent moment is more important the first-order phase transition vanishes above a critical point at a lower field strength and subsequently reappears at higher fields. We hope to achieve these different types of behavior by modification of the goethite particles with other elements. Goethite has a lot of isostructural equivalents where other cations occupy the places of Fe^{3+} [157, 158]. Therefore, it is possible to modify goethite with different elements, for example with chromium (Cr) [159, 160], aluminum (Al) [161] or cobalt (Co) [22, 162].

Apart from the nematic phase goethite can also form higher order phases. Smectic A and columnar phases have been found even in very (55%) polydisperse systems (Chapter 2) [33, 34]. All different phases of Cr-modified goethite were studied by small-angle X-ray scattering (SAXS) in a magnetic field and compared with unmodified goethite. An attempt was made to determine the magnetic properties of both systems. Al- and Co-modified goethite was also studied.

9.2. Experimental

9.2.1. Synthesis

The normal goethite (gn) dispersion used in this chapter is g35 from Chapter 2 of which the synthesis is described in Section 2.2.1.

The Cr-modified particles (gcr) were synthesized in a slightly adjusted way with part of the iron nitrate replaced by chromium nitrate ($Cr(NO_3)_3.9H_2O$, Merck, p.a.). In this case, 1 M NaOH was added to a 0.1 M chromium/iron nitrate solution until a pH of 9 was reached. After this, the precipitate was redispersed in fresh millipore water before raising the pH further to 11-12. Aging took place at 70 °C for 10 days. The dispersion obtained was centrifuged and stabilized as was done for g35. The gcr2 and gn2 dispersions were made similarly but with 14 days of aging.

Al- and Co-modified (gal/gco) goethite dispersions were synthesized in the same way using $Al(NO_3)_3.9H_2O$ (Aldrich, 98+%) or $Co(NO_3)_2.9H_2O$ (Acros, 99%). The gal system was aged for 14 days at 50 °C and the gco system for 57 days at room temperature. During synthesis, at high pH, oxidation of Co^{2+} to Co^{3+} takes place [162].

The gn3 (normal) and gal2 (Al) dispersions used for polarization microscopy studies were also made using the same method. Aging took place for 12 days, the gn3 system was kept at room temperature and the gal2 system at 45 °C. The higher temperature was used to compensate for their smaller size. At a higher temperature particles generally grow larger.

9.2.2. Characterization

TEM analysis was performed as described in Section 2.2.2.

Scanning transmission electron microscopy (STEM) in combination with energy dispersive X-ray analysis (EDX) was used to do elemental analysis. A line scan over the width of a Cr-modified particle was done to get information about the distribution of Cr over the particles. For a bulk analysis inductively coupled plasma optical emission spectroscopy (ICP OES) was used.

9.2.3. SAXS experiments

Samples were made as in Section 2.2.3. All capillaries, except the ones of the gn system, were flame sealed instead of using glue. The gn sample had been standing for about 3.5 years before doing these measurements, the gcr sample was about 1 year old and had been measured in a magnetic field two months before doing these measurements, the gal sample was 4 months old, and the gco sample 2 months. SAXS measurements were performed at the BM26 DUBBLE [56] and ID02 high brilliance [104] beamlines of the European Synchrotron Radiation Facility (ESRF, Grenoble, France). The variable permanent magnet described in Section 3.2.2 was used.

9.2.4. Magnetic properties

The magnetic properties of the particles were determined using a Micromag 2900 alternating gradient magnetometer (AGM, Princeton Measurements Cooperation). Samples were made in glass capillaries of $4 \times 4 \times 0.04$ mm^3 attached to a small piece of flexible plastic. Dispersions with a goethite volume fraction of 6% were put in the capillaries using a pipette and then dried in a magnetic field. The magnetic field was generated by a Bruker BE25v electromagnet with large flat poles. After drying the samples two-component epoxy glue (Bison Kombi rapide) was gently added to the capillary to keep the dried particles in place. Empty capillaries with glue were used as background samples.

9.2.5. Polarization microscopy

The polarization microscopy setup is described in Section 3.2.2. The capillaries used for microscopy were $0.1 \times 2.0 \times 100$ mm^3 in size.

Table 9.1. Goethite particle dimensions.

System	% Modification	$\langle L \rangle$(nm)	σ_L(%)	$\langle W \rangle$(nm)	σ_W(%)	$\langle T \rangle$(nm)	$\langle L \rangle / \langle W \rangle$
gn	0	282	35	68	32	∼25	4.1
gcr	5	227	31	68	29	∼22	3.3
gal	2	220	20	55	23	∼18	4.0
gco	9	222	44	41	41	∼14	5.4
gn2	0	237	23	57	23	∼22	4.2
gcr2	5	232	17	67	16	∼24	3.5

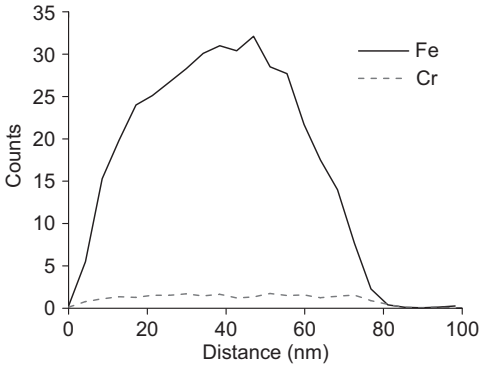

Figure 9.1. EDX lineprofile along the width of a Cr-modified goethite particle.

9.3. Results and discussion

9.3.1. Characterization

The particle dimensions of the systems used are shown in Table 9.1.

With ICP OES bulk molar concentrations of the incorporated elements were determined which can be found in Table 9.1. The line profile made by STEM-EDX along the width of a Cr-goethite particle (of the gcr system), which is shown in Figure 9.1, shows that the Cr is homogeneously distributed over the goethite particle. For the other modified systems such a line scan was not performed.

9.3.2. Influence of incorporated chromium

The general phase behavior of goethite is discussed in Chapter 5. The system discussed in that chapter is used to compare its behavior with that of a Cr-modified goethite system with a similar size polydispersity (gcr). To tune the magnetic properties of goethite a part of its Fe was replaced by Cr. This sample contains 5% (mole) Cr. In a capillary with an initial volume fraction of 7.8% the same phases were found as for the pure goethite sample. The estimated volume fraction at the I-N phase boundary is

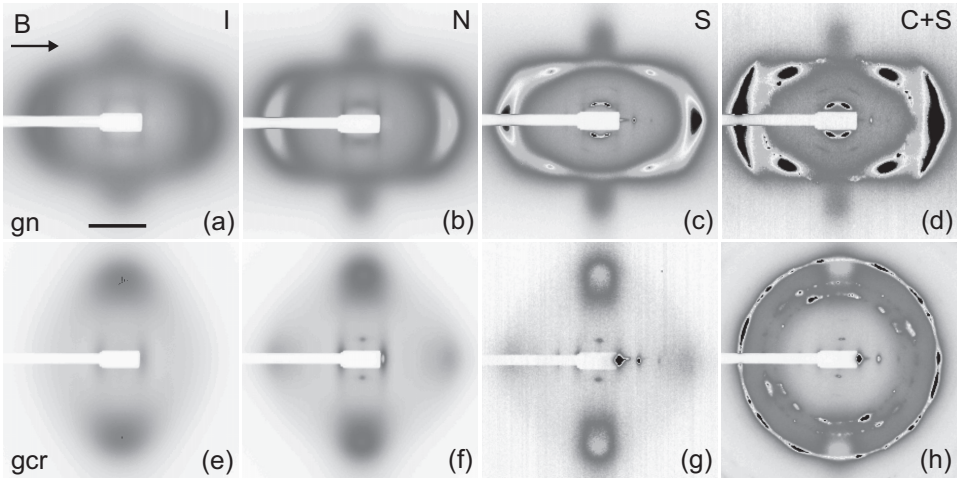

Figure 9.2. Cr-modified goethite (gcr) compared to normal goethite (gn) in a magnetic field of 0.5 T. The scale bar is 0.05 nm^{-1}.

approximately 12%, at N-SmA 13.4% and at SmA-(C+SmA) 14.4%. No clear jumps in the concentration profile were observed at the phase boundaries.

In a small magnetic field of 0.1 T, the system shows the same behavior as pure goethite; the isotropic, nematic and smectic phase are aligned parallel to the field. The coexisting columnar and smectic phases further down in the sample do not react to the magnetic field yet.

By increasing the magnetic field to 0.5 T, differences between normal and Cr-modified goethite become visible (Figure 9.2). In the upper part of the picture normal goethite (gn, a-d) is shown and in the lower part Cr-modified goethite (gcr, e-h). The isotropic and nematic phases of gn are already mostly oriented perpendicular to the field (a,b) as opposed to gcr which is still predominantly oriented parallel to the field (e,f), although a very small part of the system did turn perpendicular. When the smectic phase of gn starts to form an ordered columnar phase (c), the smectic phase of gcr is still mostly aligned with the field (g). The coexisting columnar and smectic phases of gn (d) start to form an ordered columnar phase just like the pure smectic phase (c). However, the columnar phase within the coexisting smectic and columnar phase of gcr has hardly changed and its smectic part is still mostly aligned parallel to field (h). The columnar phase of gcr is a bit peculiar because three rings are observed instead of two which are observed for normal goethite. This suggests that another kind of columnar structure is formed, probably a simple rectangular structure where a centered rectangular structure (as in Figure 5.1 C) is normally found. This is further discussed in Chapter 10.

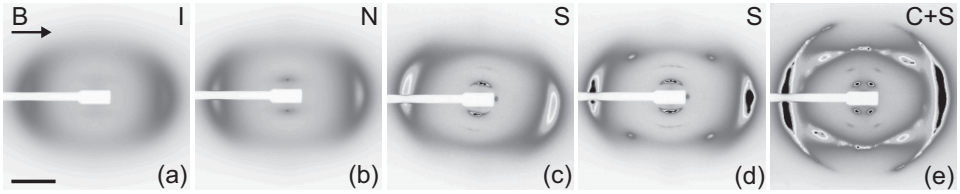

Figure 9.3. Cr-modified goethite (gcr) in a magnetic field of 1.5 T. The scale bar is 0.05 nm^{-1}.

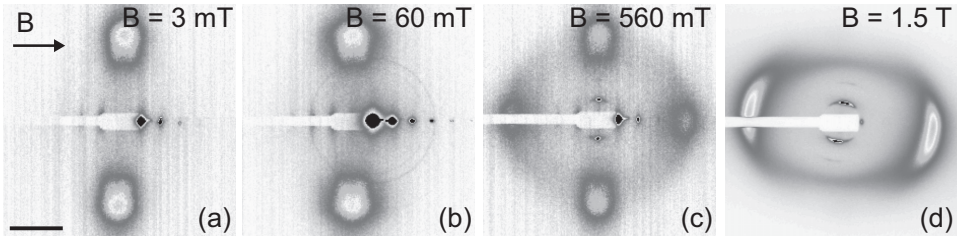

Figure 9.4. Smectic phase of Cr-modified goethite (gcr) in a magnetic field. The scale bar is 0.05 nm^{-1}.

At 1.5 T, it can be seen that the gcr system in the end does show the same behavior as normal goethite (Figure 9.3). The isotropic and nematic phase are now aligned perpendicular to the field (a,b like Figure 5.3c). In the smectic phase there are actually two different effects observed. High in the smectic phase (c) the system stays smectic but it aligns perpendicular to the field, whereas low in the smectic phase (d) it forms an ordered columnar phase as was observed for gn (Figure 5.4c,d). It seems that either the columnar phase which is already present close to the lower part of the smectic phase induces the formation of this ordered columnar phase, or the higher osmotic pressure at this height favors the transformation to a columnar phase. The columnar phase itself also starts to orient (e) but it probably needs more time to align further.

Highly ordered smectic phase. The smectic phase in the Cr-modified system shows remarkable behavior (Figure 9.4). It is already pretty well aligned in a magnetic field of 3 mT (a): a third order peak can be observed. This is possibly because of preliminary measurements carried out two months before doing these measurements where the sample had been aligned in a magnetic field. In a magnetic field of only 60 mT (b) it even shows a sixth order peak which indicates a very well ordered smectic phase. Very short measurement times of a few milliseconds were needed, together with a filter, not to oversaturate the detector. A longer measurement time was used to visualize the higher order peaks, thereby slightly oversaturating the lower order peaks causing some artifacts in the SAXS pattern (Figure 9.4b).

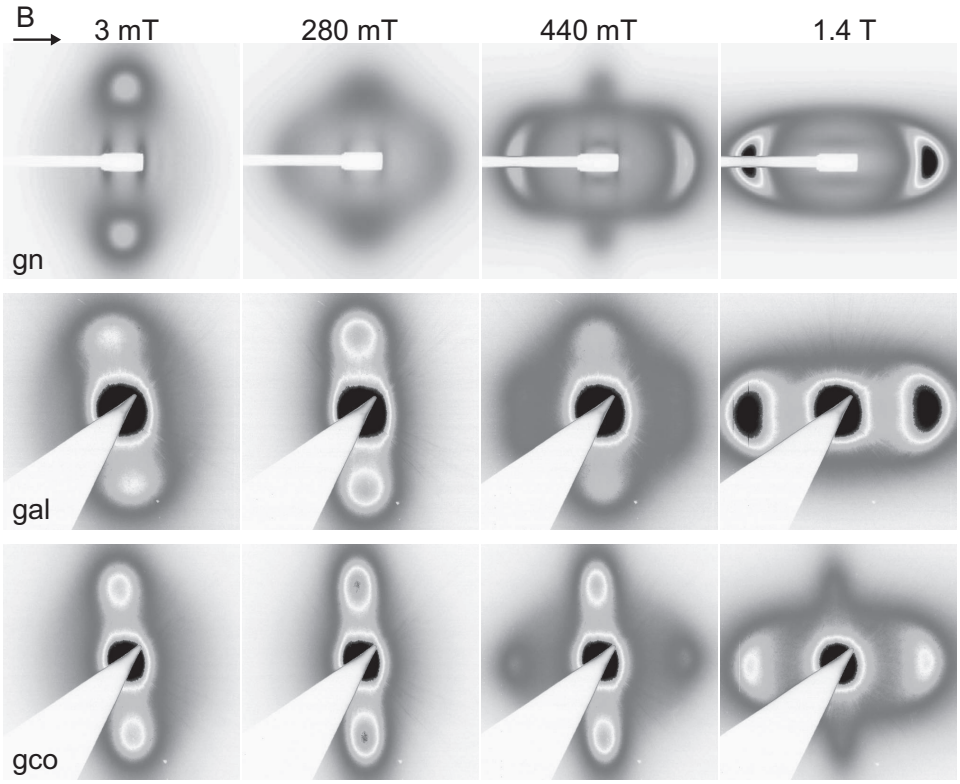

Figure 9.5. SAXS patterns of normal, Al- and Co-modified goethite in a magnetic field.

By increasing the field the order slowly decreases and at 560 mT the particles start to turn perpendicular to the field (c). At 1.5 T the smectic phase is mostly oriented perpendicular to the field (d); a second order small-angle peak can be observed. However, there are still some different domains as can be seen from the peaks at a small angle. A higher field or more time in the field are probably needed to fully align the phase.

9.3.3. Other incorporated elements

Goethite has also been modified with Al and Co (see Table 9.1). SAXS measurements of these systems and a normal system (gn) are shown in Figure 9.5.

A similar effect is observed as for Cr, the critical field strength increases when incorporating these elements. At 280 mT gn already starts to align perpendicular to the field, while gal and gco are still aligned parallel to the field. At 440 mT gal and gco also start to align perpendicular, while gn is already mostly aligned perpendicular. In

the highest field of 1.4 T gn and gal are fully aligned perpendicular to the field; in the gco system there is still a part aligned parallel to the field.

9.3.4. Magnetic properties

To study the difference in the magnetic properties of normal and Cr-modified goethite measurements were performed with AGM. Slightly different dispersions were used for these measurements: gn2 and gcr2 (Table 9.1).

Samples were dried at different field strengths to be able to determine the magnetic properties along the different axes of the particles. Dispersions dried in small field will be aligned along the field direction and in this way the permanent magnetic moment and susceptibility can be determined in the direction of the long axis of the particles. In high fields the particles will be aligned perpendicular to the field and the magnetic properties in that direction can be determined.

The measured magnetization curves of normal goethite (gn2) samples dried at 0.12 T and 1.7 T are shown in Figure 9.6. Similar results were obtained before by freezing dispersion in a certain field instead of drying them [29]. It can be seen that the curves of the 0.12 T samples show a remanent magnetic moment which confirms the presence of a permanent magnetic moment along the long axis of the particles. The 1.7 T graph crosses the origin, so no permanent magnetic moment is present along the short axes of the particles. Furthermore, a negative susceptibility anisotropy ($\chi_{\parallel} - \chi_{\perp}$) of -7·$10^{-4}$ is found. This value and the one found for the remanent moment (1.7·10^{-20} Am^2) correspond well to the values found by Lemaire *et al.* (-3·10^{-4} and 1.4·10^{-20} Am^2) [29]. Differences can occur for different goethite dispersions and there is actually a pretty large error in our measurements. The crossing point of the two lines should correspond to the critical magnetic field where the particles change orientation from parallel to perpendicular to the field. In our case, the crossing point is at a smaller (about 2-3 times) field than the actual critical field, so it is clear that the measurements are not very accurate.

The same measurements were done for a Cr-modified dispersion (gcr2) as is shown in Figure 9.7. Now there seems to be a problem because the 0.12 T and 1.7 T samples both show a remanent magnetic moment which is not expected. It is possible that the particles were not aligned completely perpendicular to the field yet, giving still a contribution of the permanent moment of the particles. The crossing point, which should be at a larger field than for normal goethite, seems to be at a very small field now. It is clear that these measurements do not show the behavior corresponding to the observations made by SAXS. Probably, there is a problem with the alignment of the particles in the dried samples.

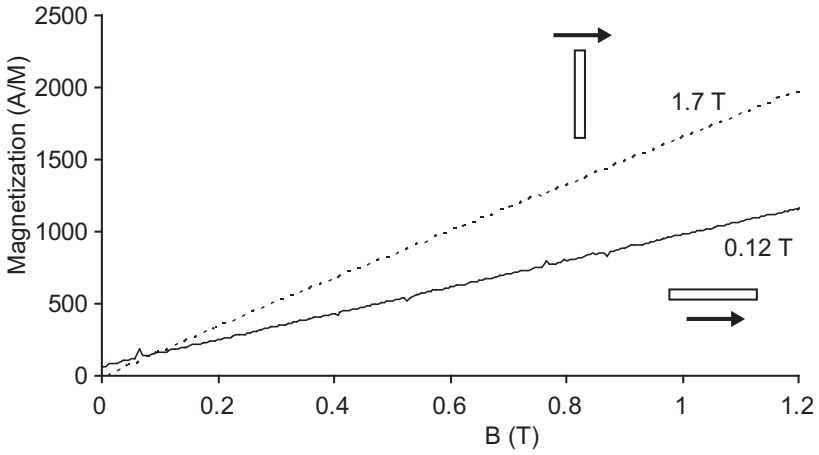

Figure 9.6. Magnetization curve for normal goethite (gn2) samples dried at 0.12 T and 1.7 T.

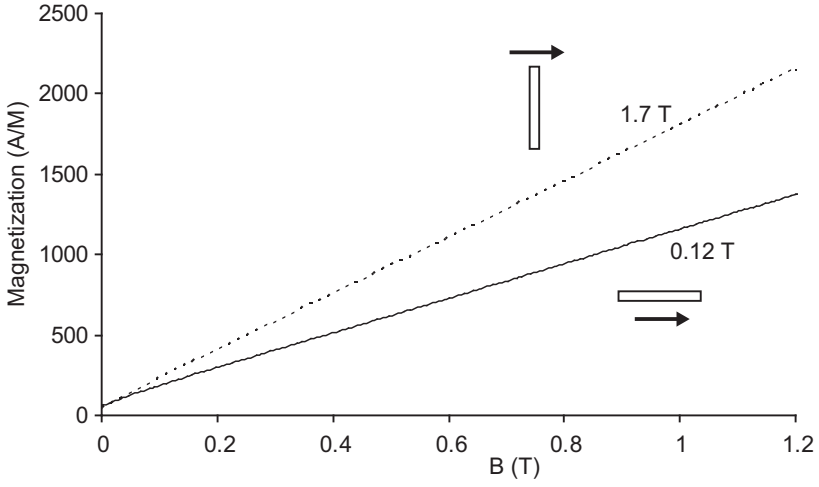

Figure 9.7. Magnetization curve for Cr-modified (gcr2) samples dried at 0.12 T and 1.7 T.

To be still able to say something about the difference between normal and Cr-goethite a study was performed on the remanent magnetization (M_r) of samples dried at different field strengths. When plotting this the initial slope gives the average permanent magnetic moment (μ_p) of the particles, according to

$$\frac{M_\mathrm{r}}{NH} = \frac{\mu_p^2 \mu_0}{3 k_\mathrm{B} T} \tag{9.1}$$

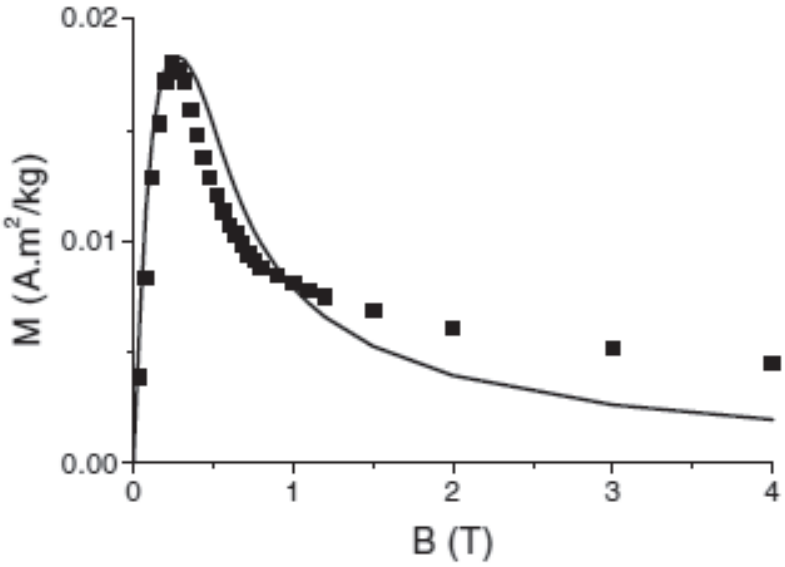

Figure 9.8. Remanent magnetization of samples frozen at different field strengths as obtained by Lemaire *et al.* [29].

with N the number of particles and H the magnetic field in A/m. At higher fields the induced moment takes over and a decrease in remanent magnetization should be observed. This type of measurements were already performed for normal goethite by Lemaire *et al.* (Figure 9.8) [29]. In this way it should be possible to distinguish between a difference in the permanent or induced moment. Measurements were performed for samples dried in fields of 7, 28 and 50 mT. This is still in the part where a straight line is expected. No difference was observed for the normal and Cr-goethite samples (Figure 9.9). The value found for μ_p is $6{\cdot}10^{-20}$ Am^2, which suggests that the remanent magnetization is overestimated if compared to the literature value of $1.4{\cdot}10^{-20}$ Am^2 [29]. The similar values for normal and Cr-goethite would suggest that there is no difference in the permanent magnetic moment of the two systems. To be sure more measurements should be done at higher fields. A difference between the systems should then be observed. Due to time constraints these measurements were not conducted yet.

If there is no difference in the permanent magnetic moment of the normal and modified particles, there should be a difference in the induced moment. This is plausible, since impurities can reduce the Neél temperature (T_N) [163]. When T_N is decreased, the system is closer to its T_N at room temperature and the susceptibility anisotropy becomes smaller. This will cause a higher critical field where the particles will rotate

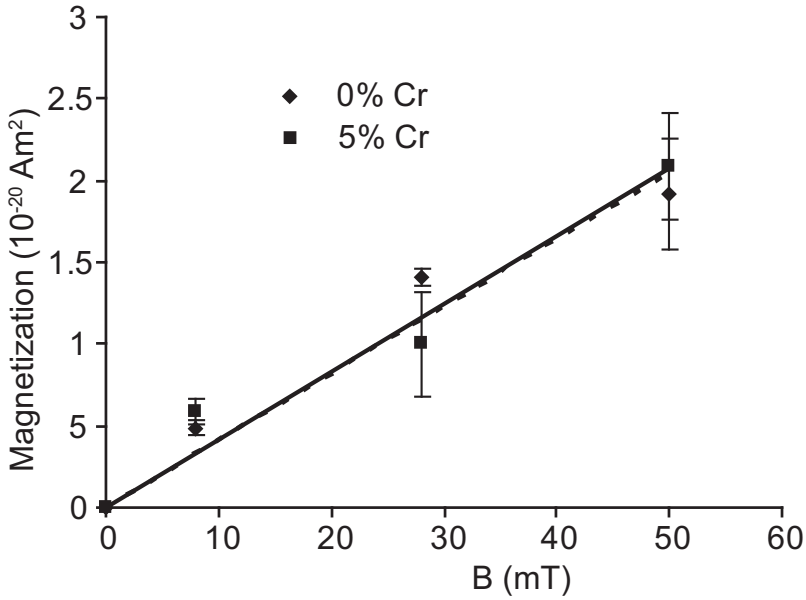

Figure 9.9. Remanent magnetization of samples dried at different field strengths.

from parallel to perpendicular to the field. A change in the permanent magnetic moment could also be possible because part of the spins is replaced by other spins. This induces more defects in the antiferromagnetic lattice and a larger remanent moment could occur.

9.3.5. Nematic-nematic phase separation

In Chapter 7 magnetic-field-induced nematic-nematic (N-N) phase separation is discussed. This occurs around the critical field strength because of polydispersity in the magnetic properties of the particles. Some particles will already start to orient perpendicular to the field, while others are still oriented parallel to the field and they separate. Another way to get this N-N phase separation, without the need of polydispersity, is by mixing a normal goethite dispersion with a modified dispersion. These two dispersions clearly have a different critical field where the particles rotate from parallel to perpendicular to the field. This should induce N-N phase separation at a field in between the two critical fields, because the normal particles will then be aligned perpendicular to the field, while the modified particles will still be parallel to the field.

N-N phase separation was indeed observed in a mixture of normal (gn3) and Al-goethite (gal2, 2% Al) with similar particle dimensions (Table 9.2). The critical fields of the two separate systems were 390 mT and 490 mT respectively and the mixture

Table 9.2. (Al-)Goethite particles used for N-N phase separation experiments.

System	% Modification	$\langle L\rangle$(nm)	σ_L(%)	$\langle W\rangle$(nm)	σ_W(%)	$\langle T\rangle$(nm)	$\langle L\rangle/\langle W\rangle$
gn3	0	180	27	36	28	∼15	5.1
gal2	2	194	27	39	28	∼17	5.2

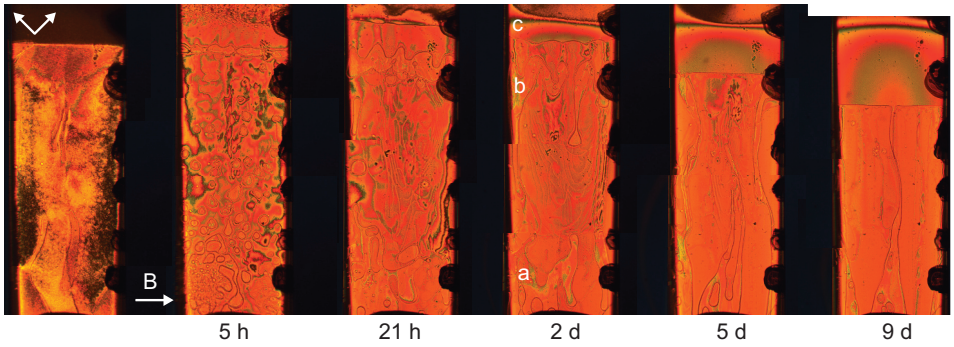

Figure 9.10. Polarization microscopy pictures of a sample of mixed normal and Al-goethite in a field of 440 mT. The width of the capillary is 2 mm.

was studied in a field of 440 mT. Polarization microscopy pictures of a sample with a 1:1 mixture of normal and Al-goethite in a field of 440 mT are shown in Figure 9.10.

In the first 5 hours, droplets were forming in the full nematic phase and also in the paranematic phase. Droplets from the paranematic phase sedimented to the nematic phase and the interface was rising. Around the position of the original I-N interface droplets coalesced and formed a region with a different orientation than the surrounding region. In time, some droplets in the nematic phase sedimented to the bottom of this phase and others went up to the region around the original I-N interface position.

After 21 hours, it could be seen that a phase was forming at the bottom of the capillary, but also the interface region had grown. In the next day everything seemed to be getting unstable. From the lower nematic phase droplets were moving up and from the interface region droplets were moving up and down. These regions seemed to have the same orientation since they connected at some points. Furthermore, the region which is even higher seemed to have the same orientation as well and was also connected to these other regions. Apparently, there is a very small density difference between the different nematic phases. If one looks carefully to the regions a, b and c (after 2 days) connections between these regions can be seen.

After 5 days, it was observed that regions a and b started to feed region c which increased in size. After 9 days, this upper nematic phase had grown even further and a connection with the lowest part of the nematic phase could still be observed. The upper

nematic phase and the remaining regions at the bottom of the nematic phase seemed to have the perpendicular orientation since it showed many interference colors and thus had a smaller birefringence (see Figure 7.6). This can be expected for the perpendicular nematic phase, because it can have all orientations from along to perpendicular to the capillary wall. The perpendicular orientation has a much smaller birefringence and will show clear birefringence colors. The other part of the nematic phase was slowly getting more homogeneous with clearly less interference colors, which indicates that it had the parallel orientation. Still some interference colors were observed in here because droplets from the other nematic phase were moving through this phase, thereby distorting the alignment.

So, in the end it seems that in this case the perpendicular nematic phase was mostly formed above the parallel nematic phase, which is opposite to the situation of a pure goethite system (Chapter 7). In that case the phase separation was based on particle dimensions and the larger particles formed the perpendicular nematic phase. In this case the N-N phase separation was not based on particle dimensions but on the magnetic properties of the normal and Al-goethite particles. The Al-goethite is expected to form the parallel phase since it switches to the perpendicular orientation at a higher field than normal goethite. The Al-particles used here were slightly larger than the normal goethite particles (Table 9.2), which might explain why the parallel nematic phase of these particles finally formed at the bottom of the capillary. The density difference between the two nematic phases seems to be smaller than in a pure goethite system and the phase separation process is slower.

The phase separated sample was frozen in liquid nitrogen and cut in pieces to be able to analyze the particles in the different nematic phases. STEM-EDX was used to determine the Al concentration in both phases. Unfortunately, 2% Al appeared to be below the resolution limit and it was not possible to see in which of the nematic phases the Al-goethite particles were present. Particles with a higher modification content would be better in this perspective, but incorporating other ions in goethite changes the particle dimensions which is an unwanted effect.

9.4. Conclusions

Goethite particles were successfully modified with Cr^{3+} ions, which were incorporated homogeneously. The modified particles show the same phase behavior as normal goethite. Furthermore, in a magnetic field similar effects are observed. The nematic phase aligns parallel to the field at a low field strength and perpendicular to a large magnetic field. The smectic phase also aligns parallel to a small magnetic field. In a higher magnetic field it aligns perpendicular to the field in the higher part of the phase and it forms a columnar phase with a distorted hexagonal structure in the lower part of the phase. The columnar phase also has the tendency to align in a magnetic field

but it reacts more slowly, probably because the particles seem to be more restricted at a higher osmotic pressure.

The difference between normal and Cr-modified goethite is that the particles turn perpendicular to the field at a considerably higher magnetic field strength. This proves that the relative importance of the permanent and induced magnetic moment can indeed be changed by incorporating different metal ions into the goethite particles. A similar effect was observed when incorporating Al or Co.

Magnetic measurements did not give conclusive evidence for the difference between normal and modified goethite, but it suggests that the permanent moment is the same. This implies that their susceptibility anisotropy is different, although this should be verified by further measurements.

In a mixture of normal and Al-goethite magnetic-field-induced N-N phase separation was observed. The process is slower than in a pure goethite system, which was discussed in Chapter 7. Furthermore, the position of the perpendicular and parallel nematic phases seems to be reversed compared to the normal situation. The perpendicular nematic phase was now mostly located above the parallel nematic phase. This might be caused by the slight difference in particle dimensions of the normal and Al-goethite.

Acknowledgements

Ben Erné is thanked for his help with the AGM measurements. Inge Storm is thanked for the nematic-nematic phase separation experiments. The staff of the ID2 and DUBBLE beamlines at ESRF are acknowledged for giving the opportunity to measure at their beamlines and giving their support, in particular Theyencheri Narayanan and Pierre Panine. EDX was carried out in collaboration with EMU, the Electron Microscopy group at Utrecht University, the Netherlands. Helen de Waard of the department of earth sciences, Geolab, is thanked for ICP OES measurements.

10

Simple rectangular columnar phase and its martensitic transition to the centered rectangular columnar phase

Abstract

Using high-resolution small-angle X-ray scattering, we observed a new type of the columnar phase with a simple rectangular (R_S) structure in colloidal goethite dispersions. Furthermore, it displays a martensitic transition into the usual centered rectangular (R_C) structure in an external magnetic field. The findings are rationalized in terms of entropic effects within a simple cell model. We interpret the results as an effect of the particle shape and the available degrees of freedom on the delicate balance between the space available for particle translations and rotations within the two structures.

10.1. Introduction

Suspensions of inorganic anisometric colloidal particles are able to self-organize into various liquid crystalline phases [11, 12]. They are very susceptible to external fields, have a high thermal stability, and are potentially suitable for applications such as photonics. Lyotropic mineral liquid crystals were found for the first time by Zocher in 1925 [13], who observed a nematic phase in suspensions of vanadium pentoxide particles. In addition to the nematic phase, which possesses only the particle orientational order, smectic or columnar phases can also be formed, which are positionally ordered in one or two dimensions, respectively. A recent intriguing example is board-like goethite particles, which shows rich liquid crystalline phase behavior, including nematic [28], smectic [33], and columnar phases [31]. The inherent polydispersity of the particles, which is usually considered to be a disadvantage of colloids, in this case enriches their phase behavior. It was found to induce the columnar phase, which coexists with a smectic phase and acts as a "waste bin" for the particles that do not fit within the smectic structure [33, 108]. The coexistence of columnar and smectic phases is rather unusual. The majority of known columnar phases are formed by flat molecules or platelike particles [164, 165]. A columnar phase can also be formed by, for example, long cylindrical micelles which do not have a fixed length [166]. For rodlike particles, apart from a few rare exceptions such as the columnar phase in suspensions of DNA molecules [167, 168] or *fd* viruses [169], a strong tendency toward smectic rather than columnar phases is observed.

In addition to their unusual phase behavior, goethite particles also have peculiar magnetic properties [28–34, 107, 108]. They possess a considerable permanent magnetic moment along their long axis, presumably due to uncompensated surface spins within their antiferromagnetic crystal structure. At the same time, their magnetic easy axis is orthogonal to the permanent magnetic moment, along the shortest particle dimension. Therefore, particles align parallel to a small external magnetic field but perpendicular to a larger magnetic field (> 250 mT). These alignment and reorientation phenomena open wide possibilities for easy manipulation of the liquid crystalline phases by an external magnetic field. Apart from the magnetic-field-induced isotropic to nematic phase transition, which has been extensively studied in various systems [32, 150, 151], goethite also shows a nematic to columnar phase transition under the influence of a magnetic field [31]. Furthermore, the particle properties can be tuned by various modification methods [22, 107, 160].

10.2. Experimental

10.2.1. Synthesis

The normal goethite particles were obtained as described in Section 2.2.1 (g35). The synthesis of the Cr-modified particles is shown in Section 9.2.1.

Particle characterization by TEM is described in Section 2.2.2, elemental analysis in Section 9.2.2.

10.2.2. SAXS

Sample preparation is discussed in Section 2.2.3. Flame sealing was used to close the capillaries. SAXS measurements were conducted at the BM26 DUBBLE and ID02 high brilliance beamline of the European Synchrotron Radiation Facility (ESRF, Grenoble, France). The microradian resolution setup was used [57].

The variable permanent magnet described in Section 3.2.2 was used.

10.3. Results and discussion

In the work presented here, a dispersion of chromium (Cr)-modified goethite particles (5:95 Cr:Fe) was studied, which is system gcr of Chapter 9. The particle dimensions are $L \times W \times T = 227 \times 68 \times 22$ nm, with a polydispersity of about 30% in all directions. Because of the incorporation of Cr, the particles have a slightly smaller L/W ratio than usually found for goethite: 3.3 while > 4 is normal [28, 108]. Except for the difference in particle dimensions, normal and modified goethite also have different magnetic properties [107]. The critical field strength (B_c) where the particles change orientation from parallel to perpendicular to the magnetic field is higher ($\sim$550 mT) for the modified particles. These modified goethite particles show the same type of phase behavior as normal goethite and have the same surface charge. In a capillary with an overall volume fraction of 7.8% four different phases were observed: an isotropic, nematic, smectic A and columnar phase upon establishment of the sedimentation equilibrium profile.

In a small-angle X-ray scattering (SAXS) experiment, the pattern displayed in Figure 10.1a was observed; the integrated intensity profile is shown in Figure 10.1b. The sharp peaks at a small angle originate from the periodicity of a smectic A phase. There is also a broad peak at a larger angle, which corresponds to the liquidlike interactions within the smectic layers. On top of this broad peak, one can see sharp and inhomogeneous scattering rings, which indicate that there is also a columnar phase present. The q-values corresponding to the first three rings are 0.062, 0.074 and 0.097 nm^{-1}. Since $0.062^2 + 0.074^2 \cong 0.097^2$, these reflections can originate from a simple rectangular (R_S, $p2mm$ symmetry group) columnar phase with unit cell dimensions of 85 and 101 nm (Figure 10.1c, one particle per cell).

More (higher order) rings can also be observed with longer exposure times. From the basis vectors, the other peak positions can be calculated and they are shown as

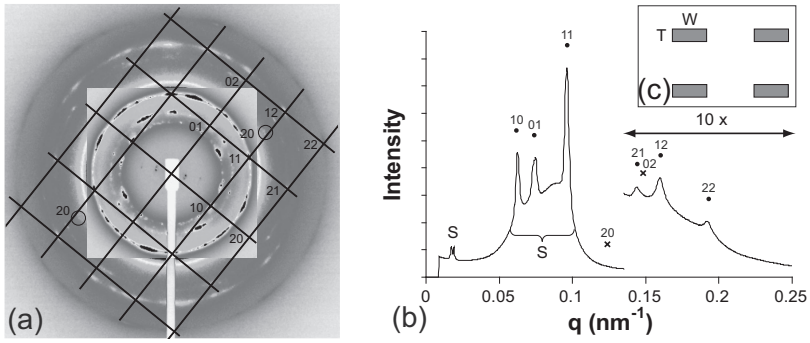

Figure 10.1. (a) SAXS pattern of the R_S phase ($p2mm$) of Cr-goethite. Two patterns measured with different exposure times are shown on top of each other. Lines highlight reflections of a domain. (b) Azimuthally integrated intensity profile (partly 10 times enlarged), with S being the smectic peaks, the dots being the columnar peaks, and the crosses being the expected columnar peaks that were not observed in the profile. (c) Unit cell.

dots and crosses in Figure 10.1b. The peaks corresponding to the dots are clearly observed, and they correspond to the following reflections: 10, 01, 11, 21, 12, and 22. The 20 reflection is weakly present as can be seen in the circles in Figure 10.1a, but it is not strong enough to be observed in the profile in Figure 10.1b. The 02 reflection was not observed, presumably due to a minimum of the particle form factor and a close vicinity of the stronger 21 reflection. The R_S structure of the columnar phase is further supported by the fact that in this powderlike pattern a few sets of reflections can be identified as originating from particular domains; one of them is highlighted in Figure 10.1a.

For comparison, in Figure 10.2, we present the results measured in a similar suspension of ordinary goethite, without doping by Cr ($282 \times 68 \times 25$ nm, volume fraction of 6%). Here only the centered rectangular (R_C, $c2mm$ symmetry group) phase has been observed; see also references [31] and [33]. The R_C columnar structure appears as less rings in a SAXS pattern (see Figure 10.2a,b). The rectangular cell of the R_C columnar phase can be seen in Figure 10.2c. In the powderlike pattern, particular domains can be found; one of them is highlighted in the figure.

The origin of the R_S structure in this Cr-modified system instead of R_C (as in ordinary goethite) is not clear yet. It is known that B_c (the critical field strength where the particles change orientation from parallel to perpendicular to the field) is significantly different for normal and modified goethite (see Chapter 9) [107]. The change of B_c might be related to the effect of the Cr substitution on the permanent magnetic moment as well as on the induced moment (by changing the susceptibility anisotropy). However,

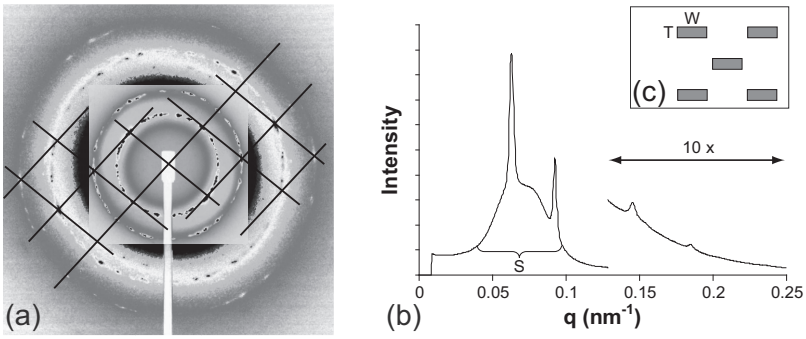

Figure 10.2. (a) SAXS pattern of the R_C phase ($c2mm$) of normal goethite. Two patterns with different exposure times are shown on top of each other. Lines highlight reflections of a domain. (b) Azimuthally integrated intensity profile (partly 10 times enlarged) and (c) unit cell.

it is expected that the dipole-dipole interactions between the particles are too weak to play a significant role when there is no field applied. Furthermore, there is a difference in the length of the particles, which could make a difference, but the effect of the particle shape should be further studied.

Interestingly, by applying a magnetic field of 1.5 T to the Cr-modified system, which is above B_c, the R_S phase transforms into the R_C columnar phase (Figure 10.3). The rectangular cell dimensions are now 130 and 132 nm (two particles per cell), and the particle density remained the same within experimental error. Since the transformation breaks the symmetry of the inter columnar structure, one can expect that the transition between R_S and R_C ordering is of first order. Because the density of the structure remained the same it is expected that it occurs via a martensitic transition, where particles only move within the unit cell by a fraction of the cell size. This externally controlled transformation is interesting from a fundamental point of view and can prove useful for possible applications of goethite self-organization, since no long-scale diffusion and no rotation of the long particle axis is involved in this transition.

Furthermore, the structure goes back to the initial (R_S) structure after removal of the field, which was observed two months later. Repeating the experiments in a magnetic field, similar behavior was observed. Waiting again for a few months, a part of the phase remained in the R_C structure, but mostly R_S was observed. A combined pattern is shown in Figure 10.4. The R_S phase seems to be the stable phase without an external field.

To elucidate the competition between both phases, a simple cell model was developed. Within this approach, the 3D space inside the crystal is split into Voronoi cells. The particles are assumed to be confined within the cells. Using the average particle

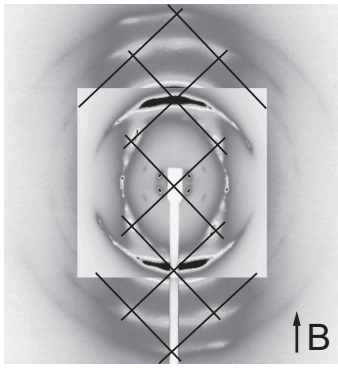

Figure 10.3. SAXS pattern of the originally R_S columnar phase ($p2mm$) which transformed into an R_C columnar phase ($c2mm$) in a magnetic field of 1.5 T. Two patterns with different intensity scales are shown on top of each other.

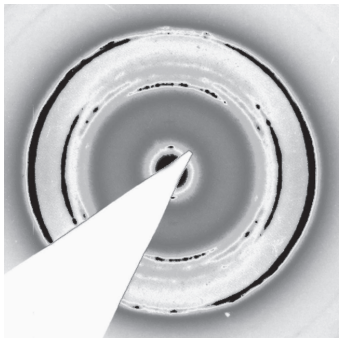

Figure 10.4. SAXS pattern of the columnar phase after being two times in a magnetic field with intervals of a few months. The rings originate from coexisting R_S and R_C columnar phases.

dimensions ($L \times W \times T = 227 \times 68 \times 22$ nm), the configurational space Ω per particle is estimated as the product of the amplitude of the particle translations Δx and Δy possible in two orthogonal directions within the cell multiplied by the amplitudes α, β, and γ of the particle rotations within the cell around three orthogonal axes. The α rotation is around the long axis L, β around the shortest axis T, and γ around the W axis (see Figure 10.5). This simple cell model was used to estimate the entropy difference $\Delta s = k_B(\ln\Omega_S - \ln\Omega_C)$ between the R_S and R_C columnar structures.

It is found that the R_S phase has a slightly higher entropy with $\Delta s = 0.32 k_B$ per particle. Moreover, the difference becomes certainly more pronounced if one accounts for the electrostatic repulsion between the particles. By simply adding the Debye length

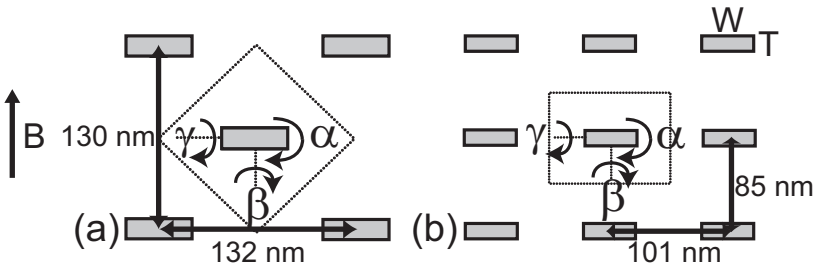

Figure 10.5. Rotations within the cell model of (a) the R_C columnar structure and (b) the R_S columnar structure.

of 10 nm to all particle sizes, one gets an upper estimate of $\Delta s = 3.4k_B$. In the presence of a strong magnetic field, one can assume that the α and γ fluctuations are frozen to ensure that the shortest particle axis stays in the field direction. In this case the cell model predicts that $\Delta s = -0.14k_B$ for bare particles and $\Delta s = -0.22k_B$ after accounting for the Debye length. This result is mostly caused by the fact that the R_C structure leaves more room for particle β rotations which are not frozen by the external field.

We note that this cell model is presumably far too simple for exact quantitative predictions of the excluded volume entropy. Moreover, possible fractionation was not taken into account which would lead to mainly the larger particles forming the columnar phase [108]. Yet, the cell model does qualitatively confirm that while the phase with R_S structure is more stable without the external field, the one with the R_C structure wins after particle alignment in a strong external magnetic field.

In our recent experiment, which was performed one year later than the measurement shown in Figure 10.4, the structure did not return back anymore to the R_S columnar phase after its field-induced transformation to the R_C structure. This observation suggests the occurrence of slow processes, which can affect the delicate balance between the phases with the R_S and R_C structures. A possible explanation is the slow densification of the system due to sedimentation, which can slowly arrest the dynamics of the system. This has been observed before in goethite samples. Additionally, it is known that fractionation plays a role which slowly changes the system [108]. One could also speculate that a slow release of ions from the goethite particles and/or capillary walls might have increased the ionic strength, thereby screening the charge of the particles. This will make them more "barelike". As one can see from the results of the simple cell model, this will reduce Δs and, therefore, will shift the equilibrium toward the R_C structure. Further study with a better control over the ionic strength would be useful.

10.4. Conclusions

In this work, we have studied a suspension of Cr-modified goethite particles. Cr substitution modifies the magnetic properties [107] and slightly influences the particle shape. In this dispersion, we found a novel columnar phase with a different structure. The most common structure of a columnar phase is the hexagonal one ($p6mm$ symmetry group), as in, for example, gibbsite dispersions [165]. For goethite particles with a rectangular cross section, a centered rectangular structure has been observed (R_C, $c2mm$ symmetry group), which can also be seen as a hexagonal structure deformed along one of the symmetry planes [31]. This type of columnar phase is also found frequently in molecular liquid crystals [170]. We have found a self-assembled simple rectangular columnar structure (R_S, $p2mm$ symmetry group), similar to those seen before in a system of helical dendrimers [171] and in a system of bolaamphiphiles with flexible lateral chains [172]. It is rather rare and has not been observed in colloidal systems before. Moreover, we have found that the columnar phase can also be switched between different structures via a magnetic-field-induced martensitic transition. The different structures can lead to different properties which can be useful for applications of goethite self-organization. A simple cell model was used to rationalize the observation. The results suggest that it is the competition for free space needed for particle translations and rotations that determines which phase is the most stable. The subtle balance between the two structures can easily be affected by external fields.

Acknowledgements

The staff of the ID02 and BM26 beamlines at ESRF are thanked for their excellent support, NWO and ESRF are acknowledged for the beamtime. EDX was carried out in collaboration with EMU, the Electron Microscopy group at Utrecht University, the Netherlands. Helen de Waard of the department of earth sciences, Geolab, is thanked for ICP OES measurements.

11

Sterically stabilized goethite: phase behavior with and without field

Abstract

The phase behavior of sterically stabilized goethite particles in toluene was studied using small-angle X-ray scattering. It was compared with that of charged particles in water, with and without magnetic field. The phase behavior was found to be similar. Furthermore, the magnetic properties remained the same after coating the particles with amino-functionalized polyisobutylene chains. The difference between the aqueous and toluene samples is that the latter one shows more tendency to form gels. Smaller domains of the different liquid crystalline phases were observed and the columnar phase does not fully develop. Also a higher field is needed to align the full sample.

11.1. Introduction

Aqueous dispersions of charged goethite particles show rich liquid crystalline phase behavior as is shown in this thesis. Nematic, biaxial nematic, smectic A and columnar phases were found in these dispersions. Furthermore, goethite particles have special magnetic properties [28]. They have a permanent magnetic moment along their long axis, but also an induced magnetic moment which is predominantly along the shortest particle axis. Therefore, the particles align parallel to a small magnetic field and perpendicular to a large magnetic field.

In theoretical work, one usually considers purely entropic systems of hard particles. Charged particles have a double layer, that depends on the ionic strength, which influences the effective particle dimensions and gives a softer interaction compared to the hard particle interaction. The effect of the electrostatic repulsion was clearly shown by changing the ionic strength of, for example, TMV and gibbsite dispersions [173, 174]. To get a better comparison with theory, particles with a nearly hard particle interaction can be obtained by sterically stabilizing them with a polymer layer and disperse them in an organic solvent.

Sterically stabilized dispersions were obtained by grafting the particles with amino-functionalized polyisobutylene (PIB) chains. This has already been successful for several inorganic liquid crystalline particles, including goethite [16, 34, 62, 100]. Before, this was usually done by an elaborate method which involves a gradual solvent substitution upon addition of the stabilizing polymer [16, 17, 175]. Here, we use an alternative, recently described method in which the particles are freeze-dried in the presence of the stabilizer [176].

11.2. Experimental

11.2.1. Synthesis

The synthesis of the g35 dispersion is described in Section 2.2.1, that of the g14 system in Section 7.2.1. g13 is comparable but the exact details are unknown. g38 was made using the same method as g35, but with a slightly different iron nitrate concentration (0.08 M for g38 and 0.11 M for g35).

Sterically stabilized dispersions were obtained using amino-modified polyisobutylene stabilizer SAP 230 TP, which has two tails of approximately 17 isobutylene subunits, according to the method described in [176]. Goethite (20 mL, 3% v/v) was added to SAP 230 TP (Infineum, U.K., 5 g), after which 1-propanol (Acros, 99%, 30 mL) was added. The mixture was shaken vigorously until the polymer and particles appeared well dispersed. The solvent was then removed by using a rotational vacuum evaporator and a highly viscous paste was obtained. This paste was spread out as a film at the inside of a round-bottom flask, then frozen in liquid nitrogen and connected to a vacuum

Table 11.1. Goethite particle dimensions

System	$\langle L \rangle$ (nm)	σ_L (%)	$\langle W \rangle$ (nm)	σ_W (%)	$\langle T \rangle$ (nm)	$\langle L \rangle / \langle W \rangle$
g38(p)	307	38	70	31	∼27	4.4
g35(p)	282	35	68	32	∼25	4.1
g14(p)	189	14	57	25	∼17	3.5
g13(p)	215	13	69	20	∼18	3.2

setup. After freeze-drying, a mixture of goethite particles and stabilizing polymer was obtained, which was easily redispersable in toluene (J.T. Baker, 99.5%). Finally, excess SAP 230 TP was removed by three cycles of centrifugation (2 h, 1425g) and redispersion in toluene.

Particle characterization by TEM is described in Section 2.2.2.

11.2.2. SAXS experiments

Sample preparation is discussed in Section 2.2.3. Capillaries were closed by flame sealing and by using glue (Araldite AW 2101). Small-angle X-ray scattering (SAXS) measurements were conducted at the BM26 DUBBLE beamline of the European Synchrotron Radiation Facility (ESRF, Grenoble, France) during measurement sessions in 2008 and 2009. The microradian resolution setup was used [57].

The variable permanent magnet described in Section 3.2.2 was used.

11.3. Results and discussion

The particle dimensions of the systems used are shown in Table 11.1. A part of each of the aqueous dispersion was used to coat the particles with PIB to get sterically stabilized dispersions in toluene (which are called gxxp). The process seems to be successful, since streaming birefringence was observed in the new dispersions. Systems with a low and high polydispersity were studied to get a complete picture of the behavior of these sterically stabilized dispersions.

11.3.1. Low polydispersity

As described in Chapter 2, charge stabilized systems with a low polydispersity form isotropic, nematic and smectic A phases. In sterically stabilized dispersions the same phases were found. The SAXS patterns of the nematic and smectic A phase of the g13p system can be seen in Figure 11.1a and f. For both phases scattering is observed at small angles corresponding to the length correlations; for the smectic phase the scattering peaks are much sharper because of the layerlike ordering and even a second-order ring is vaguely discernible. However, no scattering is observed at larger angles, which is different from the scattering obtained from aqueous dispersions (see Figure 5.3a and Figure 2.1b).

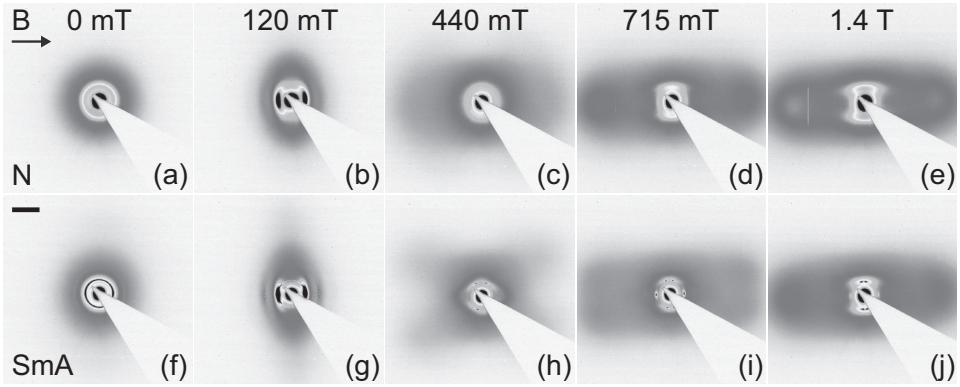

Figure 11.1. SAXS patterns of the nematic and smectic phase of the g13p system in a magnetic field. The scale bar is 0.05 nm^{-1}.

The absence of wide-angle scattering can be caused by the presence of many small domains with all different orientations. This is confirmed by the small-angle scattering which is a full ring. If the broad scattering peak at a large angle is spread over all orientations it is possible that it is not detected because the remaining intensity is too low. In the toluene samples a faster sedimentation of goethite is observed and the particles have a strong tendency to form gels. Liquid crystal phases form at a small scale but it seems that gelation takes place before large domains can form. The polymer layer of about 4 nm [17, 177] makes that the particles will probably be able to come closer together if compared to the charged particles with a Debye length of around 10 nm. Therefore, the van der Waals interaction will be stronger, which might cause the gelation.

In a field of 120 mT, the nematic and smectic phase aligned parallel to the field, as can be seen in Figure 11.1b and g. There was still no clear scattering observed at larger angles, which suggests that the alignment is not as good as in the charge stabilized dispersions. The smectic phase seems to be well aligned because second order peaks are observed. However, a ring is also still visible which implies that domains with all orientations are present even in a magnetic field of 120 mT. Lower in the same sample the smectic phase does not react to this field at all. Apparently, the structure is more gel like than in aqueous dispersions. Applying a field for a longer time might induce a better alignment.

At 440 mT, it can be seen that the particles were changing orientation (Figure 11.1c and h). Going to a field of 715 mT, the nematic phase was mostly aligned perpendicular to the field (Figure 11.1d). The smectic phase still showed domains with different orientations (Figure 11.1i). This behavior is similar to that observed in charge stabilized dispersions (Figure 6.2).

Using high fields (1.4 T), perpendicular alignment was observed everywhere in the sample (Figure 11.1e and j). In the smectic scattering pattern it can be seen that the alignment of the layers was not perfect yet, more time in the field is needed to reach that.

Samples of the charge and sterically stabilized dispersions of g14 were both measured and could be compared. The critical field strength, where the particles change orientation from parallel to perpendicular to the field, is the same for both dispersions. So, the magnetic properties of the particles do not change if coated with PIB. It was shown before that a surfactant layer on ferrofluids can cause spin-pinning, thereby creating a non-magnetic surface layer on the particles [178–180]. Apparently, this is not the case for our particles.

For this system the q-values were used to calculate distances between the particles in charge and sterically stabilized samples. For the small-angle peaks hardly any difference was found, so the particles seem to be at the same distance from each other in the length direction. Wide-angle peaks were only observed in high fields for the PIB-samples, so only those could be compared. At these high fields, the wide-angle peaks of the sterically stabilized samples were at a larger angle, meaning that the particles were closer together (45 nm compared to 60 nm). This confirms the hypothesis made earlier in this section. It might be caused by the shorter range of the interaction. A strong repulsion is present in the toluene samples around 4 nm from the particle surface (4 nm is the thickness of the polymer layer [17, 177]) when the polymer layers start to mix and deform. In the aqueous samples the Debye length is around 10 nm and the interaction is softer.

11.3.2. High polydispersity

Charge stabilized systems with a high polydispersity form isotropic, nematic, smectic A and columnar phases (Chapter 2). In sterically stabilized systems (g35p, g38p) the isotropic, nematic and smectic A (Figure 11.2a) phases were clearly observed as well. Columnar features were also recognized (Figure 11.3), but the scattering rings are not as sharp as expected for a columnar phase. It seems that the system prefers to form the columnar phase, but the particles get stuck before forming a well-defined phase. This supports the hypothesis that gelation takes place in these PIB-systems.

The smectic phase aligned in a magnetic field of 120 mT (Figure 11.2b). Reorientation occurred at 280 mT and domains with different orientations can be observed in the SAXS pattern (Figure 11.2c). In a large magnetic field of 1.4 T, the smectic phase was mostly aligned perpendicular to the field. Besides that, columnar features started to appear (Figure 11.2d). Slightly lower (0.5 mm) in the sample, this can be seen more clearly (Figure 11.4). This behavior is similar to that of charge stabilized dispersions (see Section 6.3.1).

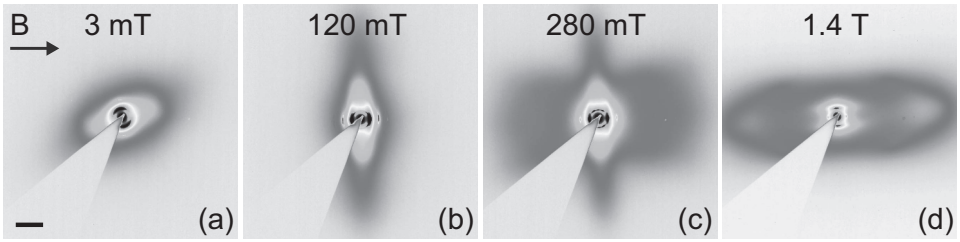

Figure 11.2. SAXS patterns of the smectic phase of the g38p system in a magnetic field. The scale bar is 0.05 nm^{-1}.

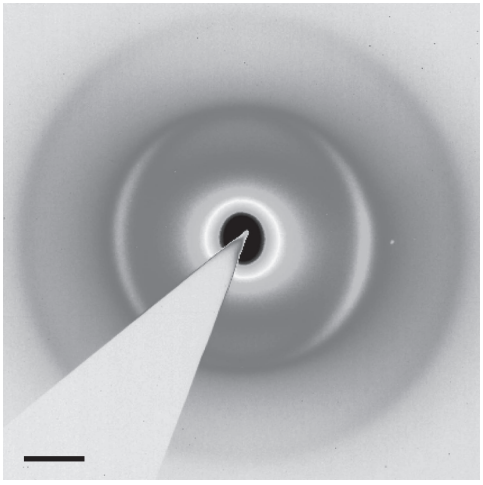

Figure 11.3. SAXS pattern of the columnar phase of the g35p system. The scale bar is 0.05 nm^{-1}.

As for the low polydisperse samples, high fields are needed to orient the full sample. Further down in the capillary the structure seems to be more gel like.

11.4. Conclusions

Sterically stabilized goethite particles in toluene were obtained and their phase behavior was studied. The phase behavior of systems with a low and high polydispersity is comparable to the equivalent aqueous dispersions. The main difference is that the PIB-systems show a stronger tendency to form gels. Therefore, smaller domains are formed and the columnar phase does not fully develop.

In a magnetic field again similar behavior is observed as for the charged systems, showing that the magnetic properties of the particles have not changed. The effect of gelation is also observed here. The lower part of the samples does not react to small fields; fields of around 1 T are needed to align the full sample.

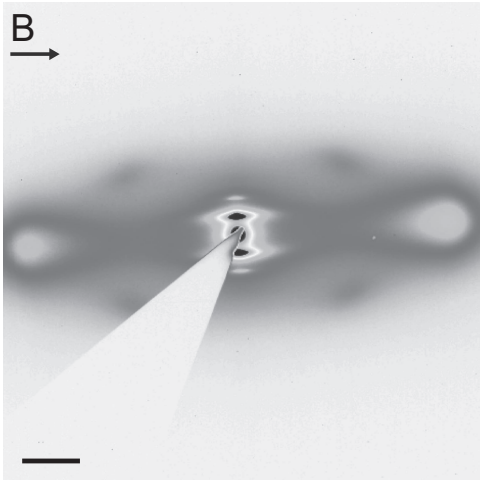

Figure 11.4. SAXS pattern of the smectic / columnar phase of the g38p system in a magnetic field of 1.4 T. The scale bar is 0.05 nm^{-1}.

For platelike particles PIB has proven to be a good stabilizer to prevent gelation and observe isotropic-nematic phase separation in systems that form gels in aqueous environments [17,62,176]. For goethite it seems that the sterically stabilized dispersions have a stronger tendency to form gels than the charge stabilized ones. This might be caused by a stronger van der Waals attraction between the particles. The 4 nm polymer layer is smaller than the 10 nm Debye length of the charged particles, so the particles of high refractive index will get closer to each other.

Acknowledgements

The staff of the BM26 DUBBLE beamline of the ESRF and Dmytro Byelov are acknowledged for their support during SAXS measurements. Maurice Mourad is thanked for his help with the PIB coating procedure.

Bibliography

[1] R. Brown. A brief account of microscopical observations made in the months of June, July and August, 1827, on the particles contained in the pollen of plants; and on the general existence of active molecules in organic and inorganic bodies. *Phil. Mag.*, 4:161–173, 1828.

[2] A. Einstein. Über die von der molekularkinetischen theorie der wärme geforderte bewegung von in ruhenden flüssigkeiten suspendierten teilchen. *Ann. Phys.*, 322(8):549–560, 1905.

[3] J. Perrin. Mouvement brownien et réalité moléculaire. *Ann. Chim. Phys.*, 18:5–114, 1909.

[4] J. Perrin. *Les atomes*. Alcan, Paris, 1913.

[5] A. Vrij, E. A. Nieuwenhuis, H. M. Fijnaut, and W. G. M. Agterof. Application of modern concepts in liquid state theory to concentrated particle dispersions. *Faraday Discuss. Chem. Soc.*, 65:101 – 113, 1978.

[6] W. Poon. Colloids as big atoms. *Science*, 304(5672):830–831, 2004.

[7] P. N. Pusey and W. van Megen. Phase behaviour of concentrated suspensions of nearly hard colloidal spheres. *Nature*, 320(6060):340–342, 1986.

[8] F. Reinitzer. Beiträge zur kenntniss des cholesterins. *Monatsh. Chem. / Chem. Monthly*, 9(1):421–441, 1888.

[9] O. Lehmann. Über fliessende krystalle. *Z. Phys. Chem.*, 4:462472, 1889.

[10] A. S. Sonin. Inorganic lyotropic liquid crystals. *J. Mater. Chem.*, 8(12):2557–2574, 1998.

[11] J. C. P. Gabriel and P. Davidson. New trends in colloidal liquid crystals based on mineral moieties. *Adv. Mater.*, 12(1):9–20, 2000.

[12] P. Davidson and J. C. P. Gabriel. Mineral liquid crystals. *Curr. Opin. Colloid Interface Sci.*, 9:377–383, 2005.

[13] H. Zocher. Concerning the spontaneous formation of structure in sols. *Z. Anorg. Allg. Chem.*, 147:91, 1925.

[14] I. Langmuir. The role of attractive and repulsive forces in the formation of tactoids, thixotropic gels, protein crystals and coacervates. *J. Chem. Phys.*, 6(12):873–896, 1938.

[15] Y. Maeda and S. Hachisu. Structure of schiller layers in β-FeOOH sols: Observation by scanning electron microscope. *Colloids Surf.*, 7(4):357–360, 1983.

[16] P. A. Buining and H. N. W. Lekkerkerker. Isotropic-nematic phase separation of a dispersion of organophilic boehmite rods. *J. Phys. Chem.*, 97(44):11510–11516, 1993.

[17] F. M. van der Kooij and H. N. W. Lekkerkerker. Formation of nematic liquid crystals in suspensions of hard colloidal platelets. *J. Phys. Chem. B*, 102(40):7829–7832, 1998.

[18] D. van der Beek and H. N. W. Lekkerkerker. Liquid crystal phases of charged colloidal platelets. *Langmuir*, 20:8582–8586, 2004.

[19] Z. Liu, J. Zhang, N. Wang, W. Liu, C. Zhang, and D. Sun. Liquid-crystalline phases of colloidal dispersions of layered double hydroxides. *Chem. Mater.*, 15:3240–3241, 2003.

[20] L. Onsager. The effects of shape on the interaction of colloidal particles. *Ann. N. Y. Acad. Sci.*, 51:627–659, 1949.

[21] S. Krehula, S. Popović, and S. Musić. Synthesis of acicular α-FeOOH particles at a very high pH. *Mater. Lett.*, 54:108–113, 2002.

[22] N. O. Nuñez, P. Tartaj, M. P Morales, R. Pozas, M. Ocaña, and C. J. Serna. Preperation, characterization, and magnetic properties of Fe-based alloy particles with elongated morphology. *Chem. Mater.*, 15:3558–3563, 2003.

[23] Q. Majorana. Sur la biréfringence magnétique. *C. R. Acad. Sci.*, 135:159, 1902.

[24] A. Cotton and H. Mouton. Sur les propriétés magnéto-optiques des colloides et des liqueurs hétérogènes. *Ann. Chim. Phys.*, 11:145, 1907.

[25] M. Faraday. Experimental researches in electricity. Nineteenth series. *Philos. Trans. R. Soc.*, 136:1–20, 1846.

[26] Q. Majorana. Su due nuovi fenomeni magneto-ottici osservati normalmente alle linee di forza. *Rend. Accad. Lincei*, 11-1:374, 1902.

[27] A. Cotton and Q. Majorana. Sur le phénomène de Majorana. *C. R. Acad. Sci.*, 141:317, 1905.

[28] B. J. Lemaire, P. Davidson, J. Ferré, J. P. Jamet, P. Panine, I. Dozov, and J. P. Jolivet. Outstanding magnetic properties of nematic suspensions of goethite (α-FeOOH) nanorods. *Phys. Rev. Lett.*, 88(12):125507, 2002.

[29] B. J. Lemaire, P. Davidson, J. Ferré, J. P. Jamet, D. Petermann, P. Panine, I. Dozov, and J. P. Jolivet. Physical properties of aqueous suspensions of goethite (α-FeOOH) nanorods: Part I: In the isotropic phase. *Eur. Phys. J. E*, 13:291–308, 2004.

[30] B. J. Lemaire, P. Davidson, D. Petermann, P. Panine, I. Dozov, D. Stoenescu, and J. P. Jolivet. Physical properties of aqueous suspensions of goethite (α-FeOOH) nanorods: Part II: In the nematic phase. *Eur. Phys. J. E*, 13:309–319, 2004.

[31] B. J. Lemaire, P. Davidson, P. Panine, and J. P. Jolivet. Magnetic-field-induced nematic-columnar phase transition in aqueous suspensions of goethite (α-FeOOH) nanorods. *Phys. Rev. Lett.*, 93:267801, 2004.

[32] B. J. Lemaire, P. Davidson, J. Ferré, J. P. Jamet, D. Petermann, P. Panine, I. Dozov, D. Stoenescu, and J. P. Jolivet. The complex phase behavior of suspensions of goethite (α-FeOOH) nanorods in a magnetic field. *Faraday Discuss.*, 128:271–283, 2005.

[33] G. J. Vroege, D. M. E. Thies-Weesie, A. V. Petukhov, B. J. Lemaire, and P. Davidson. Smectic liquid-crystalline order in suspensions of highly polydisperse goethite nanorods. *Adv. Mater.*, 18:2565–2568, 2006.

[34] D. M. E. Thies-Weesie, J. P. de Hoog, M. H. Hernandez Mendiola, A. V. Petukhov, and G. J. Vroege. Synthesis of goethite as a model colloid for mineral liquid crystals. *Chem. Mater.*, 19:5538–5546, 2007.

[35] Z. Dogic and S. Fraden. Smectic phase in a colloidal suspension of semiflexible virus particles. *Phys. Rev. Lett.*, 78(12):2417, 1997.

[36] Z. Dogic and S. Fraden. Ordered phases of filamentous viruses. *Curr. Opin. Colloid Interface Sci.*, 11(1):47–55, 2006.

[37] M. P. Lettinga, K. Kang, P. Holmqvist, A. Imhof, D. Derks, and J. K. G. Dhont. Nematic-isotropic spinodal decomposition kinetics of rodlike viruses. *Phys. Rev. E*, 73(1):11412, 2006.

[38] M. P. Lettinga and E. Grelet. Self-diffusion of rodlike viruses through smectic layers. *Phys. Rev. Lett.*, 99(19):197802, 2007.

[39] P. G. Bolhuis and D. A. Kofke. Monte Carlo study of freezing of polydisperse hard spheres. *Phys. Rev. E*, 54(1):634, 1996.

[40] P. Bartlett and P. B. Warren. Reentrant melting in polydispersed hard spheres. *Phys. Rev. Lett.*, 82(9):1979, 1999.

[41] M. A. Bates and D. Frenkel. Influence of polydispersity on the phase behavior of colloidal liquid crystals: A Monte Carlo simulation study. *J. Chem. Phys.*, 109(14):6193–6199, 1998.

[42] H. N. W. Lekkerkerker, Ph. Coulon, R. Van Der Haegen, and R. Deblieck. On the isotropic-liquid crystal phase separation in a solution of rodlike particles of different lengths. *J. Chem. Phys.*, 80(7):3427–3433, 1984.

[43] T. Odijk and H. N. W. Lekkerkerker. Theory of the isotropic-liquid crystal phase separation for a solution of bidisperse rodlike macromolecules. *J. Phys. Chem.*, 89:2090–2096, 1985.

[44] A. Speranza and P. Sollich. Simplified Onsager theory for isotropic-nematic phase equilibria of length polydisperse hard rods. *J. Chem. Phys.*, 117(11):5421–5436, 2002.

[45] A. Speranza and P. Sollich. Isotropic-nematic phase equilibria of polydisperse hard rods: the effect of fat tails in the length distribution. *J. Chem. Phys.*, 118(11):5213–5223, 2003.

[46] A. Speranza and P. Sollich. Isotropic-nematic phase equilibria in the Onsager theory of hard rods with length polydispersity. *Phys. Rev. E*, 67(6):61702, 2003.

[47] H. H. Wensink and G. J. Vroege. Isotropic-nematic phase behavior of length-polydisperse hard rods. *J. Chem. Phys.*, 119(13):6868–6882, 2003.

[48] M. Fasolo and P. Sollich. Equilibrium phase behavior of polydisperse hard spheres. *Phys. Rev. Lett.*, 91(6):68301, 2003.

[49] R. M. L. Evans, D. J. Fairhurst, and W. C. K. Poon. Universal law of fractionation for slightly polydisperse systems. *Phys. Rev. Lett.*, 81(6):1326–1329, 1998.

[50] F. M. van der Kooij, M. Vogel, and H. N. W. Lekkerkerker. Phase behavior of a mixture of platelike colloids and nonadsorbing polymer. *Phys. Rev. E*, 62(4):5397–5402, 2000.

[51] H. H. Wensink and H. N. W. Lekkerkerker. Sedimentation and multi-phase equilibria in mixtures of platelets and ideal polymer. *Europhys. Lett.*, 66(1):125–131, 2004.

[52] L. Bellier-Castella and H. Xu. Sedimentation profiles of polydisperse fluids. *J. Phys. Condens. Matter*, 15(32):5417–5428, 2003.

[53] H. Maeda and Y. Maeda. Atomic force microscopy studies for investigating the smectic structures of colloidal crystals of beta-FeOOH. *Langmuir*, 12(6):1446–1452, 1996.

[54] H. Maeda and Y. Maeda. Liquid crystal formation in suspensions of hard rodlike colloidal particles: Direct observation of particle arrangement and self-ordering behavior. *Phys. Rev. Lett.*, 90(1):018303, 2003.

[55] H. Maeda and Y. Maeda. Measurement of density distributions for colloidal β-FeOOH rods in suspensions exhibiting phase separation: The role of long-range forces in smectic ordering. *J. Chem. Phys.*, 121(24):12655–12665, 2004.

[56] W. Bras, I. P. Dolbnya, D. Detollenaere, R. van Tol, M. Malfois, G. N. Greaves, A. J. Ryan, and E. Heeley. Recent experiments on a combined small-angle/wide-angle X-ray scattering beam line at the ESRF. *J. Appl. Crystallogr.*, 36:791–794, 2003.

[57] A. V. Petukhov, J. H. H. Thijssen, D. C. 't Hart, A. Imhof, A. van Blaaderen, I. P. Dolbnya, A. Snigirev, A. Moussaid, and I. Snigireva. Microradian X-ray diffraction in colloidal photonic crystals. *J. Appl. Crystallogr.*, 39:137–144, 2006.

[58] J. S. van Duijneveldt and M. P. Allen. Free energy barriers for interlayer diffusion in the smectic-A phase of hard spherocylinders. *Mol. Phys.*, 90:243–250, 1997.

[59] A. Stroobants, H. N. W. Lekkerkerker, and D. Frenkel. Evidence for one-, two-, and three-dimensional order in a system of hard parallel spherocylinders. *Phys. Rev. A*, 36(6):2929, 1987.

[60] R. van Roij, P. Bolhuis, B. Mulder, and D. Frenkel. Transverse interlayer order in lyotropic smectic liquid crystals. *Phys. Rev. E*, 52(2):R1277, 1995.

[61] X. Wen, R. B. Meyer, and D. L. D. Caspar. Observation of smectic-A ordering in a solution of rigid-rod-like particles. *Phys. Rev. Lett.*, 63(25):2760, 1989.

[62] Z. X. Zhang and J. S. van Duijneveldt. Isotropic-nematic phase transition of nonaqueous suspensions of natural clay rods. *J. Chem. Phys.*, 124(15):154910, 2006.

[63] T. Yu, J. Park, J. Moon, K. An, Y. Piao, and T. Hyeon. Synthesis of uniform goethite nanotubes with parallelogram cross section. *J. Am. Chem. Soc.*, 129:14558–14559, 2007.

[64] L. J. Yu and A. Saupe. Observation of a biaxial nematic phase in potassium laurate-1-decanol-water mixtures. *Phys. Rev. Lett.*, 45(12):1000, 1980.

[65] G. R. Luckhurst. Liquid crystals - A missing phase found at last? *Nature*, 430(6998):413–414, 2004.

[66] J.-H. Lee, T.-K. Lim, W.-T. Kim, and J.-I. Jin. Dynamics of electro-optical switching processes in surface stabilized biaxial nematic phase found in bent-core liquid crystal. *J. Appl. Phys.*, 101(3):34105, 2007.

[67] L. M. Blinov. On the way to polar achiral liquid crystals. *Liq. Cryst.*, 24:143–152, 1998.

[68] T. Watanabe, S. Miyata, T. Furukawa, H. Takezoe, T. Nishi, M. Sone, A. Migita, and J. Watanabe. Nematic liquid crystals with polar ordering formed from simple aromatic polyester. *Jpn. J. Appl. Phys. Part 2*, 35(4B):505–507, 1996.

[69] O. Francescangeli, V. Stanic, S. I. Torgova, A. Strigazzi, N. Scaramuzza, C. Ferrero, I. P. Dolbnya, T. M. Weiss, R. Berardi, L. Muccioli, S. Orlandi, and C. Zannoni. Ferroelectric response and induced biaxiality in the nematic phase of a bent-core mesogen. *Adv. Funct. Mater.*, 19(16):2592–2600, 2009.

[70] M. J. Freiser. Ordered states of a nematic liquid. *Phys. Rev. Lett.*, 24(19):1041, 1970.

[71] R. Alben. Phase transitions in a fluid of biaxial particles. *Phys. Rev. Lett.*, 30(17):778, 1973.

[72] J. P. Straley. Ordered phases of a liquid of biaxial particles. *Phys. Rev. A*, 10(5):1881, 1974.

[73] F. Biscarini, C. Chiccoli, P. Pasini, F. Semeria, and C. Zannoni. Phase diagram and orientational order in a biaxial lattice model: a Monte Carlo study. *Phys. Rev. Lett.*, 75(9):1803, 1995.

[74] P. J. Camp and M. P. Allen. Phase diagram of the hard biaxial ellipsoid fluid. *J. Chem. Phys.*, 106(16):6681–6688, 1997.

[75] M. P. Taylor and J. Herzfeld. Nematic and smectic order in a fluid of biaxial hard particles. *Phys. Rev. A*, 44(6):3742, 1991.

[76] A. G. Vanakaras, M. A. Bates, and D. J. Photinos. Theory and simulation of biaxial nematic and orthogonal smectic phases formed by mixtures of board-like molecules. *Phys. Chem. Chem. Phys.*, 5(17):3700–3706, 2003.

[77] C. M. Care and D. J. Cleaver. Computer simulation of liquid crystals. *Rep. Prog. Phys.*, 68(11):2665–2700, 2005.

[78] C. McBride and E. Lomba. Hard biaxial ellipsoids revisited: Numerical results. *Fluid Phase Equilib.*, 255(1):37–45, 2007.

[79] R. Berardi, L. Muccioli, S. Orlandi, M. Ricci, and C. Zannoni. Computer simulations of biaxial nematics. *J. Phys. Condens. Matter*, 20(46):463101, 2008.

[80] R. Alben. Liquid crystal phase transitions in mixtures of rodlike and platelike molecules. *J. Chem. Phys.*, 59(8):4299–4304, 1973.

[81] A. Cuetos, A. Galindo, and G. Jackson. Thermotropic biaxial liquid crystalline phases in a mixture of attractive uniaxial rod and disk particles. *Phys. Rev. Lett.*, 101(23):237802, 2008.

[82] A. Stroobants and H. N. W. Lekkerkerker. Liquid crystal phase transitions in a solution of rodlike and disklike particles. *J. Phys. Chem.*, 88(16):3669–3674, 1984.

[83] P. J. Camp, M. P. Allen, P. G. Bolhuis, and D. Frenkel. Demixing in hard ellipsoid rod-plate mixtures. *J. Chem. Phys.*, 106(22):9270–9275, 1997.

[84] H. H. Wensink, G. J. Vroege, and H. N. W. Lekkerkerker. Biaxial versus uniaxial nematic stability in asymmetric rod-plate mixtures. *Phys. Rev. E*, 66(4):41704, 2002.

[85] S. Varga, A. Galindo, and G. Jackson. Ordering transitions, biaxiality, and demixing in the symmetric binary mixture of rod and plate molecules described with the Onsager theory. *Phys. Rev. E*, 66(1):11707, 2002.

[86] Y. Galerne, A. M. Figueiredo Neto, and L. Liebert. Microscopical structure of the uniaxial and biaxial lyotropic nematics. *J. Chem. Phys.*, 87(3):1851–1856, 1987.

[87] L. A. Madsen, T. J. Dingemans, M. Nakata, and E. T. Samulski. Thermotropic biaxial nematic liquid crystals. *Phys. Rev. Lett.*, 92(14):145505, 2004.

[88] B. R. Acharya, A. Primak, and S. Kumar. Biaxial nematic phase in bent-core thermotropic mesogens. *Phys. Rev. Lett.*, 92(14):145506, 2004.

[89] G. R. Luckhurst. Biaxial nematic liquid crystals: fact or fiction? *Thin Solid Films*, 393(1-2):40–52, 2001.

[90] Y. Galerne. Comment on "Thermotropic biaxial nematic liquid crystals". *Phys. Rev. Lett.*, 96(21):219803, 2006.

[91] L. A. Madsen, T. J. Dingemans, M. Nakata, and E. T. Samulski. Madsen et al. reply. *Phys. Rev. Lett.*, 96(21):219804, 2006.

[92] K. Van Le, M. Mathews, M. Chambers, J. Harden, Q. Li, H. Takezoe, and A. Jakli. Electro-optic technique to study biaxiality of liquid crystals with positive dielectric anisotropy: The case of a bent-core material. *Phys. Rev. E*, 79(3):30701, 2009.

[93] N. Vaupotic, J. Szydlowska, M. Salamonczyk, A. Kovarova, J. Svoboda, M. Osipov, D. Pociecha, and E. Gorecka. Structure studies of the nematic phase formed by bent-core molecules. *Phys. Rev. E*, 80(3):30701, 2009.

[94] H. F. Leube and H. Finkelmann. Optical investigations on a liquid-crystalline side-chain polymer with biaxial nematic and biaxial smectic A phase. *Makromol. Chem.*, 192(6):1317–1328, 1991.

[95] R. Pratibha, N. V. Madhusudana, and B. K. Sadashiva. An orientational transition of bent-core molecules in an anisotropic matrix. *Science*, 288(5474):2184–2187, 2000.

[96] T. Hegmann, J. Kain, S. Diele, G. Pelzl, and C. Tschierske. Evidence for the existence of the McMillan phase in a binary system of a metallomesogen and 2,4,7-trinitrofluorenone. *Angew. Chem.*, 113(5):911–914, 2001.

[97] X. Commeinhes, P. Davidson, C. Bourgaux, and J. Livage. Orientation of liquid-crystalline suspensions of vanadium pentoxide ribbons by a magnetic field. *Advanced Materials*, 9(11):900–903, 1997.

[98] D. van der Beek, A. V. Petukhov, P. Davidson, J. Ferre, J. P. Jamet, H. H. Wensink, G. J. Vroege, W. Bras, and H. N. W. Lekkerkerker. Magnetic-field-induced orientational order in the isotropic phase of hard colloidal platelets. *Phys. Rev. E*, 73(4):41402, 2006.

[99] L. J. Michot, I. Bihannic, S. Maddi, S. S. Funari, C. Baravian, P. Levitz, and P. Davidson. Liquid-crystalline aqueous clay suspensions. *Proc. Natl. Acad. Sci.*, 103(44):16101–16104, 2006.

[100] F. M. van der Kooij, K. Kassapidou, and H. N. W. Lekkerkerker. Liquid crystal phase transition in suspensions of polydisperse plate-like particles. *Nature*, 406:868–871, 2000.

[101] O. Pelletier, C. Bourgaux, O. Diat, P. Davidson, and J. Livage. A biaxial nematic gel phase in aqueous vanadium pentoxide suspensions. *Eur. Phys. J. B*, 12(4):541–546, 1999.

[102] V. Petkov, P. N. Trikalitis, E. S. Bozin, S. J. L. Billinge, T. Vogt, and M. G. Kanatzidis. Structure of $V_2O_5{\cdot}nH_2O$ xerogel solved by the atomic pair distribution function technique. *J. Am. Chem. Soc.*, 124(34):10157–10162, 2002.

[103] E. van den Pol, A. V. Petukhov, D. M. E. Thies-Weesie, D. V. Byelov, and G. J. Vroege. Experimental realization of biaxial liquid crystal phases in colloidal dispersions of boardlike particles. *Phys. Rev. Lett.*, 103(25):258301, 2009.

[104] T. Narayanan, O. Diat, and P. Bösecke. SAXS and USAXS on the high brilliance beamline at the ESRF. *Nucl. Instrum. Meth. A*, 467-468(Part 2):1005–1009, 2001.

[105] S. Fraden, A. J. Hurd, R. B. Meyer, M. Cahoon, and D. L. D. Caspar. Magnetic-field-induced alignment and instabilities in ordered colloids of tobacco mosaic virus. *J. Phys. Colloq.*, 46(C3):85–113, 1985.

[106] P. G. de Gennes and J. Prost. *The physics of liquid crystals*. Clarendon, Oxford, U.K., 1995.

[107] E. van den Pol, D. M. E. Thies-Weesie, A. V. Petukhov, P. Panine, and G. J. Vroege. Chromium-modified goethite in an external magnetic field. *J. Phys. Condens. Matter*, 20:404219, 2008.

[108] E. van den Pol, D. M. E. Thies-Weesie, A. V. Petukhov, G. J. Vroege, and K. Kvashnina. Influence of polydispersity on the phase behavior of colloidal goethite. *J. Chem. Phys.*, 129(16):164715, 2008.

[109] J. Als-Nielsen, R. J. Birgeneau, M. Kaplan, J. D. Litster, and C. R. Safinya. Experimental observation of anomalous ordering in a Landau-Peierls system. *Phys. Rev. Lett.*, 39(26):1668, 1977.

[110] J. Als-Nielsen, J. D. Litster, R. J. Birgeneau, M. Kaplan, C. R. Safinya, A. Lindegaard-Andersen, and S. Mathiesen. Observation of algebraic decay of positional order in a smectic liquid crystal. *Phys. Rev. B*, 22(1):312, 1980.

[111] V. M. Kaganer, B. I. Ostrovskii, and W. H. de Jeu. X-ray scattering in smectic liquid crystals: From ideal- to real-structure effects. *Phys. Rev. A*, 44(12):8158, 1991.

[112] C. R. Safinya, D. Roux, G. S. Smith, S. K. Sinha, P. Dimon, N. A. Clark, and A. M. Bellocq. Steric interactions in a model multimembrane system: A synchrotron X-ray study. *Phys. Rev. Lett.*, 57(21):2718, 1986.

[113] G. S. Smith, C. R. Safinya, D. Roux, and N. A. Clark. X-ray study of freely suspended films of a multilamellar lipid system. *Mol. Cryst. Liq. Cryst.*, 144:235–255, 1987.

[114] D. C. Wack and W. W. Webb. Measurement by x-ray diffraction methods of the layer compressional elastic constant B in the lyotropic smectic-A (L_α) phase of the lecithin-water system. *Phys. Rev. A*, 40(3):1627, 1989.

[115] P. Bassereau, J. Marignan, G. Porte, and R. May. Experimental measure of the anisotropy of the Bragg singularity in lyotropic smectics. *Europhys. Lett.*, 15(7):753, 1991.

[116] T. Salditt, M. Vogel, and W. Fenzl. Thermal fluctuations and positional correlations in oriented lipid membranes. *Phys. Rev. Lett.*, 90(17):178101, 2003.

[117] E. Schneck, F. Rehfeldt, R. G. Oliveira, C. Gege, B. Demé, and M. Tanaka. Modulation of intermembrane interaction and bending rigidity of biomembrane models via carbohydrates investigated by specular and off-specular neutron scattering. *Phys. Rev. E*, 78(6):061924, 2008.

[118] E. Schneck, R. G. Oliveira, F. Rehfeldt, B. Demé, K. Brandenburg, U. Seydel, and M. Tanaka. Mechanical properties of interacting lipopolysaccharide membranes from bacteria mutants studied by specular and off-specular neutron scattering. *Phys. Rev. E*, 80(4):041929, 2009.

[119] E. Nachaliel, E. N. Keller, D. Davidov, and C. Boeffel. Algebraic dependence of the structure factor and possible anharmonicity in a high-resolution x-ray study of a side-group polymeric liquid crystal. *Phys. Rev. A*, 43(6):2897, 1991.

[120] P. Ŝtêpánek, F. Nallet, O. Diat, K. Almdal, and P. Panine. Undulation properties of the lamellar phase of a diblock copolymer: SAXS experiments. *Macromol.*, 35(19):7287–7292, 2002.

[121] E. P. Obraztsov, A. S. Muresan, B. I. Ostrovskii, and W. H. de Jeu. Road to disorder in smectic elastomers. *Phys. Rev. E*, 77(2):021706, 2008.

[122] P. M. Chaikin and T. C. Lubensky. *Principles of condensed matter physics*. Cambridge University Press, 1995.

[123] B. T. M. Willis and A. W. Pryor. *Thermal vibrations in crystallography*. Cambridge University Press, 1975.

[124] P. Davidson. Private communication, 2009.

[125] E. van den Pol, D. M. E. Thies-Weesie, A. V. Petukhov, D. V. Byelov, and G. J. Vroege. Uniaxial and biaxial liquid crystal phases in colloidal dispersions of boardlike particles. *Liq. Cryst.*, Accepted for publication.

[126] E. van den Pol, A. V. Petukhov, D. M. E. Thies-Weesie, and G. J. Vroege. Simple rectangular columnar phase of goethite nanorods and its martensitic transition to the centered rectangular columnar phase. *Langmuir*, 26(3):15791582, 2010.

[127] J. W. Emsley, J. E. Long, G. R. Luckhurst, and P. Pedrielli. Magnetic field induced alignment of the directors of a smectic-A liquid crystal. *Phys. Rev. E*, 60(2):1831, 1999.

[128] J. W. Emsley, G. R. Luckhurst, and P. Pedrielli. Magnetic field induced alignment of the director in a smectic A phase: surface effects. *Chem. Phys. Lett.*, 320(3-4):255–261, 2000.

[129] W. Bras, J. W. Emsley, Y. K. Levine, G. R. Luckhurst, J. M. Seddon, and B. A. Timimi. Field-induced alignment of a smectic-A phase: A time-resolved X-ray diffraction investigation. *J. Chem. Phys.*, 121(9):4397–4413, 2004.

[130] P. D. Brimicombe, S. D. Siemianowski, S. Jaradat, Y. K. Levine, P. Thompson, W. Bras, and H. F. Gleeson. Time-resolved X-ray studies of the dynamics of smectic-A layer realignment by magnetic fields. *Phys. Rev. E*, 79(3):31706, 2009.

[131] C. Rau, V. Crecea, K. M. Peterson, P. R. Jemian, C. P. Richter, U. Neuhäusler, G. Schneider, X. Yu, P. V. Braun, and I. K. Robinson. A full-field KB-FZP microscope for hard X-ray imaging with sub-100 nm resolution. *Proc. 8th Int. Conf. X-ray Microscopy; IPAP Conf. Series*, 7:7–8, 2006.

[132] A. Snigirev, V. Kohn, I. Snigireva, and B. Lengeler. A compound refractive lens for focusing high-energy X-rays. *Nature*, 384(6604):49–51, 1996.

[133] V. Kohn, I. Snigireva, and A. Snigirev. Diffraction theory of imaging with X-ray compound refractive lens. *Opt. Commun.*, 216(4-6):247–260, 2003.

[134] M. Drakopoulos, A. Snigirev, I. Snigireva, and J. Schilling. X-ray high-resolution diffraction using refractive lenses. *Appl. Phys. Lett.*, 86(1):014102, 2005.

[135] D. V. Byelov et al. To be published.

[136] A. Abe and P. J. Flory. Statistical thermodynamics of mixtures of rodlike particles. 2. Ternary systems. *Macromol.*, 11(6):1122–1126, 1978.

[137] T. M. Birshtein, B. I. Kolegov, and V. A. Pryamitsyn. Theory of athermal lyotropic liquid crystal systems. *Polym. Sci. USSR*, 30(2):316–324, 1988.

[138] G. J. Vroege and H. N. W. Lekkerkerker. Theory of the isotropic-nematic-nematic phase separation for a solution of bidisperse rodlike particles. *J. Phys. Chem.*, 97(14):3601–3605, 1993.

[139] R. van Roij and B. Mulder. Demixing versus ordering in hard-rod mixtures. *Phys. Rev. E*, 54(6):6430, 1996.

[140] R. van Roij and B. Mulder. Absence of high-density consolute point in nematic hard rod mixtures. *J. Chem. Phys.*, 105(24):11237–11245, 1996.

[141] R. van Roij, B. Mulder, and M. Dijkstra. Phase behavior of binary mixtures of thick and thin hard rods. *Physica A*, 261(3-4):374–390, 1998.

[142] P. C. Hemmer. Phase transitions in a solution of rodlike macromolecules of two different sizes. *Mol. Phys.*, 96(8):1153 – 1157, 1999.

[143] S. Varga, A. Galindo, and G. Jackson. New types of phase behaviour in binary mixtures of hard rod-like particles. *Mol. Phys.*, 101(6):817–825, 2003.

[144] H. H. Wensink and G. J. Vroege. Demixing in binary mixtures of anisometric colloids. *J. Phys. Condens. Matter*, 16:S2015, 2004.

[145] S. Varga, K. Purdy, A. Galindo, S. Fraden, and G. Jackson. Nematic-nematic phase separation in binary mixtures of thick and thin hard rods: Results from Onsager-like theories. *Phys. Rev. E*, 72(5):51704, 2005.

[146] G. J. Vroege and H. N. W. Lekkerkerker. Phase transitions in lyotropic colloidal and polymer liquid crystals. *Rep. Prog. Phys.*, 55(8):1241–1309, 1992.

[147] T. Odijk. Osmotic pressure of a nematic solution of polydisperse rod-like macromolecules. *Liquid Crystals*, 1(1):97–100, 1986.

[148] K. R. Purdy, S. Varga, A. Galindo, G. Jackson, and S. Fraden. Nematic phase transitions in mixtures of thin and thick colloidal rods. *Phys. Rev. Lett.*, 94(5):57801, 2005.

[149] T. Itou and A. Teramoto. Triphase equilibrium in aqueous solutions of the rodlike polysaccharide schizophyllan. *Macromol.*, 17(7):1419–1420, 1984.

[150] J. Tang and S. Fraden. Magnetic-field-induced isotropic-nematic phase transition in a colloidal suspension. *Phys. Rev. Lett.*, 71(21):3509, 1993.

[151] D. van der Beek, P. Davidson, H. H. Wensink, G. J. Vroege, and H. N. W. Lekkerkerker. Influence of a magnetic field on the nematic phase of hard colloidal platelets. *Phys. Rev. E*, 77(3):031708, 2008.

[152] H. H. Wensink and G. J. Vroege. Nematic order of model goethite nanorods in a magnetic field. *Phys. Rev. E*, 72(3):31708, 2005.

[153] H. H. Wensink. Private communication, 2009.

[154] D. G. A. L. Aarts. The interface in demixed colloid-polymer systems: wetting, waves and droplets. *Soft Matter*, 3(1):19–23, 2007.

[155] J. Hanus. Effect of the molecular interaction between anisotropic molecules on the optical Kerr effect. Field-induced phase transition. *Phys. Rev.*, 178(1):420, 1969.

[156] A. R. Khokhlov and A. N. Semenov. Influence of external field on the liquid-crystalline ordering in solutions of stiff-chain macromolecules. *Macromol.*, 15:1272–1277, 1982.

[157] R. M. Cornell and U. Schwertmann. *The iron oxides*. VCH, Weinheim, 1996.

[158] U. Schwertmann and R. M. Cornell. *Iron oxides in the laboratory: preparation and characterization*. Wiley-VCH, Weinheim, second edition, 2000.

[159] U. Schwertmann, U. Gasser, and H. Sticher. Chromium-for-iron substitution in synthetic goethites. *Geochim. Cosmochim. Acta*, 53(6):1293–1297, 1989.

[160] E. E. Sileo, A. Y. Ramos, G. E. Magaz, and M. A. Blesa. Long range vs. short-range ordering in synthetic Cr-substituted goethites. *Geochim. Cosmochim. Acta*, 68(14):3053–3063, 2004.

[161] N. O. Nuñez, R. Pozas, M. P Morales, P. Tartaj, P. Bonville, A. R. González-Elipe, A. Caballero, M. Ocaña, and C. J. Serna. Acicular metallic particles obtained from Al-doped goethite precursors. *Chem. Mater.*, 15:951–957, 2003.

[162] R. Pozas, T. C. Rojas, M. Ocaña, and C. J. Serna. The nature of Co in synthetic Co-substituted goethites. *Clays Clay Miner.*, 52(6):760–766, 2004.

[163] Q. Liu, J. Torrent, Y. Yu, and C. Deng. Mechanism of the parasitic remanence of aluminous goethite [α-(Fe, Al)OOH]. *J. Geophys. Res.*, 109, 2004.

[164] S. Chandrasekhar and G. S. Ranganath. Discotic liquid-crystals. *Rep. Prog. Phys.*, 53(1):57–84, 1990.

[165] D. van der Beek, A. V. Petukhov, S. M. Oversteegen, G. J. Vroege, and H. N. W. Lekkerkerker. Evidence of the hexagonal columnar liquid-crystal phase of hard colloidal platelets by high-resolution SAXS. *Eur. Phys. J. E*, 16(3):253–258, 2005.

[166] V. Luzzati and F. Husson. The structure of the liquid-crystalline phases of lipid-water systems. *J. Cell Biol.*, 12:207–219, 1962.

[167] F. Livolant, A. M. Levelut, J. Doucet, and J. P. Benoit. The highly concentrated liquid-crystalline phase of DNA is columnar hexagonal. *Nature*, 339(6227):724–726, 1989.

[168] F. Livolant and A. Leforestier. Condensed phases of DNA: structures and phase transitions. *Prog. Polym. Sci.*, 21(6):1115–1164, 1996.

[169] E. Grelet. Hexagonal order in crystalline and columnar phases of hard rods. *Phys. Rev. Lett.*, 100(16):168301, 2008.

[170] C. Tschierske. Liquid crystal engineering - new complex mesophase structures and their relations to polymer morphologies, nanoscale patterning and crystal engineering. *Chem. Soc. Rev.*, 36:1930–1970, 2007.

[171] V. Percec, M. Glodde, T. K. Bera, Y. Miura, I. Shiyanovskaya, K. D. Singer, V. S. K. Balagurusamy, P. A. Heiney, I. Schnell, A. Rapp, H. W. Spiess, S. D. Hudson, and H. Duan. Self-organization of supramolecular helical dendrimers into complex electronic materials. *Nature*, 417(6905):384–387, 2002.

[172] M. Prehm, S. Diele, M. K. Das, and C. Tschierske. Correlated layer structures: a novel type of liquid crystalline phase with 2D-lattice. *J. Am. Chem. Soc.*, 125(3):614–615, 2003.

[173] S. Fraden, G. Maret, and D. L. D. Caspar. Angular correlations and the isotropic-nematic phase transition in suspensions of tobacco mosaic virus. *Phys. Rev. E*, 48(4):2816, 1993.

[174] M. C. D. Mourad, J. E. G. J. Wijnhoven, D. D. van 't Zand, D. van der Beek, and H. N. W. Lekkerkerker. Gelation versus liquid crystal phase transitions in suspensions of plate-like particles. *Philos. Trans. R. Soc. A*, 364(1847):2807–2816, 2006.

[175] C. Pathmamanoharan. Preparation of monodisperse polyisobutene grafted silica dispersion. *Colloids Surf.*, 34(1):81–88, 1988.

[176] M. C. D. Mourad, E. J. Devid, M. M. van Schooneveld, C. Vonk, and H. N. W. Lekkerkerker. Formation of nematic liquid crystals of sterically stabilized layered double hydroxide platelets. *J. Phys. Chem. B*, 112(33):10142–10152, 2008.

[177] C. Smits, W. Briels, J. Dhont, and H. Lekkerkerker. Influence of the stabilizing coating on the rate of crystallization of colloidal systems. *Prog. Colloid Polym. Sci.*, 79:287–292, 1989.

[178] R. Kaiser and G. Miskolczy. Magnetic properties of stable dispersions of subdomain magnetite particles. *J. Appl. Phys.*, 41(3):1064–1072, 1970.

[179] S. Mørup. Mössbauer spectroscopy studies of suspensions of Fe_3O_4 microcrystals. *J. Magn. Magn. Mater.*, 39(1-2):45–47, 1983.

[180] C. Caizer. T^2 law for magnetite-based ferrofluids. *J. Phys. Condens. Matter*, 15(6):765, 2003.

Summary

In this thesis the liquid crystal phase behavior of colloidal, boardlike, goethite (α-FeOOH) particles is described. The main technique to study this has been small-angle X-ray scattering, while also polarization microscopy was used. Except for the last chapter, aqueous dispersions were studied.

Part 1 describes the general phase behavior of goethite. In Chapter 2 it is shown that polydispersity plays a large role in the phase behavior. Systems with a low polydispersity show an isotropic, nematic and smectic A phase. A high polydispersity induces the formation of a columnar phase, but still a smectic phase is observed as well. Strong fractionation occurs which is able to reduce the local length polydispersity by up to a factor two. The larger particles that do not fit into the smectic layers seem to be accommodated by the columnar phase. Chapter 3 describes the existence of a special type of liquid crystals, the biaxial liquid crystals. It is shown that particles with specific dimensions, exactly in between rodlike and platelike, spontaneously form biaxial phases, which confirms theoretical predictions. The 3D structure of the biaxial nematic and biaxial smectic A phase was determined by aligning the domains using a small magnetic field during small-angle X-ray scattering measurements. In Chapter 4 a closer look is taken at the smectic A phase. Information about undulation fluctuations in this phase is obtained by the analysis of the peak shape of X-ray reflections. An unusual peak shape was observed which is rationalized by the occurrence of sliding fluctuations, in which the layers undulate by sliding the particles along each other while keeping the particle director fixed.

An external magnetic field was used to manipulate the phase behavior in Part 2. Chapter 5 describes the general behavior of the different liquid crystal phases in a magnetic field. In the isotropic and nematic phase alignment along the field is observed in small fields. Applying a larger field causes the particles to rotate to an orientation perpendicular to the field. The columnar phase hardly reacts to a small field, but it aligns perpendicular to large fields. The smectic phase shows more complicated behavior, which is studied in more detail in Chapter 6. In systems with a low polydispersity the smectic phase shows behavior similar to the isotropic and nematic phase. The reorientation behavior is more complicated though; the particle and layer orientation seem to be able to decouple during rotation. Systems with a higher polydispersity align parallel to a small field as well, but at higher fields the smectic phase transforms into an aligned columnar phase.

Chapter 7 shows that nematic-nematic phase separation can occur in a magnetic field. When a field is applied around the critical magnetic field, where the particles rotate from parallel to perpendicular to the field, the nematic phase separates into two nematic phases with orthogonal orientations. The large excluded volume between these orientations causes macroscopic phase separation. The nematic-nematic phase separation seems to be induced by a polydispersity in the magnetic properties of the particles. Around the isotropic-nematic interface also various effects are observed when following it over time in a magnetic field, as is shown in Chapter 8. Depending on the field strength the level of the interface rises or lowers, which seems to couple to the occurrence of nematic-nematic phase separation. Furthermore, from a certain field strength onwards nematic droplets are being formed in the aligned isotropic (paranematic) phase. In the paranematic phase also regions with different orientations coexist around the critical field strength.

In Part 3, modified goethite dispersions are discussed. Goethite particles are modified, replacing Fe with a few percent of the elements Cr, Al or Co in Chapter 9. The magnetic properties of these particles are different from the pure goethite particles, which results in a higher critical field strength. Apart from that, the phase behavior is similar to that of normal goethite. Nematic-nematic phase separation is observed in a mixed sample of normal and Al-goethite. Chapter 10 describes the formation of a simple rectangular columnar phase in a Cr-goethite dispersion. In a large magnetic field it is transformed into the centered rectangular columnar phase, which is the structure that is usually found for goethite. This is rationalized in terms of entropic effects using a simple cell model. The last chapter (11) shows the phase behavior of sterically stabilized goethite which is compared to that of charged goethite. The magnetic properties remain the same and the phase behavior is similar. However, in the sterically stabilized dispersions a stronger tendency to form gels is observed. This might be caused by a stronger van der Waals interaction because the particles can come closer together.

Samenvatting

In dit proefschrift wordt het vloeibaar kristallijne fasegedrag van colloïdaal goethiet onderzocht. Hierbij is veelvuldig gebruik gemaakt van een magneetveld om het gedrag te beïnvloeden. Een aantal belangrijke begrippen wordt hieronder, in de eerste drie paragrafen, uitgelegd waarna de behaalde resultaten beschreven worden.

Colloïden

Colloïden zijn deeltjes waarvan tenminste één dimensie (lengte/breedte/dikte) een grootte heeft tussen de nanometer en micrometer ($10^{-9} - 10^{-6}$ m; een haar is ongeveer 100 micrometer dik). Ze vormen een stabiel mengsel met het medium waar ze in zitten. De colloïden en het medium kunnen gasvormig, vloeibaar of vast zijn. Deze colloïdale dispersies (mengsels) komen overal in het dagelijks leven voor. Een aantal voorbeelden zijn melk, verf, crème, klei, inkt, bloed, mist en rook.

Een belangrijke eigenschap van colloïden is dat ze Brownse beweging vertonen. Dit is de willekeurige beweging van deeltjes in een medium. Het wordt veroorzaakt door de thermische beweging van de moleculen van het medium die daardoor voortdurend tegen de colloïden botsen en deze zo ook continu laten bewegen. Deze beweging zorgt er voor dat colloïden met een grotere dichtheid dan het medium niet bezinken maar blijven zweven.

De vele toepassingen, zoals de hierboven genoemde voorbeelden, maken dat colloïden interessant zijn om te bestuderen. Daarnaast kunnen ze ook model staan voor het gedrag van atomen of moleculen. Het is gebleken dat deze systemen vaak vergelijkbaar gedrag vertonen. Het voordeel van colloïden is dat ze groot zijn vergeleken met atomen en moleculen en daardoor makkelijker zijn te bestuderen. Ze zijn makkelijker te bekijken met een microscoop en beter te volgen omdat ze trager zijn. Daarbij kunnen ze in allerlei vormen en maten gemaakt worden met ook nog eens verschillende soorten interacties tussen de deeltjes. Hierdoor is een breed onderzoeksgebied ontstaan met steeds groeiende mogelijkheden.

Vormen en vloeibare kistallen

Veel onderzoek is gedaan naar bolvormige colloïden. Deze deeltjes kunnen in een oplosmiddel een gas-, vloeistof- en kristalfase aannemen. Welke fase ze vormen is afhankelijk van de concentratie. Als de concentratie heel laag is zijn de deeltjes zo ver uit elkaar dat ze zich gedragen als een gas. Bij een toenemende concentratie wordt

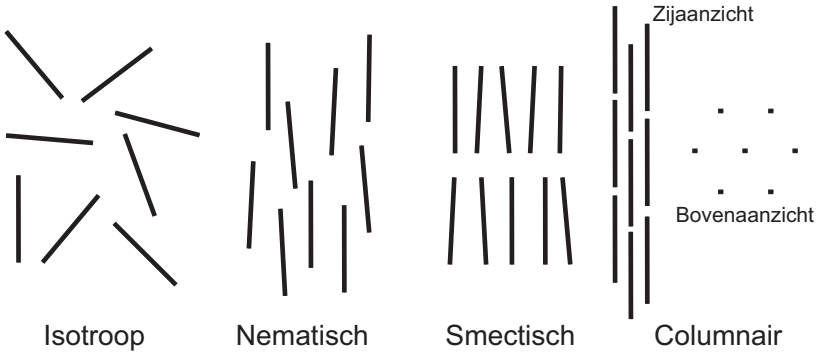

FIGUUR 1. Schematische weergave van de structuur van de isotrope, nematische, smectische en columnaire fase.

het gedrag vergelijkbaar met een vloeistof en op een gegeven moment zullen de deeltjes kristalliseren en zich daarmee driedimensionaal ordenen.

Als de deeltjes niet bolvormig maar bijvoorbeeld staaf- of plaatvormig zijn, ontstaan er nieuwe mogelijkheden. Ze kunnen nu behalve positie-ordening, zoals in een kristal, ook ordening van de oriëntatie hebben. Op deze manier kunnen vloeibare kristallen worden verkregen; deze hebben deels kristallijne eigenschappen maar vloeien nog wel als een vloeistof. Deeltjes zullen zich ordenen vanaf een bepaalde concentratie. Bij een lage concentratie hebben de deeltjes veel ruimte en zullen ze willekeurige oriëntaties aannemen (dit wordt isotroop genoemd, Figuur 1). Als de concentratie hoger wordt, wordt de bewegingsvrijheid van de deeltjes beperkt als ze ongeordend blijven. Door allemaal dezelfde oriëntatie aan te nemen kunnen ze makkelijker langs elkaar bewegen.

De simpelste vloeibaar-kristalvorm wordt de nematische fase genoemd, hierbij zijn alle deeltjes in één richting opgelijnd maar hun posities zijn nog steeds willekeurig (Figuur 1). Als behalve het oplijnen ook ééndimensionale ordening van de positie optreedt ontstaan er lagen in het systeem. Binnen deze lagen bewegen de deeltjes willekeurig. Dit wordt de smectische fase genoemd. De deeltjes kunnen ook een tweedimensionale positie-ordening hebben als ze kolommen vormen. De kolommen ordenen zichzelf daarbij in een regelmatige structuur. Dit is de columnaire fase.

Een speciale vorm van de vloeibare kristallen kan ontstaan als de deeltjes een vorm hebben tussen staven en platen in, dat wil zeggen plankvormig (met drie verschillende dimensies, zoals in Figuur 4a). In dat geval kan het voorkomen dat alle drie de assen van de deeltjes zich oplijnen, waar dit normaal gesproken maar voor één as gebeurt. Zo'n fase wordt een biaxiale fase genoemd (uitlijning van twee assen geeft automatisch ook uitlijning van de derde as).

Vloeibare kristallen worden veelvuldig toegepast in schermen, denk aan LCDs (liquid crystal displays; vloeibaar-kristalschermen). De kristaleigenschappen zorgen ervoor dat

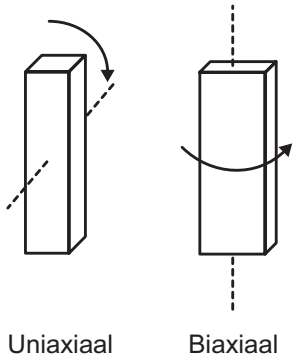

Figuur 2. Schematische weergave van het uitlijnen van de uniaxiale en biaxial fase.

licht beïnvloed kan worden en de vloeistofeigenschappen zorgen dat de uitlijning makkelijk gerealiseerd kan worden met bijvoorbeeld een elektrisch of magneetveld. Door het veld aan te passen kan beïnvloed worden hoeveel licht er doorgelaten wordt. Veelbelovend voor toepassingen zijn de biaxiale vloeibare kristallen omdat hierbij alleen de kortste as van het deeltje van richting veranderd hoeft te worden in plaats van de lange as (Figuur 2). Hierdoor kan het oplijningsproces sneller worden. Deze biaxiale vloeibare kristallen kunnen mogelijk ook een rol spelen in driedimensionale optische toepassingen omdat licht vanuit drie verschillende richtigen gestuurd kan worden.

Goethiet

In dit proefschrift wordt gekeken naar vloeibare kristallen van goethiet. Goethiet is een mineraal dat bestaat uit ijzer oxyhydroxide (FeOOH, een soort roest). Het is overal op de wereld in de natuur te vinden en het wordt al sinds de prehistorie gebruikt als geelbruin pigment (kleurstof in bijvoorbeeld verf).

Goethiet kan ook gemaakt worden als colloïdaal systeem. Dit levert plankvormige deeltjes op die stabiel zijn in water. Vanwege de vorm kunnen ze vloeibare kristallen vormen. De magnetische eigenschappen van het materiaal zorgen ervoor dat de deeltjes makkelijk gestuurd kunnen worden met een magneetveld.

Het is uit eerder onderzoek, ruim 100 jaar geleden begonnen en in meer detail de laatste jaren, gebleken dat de goethiet deeltjes zeer speciaal gedrag vertonen in een magneetveld. In een klein veld lijnen de deeltjes op langs het veld, maar in een groter veld draaien de deeltjes zodat ze loodrecht op het veld staan (Figuur 3). Dit gedrag is waargenomen in de ongeordende (isotrope) fase en ook in de nematische fase. Verder is gebleken dat de deeltjes een columnaire fase kunnen vormen bij voldoende hoge concentratie aan deeltjes. Bijzonder is dat de nematische fase in een groot magneetveld overgaat in de columnaire fase, waarbij de deeltjes dus van soort ordening veranderen.

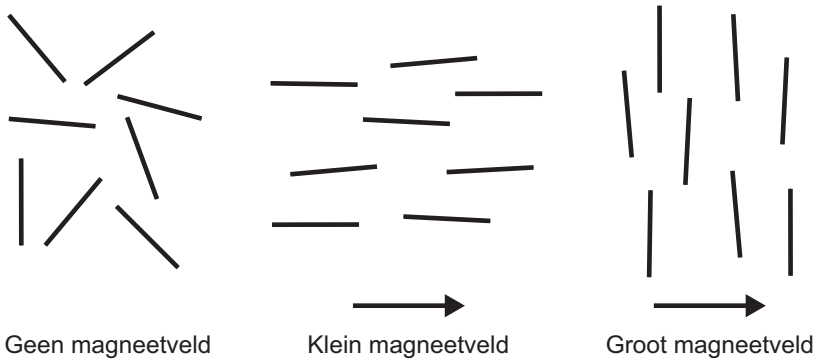

FIGUUR 3. Het gedrag van goethiet deeltjes in een magneetveld.

FASEGEDRAG VAN GOETHIET

Uitgaande van het bekende gedrag is er verder gekeken naar de verschillende vloeibare kristallen van goethiet. Het pure gedrag is bekeken in deel 1 van dit proefschrift.

Invloed van de variatie in de deeltjesgrootte

Als colloïden gemaakt worden hebben ze nooit allemaal exact dezelfde afmeting. Er is een spreiding in de deeltjesgrootte en een maat hiervoor is de polydispersiteit: de standaarddeviatie gedeeld door het gemiddelde. Afhankelijk van de manier waarop de deeltjes gemaakt worden, kunnen systemen verkregen worden met een lage of hoge polydispersiteit.

Er is in hoofdstuk 2 gekeken naar het fasegedrag van goethietsystemen met verschillende polydispersiteiten. Systemen met een lage polydispersiteit vormen de nematische en smectische fase, afhankelijk van de concentratie (zie Figuur 1). Als de polydispersiteit hoog wordt dan wordt er ook een columnaire fase gevormd. Verrassend genoeg wordt de smectische fase ook nog waargenomen. Dit werd niet verwacht omdat het vormen van lagen niet gunstig is als er veel verschil is in de lengte van de deeltjes. In een columnaire fase is het makkelijker verschillende lengtes in te passen. Het blijkt dat het systeem zich zo aanpast dat deeltjes van ongeveer dezelfde lengte de smectische fase vormen en dat met name de deeltjes die te lang zijn om in de lagen te passen de columnaire fase vormen.

Biaxiale fasen

Vanwege de vorm van de goethiet deeltjes, namelijk plankvormig, zijn ze een kandidaat om biaxiale vloeibaar-kristalfasen te kunnen vormen. In hoofdstuk 3 wordt aangetoond dat ze dat inderdaad doen. Deeltjes met speciale verhoudingen van lengte, breedte en dikte (lengte/breedte = breedte/dikte) vormen spontaan een biaxiale nematische en biaxiale smectische fase. 40 jaar eerder was theoretisch al voorspeld dat

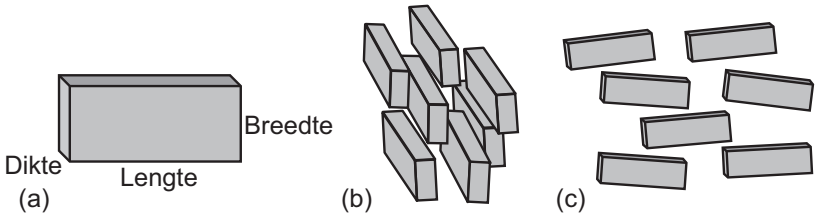

Figuur 4. (a) Vorm van een goethiet deeltje, (b) biaxiale nematische fase met de lange as loodrecht op het papier, (c) biaxiale nematische fase met de lange as gericht langs het papier.

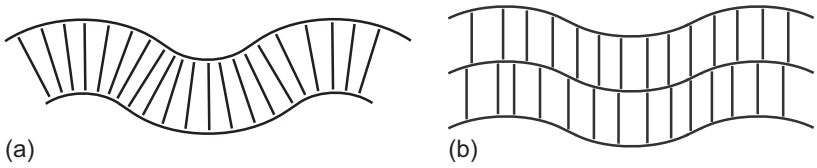

Figuur 5. Fluctuaties in de smectische fase.

deeltjes met deze verhoudingen biaxiale fasen zouden vormen; hier hebben wij voor het eerst het experimentele bewijs geleverd. Voor de structuur zie Figuur 4.

De smectische fase

In hoofdstuk 4 is er in meer detail gekeken naar de smectische fase. De lagen in deze fase kunnen verschillende soorten fluctuaties vertonen. Er wordt voor de smectische fase meestal uitgegaan van fluctuaties zoals te zien in Figuur 5a, waarbij de laagafstand gelijk blijft maar de deeltjesoriëntatie varieert. In het bestudeerde systeem zijn aanwijzingen gevonden voor een ander type fluctuaties, zoals weergegeven in Figuur 5b. Hierbij blijft de oriëntatie van de deeltjes gelijk maar varieert de laagafstand. Bij de gebruikte deeltjes kost het waarschijnlijk meer energie om de oriëntatie ten opzichte van elkaar te veranderen dan om ze een beetje langs elkaar te schuiven.

Goethiet in een magneetveld

Deel 2 van het proefschrift beschrijft het gedrag van de vloeibaar-kristalfasen van goethiet in een magneetveld.

Algemeen gedrag van de verschillende fasen

Het gedrag van de verschillende vloeibare kristalfasen in een magneetveld is beschreven in hoofdstuk 5. In de nematische fase lijkt het gedrag in een magneetveld op het gedrag van de enkele deeltjes. De fase lijnt op parallel aan het veld in kleine magneetvelden. Vanaf een bepaalde veldsterkte gaan de deeltjes draaien naar een loodrechte oriëntatie. De smectische fase lijnt ook op parallel aan een klein veld, maar in grote

velden wordt het gedrag ingewikkelder. Het systeem beschreven in dit hoofdstuk gaat over naar een columnaire fase. In het volgende hoofdstuk is nader ingegaan op het gedrag van de smectische fase. De columnaire fase wordt nauwelijks beïnvloed door lage velden, maar lijnt wel op in hoge velden. Daar is de oriëntatie met de deeltjes loodrecht op het veld.

De smectische fase

Het gedrag van de smectische fase in een magneetveld hangt af van de polydispersiteit van het systeem. Dit is bestudeerd in hoofdstuk 6. In systemen met een lage polydispersiteit lijkt het gedrag op dat van de nematische fase. In een klein veld lijnen de deeltjes op parallel aan het veld, en in een groot veld loodrecht. De reoriëntatie is in dit geval ingewikkelder omdat de lagen van de smectische fase niet gemakkelijk als geheel kunnen draaien. Het lijkt erop dat de lagen tijdelijk opbreken in kleine stukjes om later in de nieuwe oriëntatie zich opnieuw te vormen. Systemen met een hoge polydispersiteit lijnen ook op parallel aan een klein magneetveld, maar in hoge velden vertonen ze ander gedrag. De smectische fase transformeert naar de columnaire fase. In deze systemen is de columnaire fase ook al aanwezig zonder magneetveld (zoals gezien in hoofdstuk 2) en die wordt dus stabieler in een groot magneetveld.

Scheiding van twee verschillende nematische fasen

In hoofdstuk 7 is gekeken naar het gedrag van de nematische fase als deze geplaatst wordt in een magneetveld rond het kritische veld waarbij de deeltjes gaan draaien van parallel aan naar loodrecht op het veld. In ongeveer een dag tijd vindt er scheiding plaats tussen twee verschillende nematische fasen. De ene heeft een oriëntatie parallel aan het veld en de andere loodrecht op het veld. Als een deel van de deeltjes al wil gaan draaien, maar een ander deel niet dan gaan ze elkaar zo in de weg zitten dat het gunstiger is om te splitsen in twee fasen met een onderling loodrechte oriëntatie.

Het isotroop-nemaat grensvlak

De isotrope en nematische fase worden gescheiden door een grensvlak. Hoofdstuk 8 beschrijft de invloed van een magneetveld op dit grensvlak. In een klein magneetveld lijnen beide fasen op langs het veld en is het verschil niet goed meer te zien. Bij hogere velden treden er veranderingen op in de positie van het grensvlak. Er zijn verschillende effecten die hierbij een rol spelen. Ten eerste lijkt er een effect te zijn van wat er in de nematische fase zelf gebeurt. Als daar een scheiding optreedt in twee nematische fasen heeft tenminste één van de twee een hogere dichtheid dan voordat het in een magneetveld is geweest. De hogere dichtheid zorgt ervoor dat de nematische fase compacter wordt en het grensvlak verplaatst naar beneden. Tegelijk is er ook een ander effect dat optreedt. In een magneetveld wordt de geordende nematische fase voordeliger om te vormen ten opzichte van de isotrope fase. Er vormen zich dan ook

nematische druppels in de isotrope fase die naar de nematische fase toe zakken en deze fase laten groeien waardoor het grensvlak stijgt. Het hangt van de veldsterkte af welk effect belangrijker is. Bij erg grote magneetvelden zal het verschil tussen de isotrope en nematische fase volledig verdwijnen.

Gemodificeerd goethiet

In deel 3 van het proefschrift is goethiet op verschillende manieren gemodificeerd. Er is gekeken in welke mate deze modificaties het gedrag beïnvloeden.

Vervanging van een deel van het ijzer door andere elementen

Een klein deel van het ijzer in goethiet kan vervangen worden door andere elementen zonder de vorm van de deeltjes teveel te veranderen. In hoofdstuk 9 is eerst gekeken naar deeltjes met chroom. Het blijkt dat deze deeltjes nog steeds dezelfde vloeibare kristallen vormen. Wel is er iets veranderd aan de magnetische eigenschappen. Er is een groter magneetveld nodig om de deeltjes te laten draaien van parallel aan naar loodrecht op het veld. Deeltjes met aluminium of cobalt vertonen een vergelijkbaar effect. Dit soort deeltjes kan bijvoorbeeld gebruikt worden om een scheiding in twee nematische fasen te krijgen op een iets andere manier dan beschreven in hoofdstuk 7. Een mengsel van gewoon goethiet en gemodificeerd goethiet is bestudeerd in een magneetveld. Bij een bepaalde veldsterkte oriënteert het gewone goethiet zich loodrecht op het veld, terwijl de gemodificeerde deeltjes parallel aan het veld zullen uitlijnen. Er vindt dan scheiding plaats in twee verschillende nematische fasen: één met de gewone deeltjes loodrecht op het veld en één met de gemodificeerde deeltjes parallel aan het veld.

Speciale vorm van de columnaire fase

In een goethiet systeem met chroom is een andere structuur van de columnaire fase gevonden (hoofdstuk 10). De gebruikelijke structuur is te zien in Figuur 6a. In dit geval bleek de structuur anders te zijn, namelijk zoals die in Figuur 6b. Wanneer deze vervolgens in een magneetveld wordt gebracht, gaat de structuur over naar de normale structuur (Figuur 6a). Een simpel model, waarbij is gekeken naar de bewegingsvrijheid van de deeltjes in de verschillende structuren, is gebruikt om dit te verklaren.

Behaarde deeltjes

Alle hiervoorgenoemde systemen bestaan uit deeltjes in water. Het gebruikte water heeft een pH van 3 en in die omstandigheden hebben de deeltjes een positieve lading. Deze lading zorgt ervoor dat de deeltjes elkaar afstoten en niet te dicht bij elkaar kunnen komen. Als ze elkaar te dicht zouden kunnen naderen aggregeren ze (klonteren ze samen) en zinken ze naar de bodem. Losse deeltjes blijven mooi stabiel in het water zweven. Een andere manier om de deeltjes stabiel te maken is door ze te beharen met polymeren op het oppervlak. Deze haren zorgen er nu voor dat de deeltjes zelf elkaar

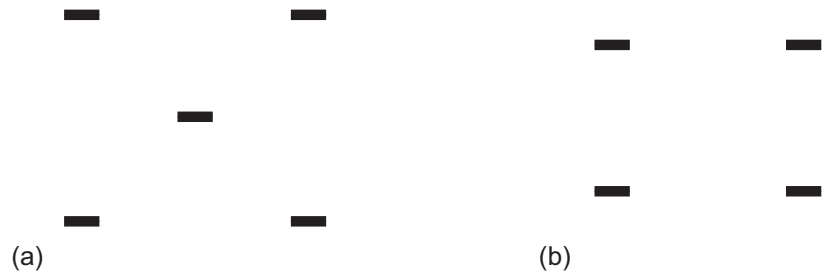

FIGUUR 6. Schematische weergave van het bovenaanzicht van de structuur van twee typen columnaire fasen.

niet kunnen raken. Dit soort deeltjes, met als oplosmiddel tolueen, is bestudeerd en vergeleken met de geladen deeltjes in water in hoofdstuk 11.

De twee soorten systemen vormen dezelfde typen vloeibare kristallen en hebben dezelfde magnetische eigenschappen. Dit is waargenomen voor systemen met een lage en een hoge polydispersiteit. Het is echter gebleken dat de behaarde deeltjes eerder een gel vormen dan de geladen deeltjes. Een gel is een soort netwerk van deeltjes en is erg viskeus (stroperig). Hierdoor vormen ze de vloeibare kristallen op een kleinere schaal en zijn ze niet makkelijk uit te lijnen in een magneetveld. De haren op de deeltjes lijken dus de deeltjes minder goed van elkaar af te houden dan de lading dat doet.

NUT VAN HET ONDERZOEK

Het onderzoek beschreven in dit proefschrift valt in de categorie fundamenteel onderzoek. Dit betekent dat het onderzoek vooral bedoeld is om nieuwe kennis op te doen en niet direct om het toe te passen in de praktijk. Meestal is niet vantevoren te voorspellen waarvoor de opgedane kennis uiteindelijk gebruikt zal worden. Dat wil niet zeggen dat de resultaten nooit toegepast zullen worden. De opgedane kennis kan gebruikt worden in meer toegepast onderzoek wat dan op de langere termijn kan leiden tot een bruikbaar product.

Vloeibare kristallen worden vooral gebruikt in de eerder genoemde LCDs en andere optische toepassingen. De colloïden beschreven in dit proefschrift zullen niet direct hiervoor toegepast worden omdat ze te groot (en daarmee te langzaam) zijn en ook nog eens gekleurd. Wel kunnen ze model staan voor wat er allemaal mogelijk is. Dit soort deeltjes vormt een simpel model voor de ingewikkeldere moleculen die echt toegepast worden.

Dankwoord

Dit promotieonderzoek had ik nooit uit kunnen voeren zonder de hulp van anderen. Er zijn dan ook veel mensen die ik wil bedanken voor hun bijdrage. Ik begin hierbij met mijn meest directe begeleider, en co-promotor, Gert Jan. Ik vond het erg prettig om met je samen te werken. Je bent de rustige basis geweest voor mijn werk. Veel plezier in Italië! Mijn beide andere co-promotoren hebben ook een belangrijke bijdrage geleverd. Andrei, je was vooral de man voor de röntgenverstrooiingsmetingen in Grenoble. Je hebt me erg enthousiast weten te maken voor deze, ook vaak nachtelijke, metingen. Ook terug in het lab kon ik altijd bij je terecht met vragen en heb je me goed geholpen. Dominique, bedankt voor al het werk dat je al gedaan had voordat ik begon, een aantal van jouw samples heeft mij erg mooie resultaten gegeven. Het was altijd gezellig met jou erbij.

Natuurlijk wil ik ook mijn promotor, Henk, bedanken. Je begeleiding is niet zo direct geweest, maar op een afstand was je toch prettig aanwezig. Je persoonlijke interesse was altijd fijn om te ervaren.

Ondersteuning heb ik verder gekregen van verschillende andere mensen op het lab. Met computerproblemen kon ik altijd bij Emile terecht. We hebben ook veel tijd samen aan de koffietafel doorgebracht, als voorstanders van een wat vroegere koffiepauze. De hulp van Bonny heb ik ook altijd gewaardeerd. Bedankt voor je mooie ontwerpen van de verschillende soorten magneten die ik wilde hebben. De werkplaats heeft vervolgens een goed vervolg gegeven aan deze ontwerpen waardoor ik weer verder kon. Ben, bedankt voor je ideeën hoe we de magnetische eigenschappen van mijn deeltjes konden bepalen. Het was ook prettig met je samen te werken bij de verschillende onderwijsverplichtingen. Marina, bedankt voor je inzet om alles goed te laten verlopen, met name met het zo geliefde Metis systeem.

Met Sandra heb ik veel lol gehad op het lab. Het was erg leuk om je paranimf te zijn en zo alles alvast eens van wat dichterbij mee te maken. Nu zullen de rollen omgedraaid zijn. Lia, we zijn veel naar dezelfde conferenties gegaan, ik vond dat altijd erg gezellig. Ook in het lab was het prettig om dingen met je samen te doen. Helaas zal ik jouw verdediging gaan missen. Succes nog met de laatste loodjes! Op het lab heb ik ook veel gehad aan Maurice. Je hebt me een aantal nuttige dingen laten zien.

Mijn kamergenoten, Maria, Roberto, Bob, Rob en op de valreep nog Susanne, wil ik ook bedanken. We zijn nooit een drukke kamer geweest, maar ik heb jullie aanwezigheid zeker gewaardeerd.

Tijdens mijn onderzoek heb ik ook een aantal studenten begeleid. Edwin, Anoeska en Inge bedankt voor jullie inzet. Also thanks to Andreea en Mihai for your nice work.

Alle andere promovendi, postdocs, medewerkers en studenten bedankt voor de sfeer op het lab. Ik heb het erg naar mijn zin gehad. Ook de mensen van Soft Condensed Matter wil ik bedanken voor de gezellige tijd tijdens conferenties, scholen en andere bijeenkomsten.

Buiten ons eigen lab heb ik ook de nodige hulp gehad. Om dichtbij te beginnen, Hans, bedankt voor de hulp met de elektronenmicroscoop en in het bijzonder met de elementanalyse (EDX). Patrick, thanks for all your input and having me over to perform some measurements in Orsay. I also went many times to the ESRF in Grenoble for small-angle X-ray scattering measurements. First of all, I want to thank Dima for his help during these measurements. Furthermore, I would like to thank the people of the BM26 DUBBLE beamline and the ID02 beamline for all their help and NWO for the opportunity to do the measurements.

Daniëlle, het was erg fijn om van alles met je te kunnen delen, ook al was het vanaf een wat grotere afstand. Jij hebt je proefschrift inmiddels met succes verdedigd, knap hoe je dat voor elkaar gekregen hebt. Erg leuk dat je komt om mijn paranimf te zijn. Stefan, bedankt voor het oprichten van het forum. Het bezorgt de nodige dagelijkse afleiding en is een goede plek om lekker te klagen. Dennis, bedankt voor de gezellige etentjes. Veel succes in België.

Gelukkig heb ik me naast mijn promotie kunnen ontspannen en inspannen op de atletiekbaan. Al mijn trainingsgenoten en trainers bij Altis en Phoenix, bedankt voor de gezelligheid.

Ik wil ook mijn familie bedanken. Kees, Ineke, Peter en Veerle bedankt voor de steun, de leuke momenten samen en de pogingen om te begrijpen wat ik nou eigenlijk allemaal doe.

Ronald, als laatste wil ik jou bedanken. Je bent heel belangrijk geweest bij het tot stand komen van dit boekje en ik vind het fijn dat ik al die jaren met jou samen heb meegemaakt. En nu eerst lekker samen op reis.

List of publications

This thesis is based on the following publications:

- E. van den Pol, D. M. E. Thies-Weesie, A. V. Petukhov, K. Kvashnina, G. J. Vroege, *Influence of polydispersity on the phase behavior of colloidal goethite*, J. Chem. Phys. **129**, 164715 (2008). (Chapter 2)
- E. van den Pol, A. V. Petukhov, D. M. E. Thies-Weesie, D. V. Byelov, G. J. Vroege, *Experimental realization of biaxial liquid crystal phases in colloidal dispersions of boardlike particles*, Phys. Rev. Lett. **103**, 258301 (2009). (Chapter 3)
- E. van den Pol, A. V. Petukhov, D. M. E. Thies-Weesie, D. V. Byelov, G. J. Vroege, *Uniaxial and biaxial liquid crystal phases in colloidal dispersions of boardlike particles*, accepted for a special issue in Liq. Cryst. (2010). (Chapter 3)
- E. van den Pol, D. M. E. Thies-Weesie, A. V. Petukhov, P. Panine, G. J. Vroege, *Chromium-modified goethite in an external magnetic field*, J. Phys. Condens. Matter **20**, 404219 (2008). (Chapter 5 and 9)
- E. van den Pol, A. V. Petukhov, D. M. E. Thies-Weesie, G. J. Vroege, *Simple rectangular columnar phase of goethite nanorods and its martensitic transition to the centered rectangular columnar phase*, Langmuir **26**, 1579 (2010). (Chapter 10)

Manuscripts in preparation:

- A. V. Petukhov, E. van den Pol, D. V. Byelov, D. M. E. Thies-Weesie, P. Davidson, R. van Silfhout, G. J. Vroege, *Sliding undulation fluctuations in the smectic A phase of colloidal goethite.* (Chapter 4)
- E. van den Pol, A. V. Petukhov, D. V. Byelov, D. M. E. Thies-Weesie, A. Snigirev, G. J. Vroege, *Behavior of the smectic A phase of goethite in a magnetic field.* (Chapter 6)
- E. van den Pol, A. Lupascu, M. A. Diaconeasa, A. V. Petukhov, D. V. Byelov, G. J. Vroege, *Onsager revisited: Magnetic field induced nematic-nematic phase separation in dispersions of goethite nanorods.* (Chapter 7)
- E. van den Pol, A. Lupascu, G. J. Vroege, *The isotropic-nematic interface of colloidal goethite in an external magnetic field.* (Chapter 8)
- E. van den Pol, A. V. Petukhov, D. M. E. Thies-Weesie, D. V. Byelov, G. J. Vroege, *Sterically stabilized goethite: phase behavior with and without magnetic field.* (Chapter 11)

Other papers by the author:

- P. Vergeer, E. van den Pol, A. Meijerink, *Time and temperature dependence of the emissions from the quantum-cutting phosphor $LiGdF_4$:Eu^{3+}*, J. Lumin. **121**, 456 (2006).
- B. H. Erné, E. van den Pol, G. J. Vroege, T. Visser, H.H. Wensink, *Size fractionation in a phase-separated colloidal fluid*, Langmuir **21**, 1802 (2005).

Curriculum Vitae

Esther van den Pol was born on the 1^{st} of August, 1982 in Middelburg, The Netherlands. In 2000 she graduated from the Buys Ballot College in Goes. She studied Chemistry at Utrecht University from 2000 until 2005. As part of the Bachelor program she performed a project on size fractionation in phase separated ferrofluids at the Van 't Hoff Laboratory for Physical and Colloid Chemistry under supervision of Ben Erné. During the master Chemistry and Physics, she did her main research project at the group of Condensed Matter and Interfaces under supervision of Peter Vergeer and Andries Meijerink on quantum cutting phosphors. Also as part of her masters she performed an internship at Akzo Nobel Coatings Research in Arnhem under supervision of Anthonie Stuiver and Willem Kegel on interactions between thickener molecules and latex or pigment particles in waterborn paints. In 2006 she started her PhD research at the Van 't Hoff Laboratory of Physical and Colloid Chemistry at Utrecht University under supervision of Henk Lekkerkerker, Gert Jan Vroege, Andrei Petukhov and Dominique Thies-Weesie. She was employed by the 'Stichting voor Fundamenteel Onderzoek der Materie' (FOM). Her research on goethite liquid crystals and the manipulation by an external magnetic field is described in this thesis.